# NOVEL ANALYTICAL TOOLS FOR STUDYING A POTENTIAL TYPE-1 DIABETES THERAPY

Ву

**Cody Pinger** 

# A DISSERTATION

Submitted to
Michigan State University
in partial fulfillment of the requirements
for the degree of

Chemistry – Doctor of Philosophy

2018

#### **ABSTRACT**

### NOVEL ANALYTICAL TOOLS FOR STUDYING A POTENTIAL TYPE-1 DIABETES THERAPY

By

### **Cody Pinger**

Red blood cells (RBCs) are known to play an important role in regulating microvascular circulation by releasing the signaling molecule adenosine triphosphate (ATP). Extracellular ATP in the bloodstream reacts with endothelial cells lining the blood vessel via a P2Y purinergic receptor, causing the endothelial cells to create and release nitric oxide, a known vasodilator. Interestingly, RBCs from Type-1 diabetic (T1D) subjects release significantly less ATP than RBCs from non-diabetic subjects. This effect is believed to impair microvascular blood flow and be a potential cause of the prevalent downstream microvascular complications seen in T1D.

In T1D, the immune system destroys the pancreatic  $\beta$ -cells, therefore creating a deficiency of the hormones normally secreted by these cells. Since the early 1920's, T1D patients have been administering the pancreatic  $\beta$ -cell secretion insulin to manage their blood sugar and stay alive. However, insulin treatment alone with diet and exercise does not prevent the microvascular complications seen in the disease. C-peptide is a 31-amino acid peptide that is co-secreted with insulin from the pancreatic  $\beta$ -cells along with Zn<sup>2+</sup>. Researchers have found that treating T1D RBCs with a combination of C-peptide and Zn<sup>2+</sup> in the presence of albumin, a prevalent bloodstream protein, can significantly increase the amount of ATP released from the cells. However, RBCs are unaffected when treated with C-peptide and Zn<sup>2+</sup> in the absence of albumin. Researchers have shown that albumin from diabetic patients has different properties than albumin from non-diabetic subjects. Therefore, the hypothesis of the work in this thesis is that diabetic albumin interferes with the interaction of RBCs with C-peptide and Zn<sup>2+</sup>.

The work in this dissertation is focused on the role of albumin and its interactions with C-peptide,  $Zn^{2+}$ , and RBCs. 3D-printing technology was used in order to create novel devices to study interactions between albumin and C-peptide and  $Zn^{2+}$  under diabetic conditions. A 3D-printed equilibrium dialysis device was used to measure the binding affinity between human serum albumin (HSA) and  $Zn^{2+}$  ( $K_d$ = 562  $\pm$  93 nanomolar). It was found that the affinity of this interaction was decreased by glycation of albumin, but not by immediate addition of glucose. The device was also used to measure that C-peptide does not alter the affinity of  $Zn^{2+}$ to albumin. The dialysis device is compatible with plate-reader technology and enables automated and direct measurements of certain analyte ligands. Further, a 3D-printed ultrafiltration device was created in order to measure the binding affinity between HSA and C-peptide ( $K_d$ = 2.4  $\pm$  0.3 micromolar). The affinity of this interaction was not altered by  $Zn^{2+}$ , glucose, or glycation of albumin. Novel 3D-printing techniques were developed in order to create these devices, such as the *Print-Pause-Print* method for integrating membranes directly into 3D-printed devices, and a support-free Polyjet printing technique.

Lastly, the interaction of RBCs with C-peptide and  $Zn^{2+}$  was measured in the presence of normal and glycated albumin. The ability of RBCs to release ATP under flow conditions was increased significantly in the presence of C-peptide/ $Zn^{2+}$  and normal albumin (p<0.05); whereas the RBCs treated with C-peptide/ $Zn^{2+}$  and glycated albumin did not release statistically more ATP than the control (n=4 blood draws). The ability of C-peptide to bind to RBCs in the presence of normal and glycated albumin was also measured. Approximately 1.8  $\pm$  0.1 picomoles of C-peptide bound to RBCs in the presence of normal albumin, whereas 0.8  $\pm$  0.1 picomoles bound in the presence of glycated albumin (n=3 blood draws, p<0.05). Therefore, the ability of C-peptide to bind and affect RBCs was affected by the presence of glycated albumin, such as seen in diabetes. The results of the studies reported in this thesis should be taken into consideration by those studying C-peptide as a replacement therapy in T1D.

### **ACKNOWLEDGMENTS**

Firstly, I would like to thank all of the members of my family for their love and support in helping me obtain my Ph.D. Also, I would like to acknowledge and thank Dana Spence for his scientific guidance, mentorship, and friendship over the past four and a half years. His unique approach to scientific mentoring, including proper work-life balance and treating us students like family, created a very positive graduate school experience for me. I would also like to acknowledge and thank David Karpovich for sparking my initial interest in analytical chemistry and inspiring me to be both excited and curious in the lab. Other mentors I would like to recognize are: Merlin Bruening, Dan Jones, Gary Blanchard, and Kathy Severin, who have always made time to go out of their way to help me become a better scientist.

I could not have kept my sanity over the years without the tremendous help of my graduate (and undergraduate) student colleagues and the members of the Spence group. Thank you for your love and friendship. Also, a huge shout-out to all of my friends for always being there for me, and a special thanks to Kathryn for your support and patience while I prepared this thesis and defense-presentation. Praise be to God.

"Wimps go up to rebound with one hand, not two."

- Tom Izzo

"One should not pursue goals that are easily achieved. One must develop an instinct for what one can just barely achieve through one's greatest efforts."

-Albert Einstein

# TABLE OF CONTENTS

LIST OF FIGURES	vii
Chapter 1: Type 1 Diabetes History, Complications, and C-peptide	1
1.1 Diabetes Mellitus	1
1.2 A Brief History of Diabetes Research	
1.3 Insulin Secretion and Action	3 7
1.4 Diabetes Complications	10
1.5 C-peptide	14
1.6 Effect of C-peptide on ATP Release from Red Blood Cells	17
1.7 Fluidic Device for Advanced in vitro Studies of C-peptide	19
1.8 Successful-Rodent, Failed-Human Trials of C-peptide Replacement	21
REFERENCES	25
Chapter 2: 3D-Printed Device for Equilibrium Dialysis Binding Measurements	34
2.1 Prologue	34
2.2 Introduction	35
2.3 Fabrication and Preparation Methods	39
2.3.1 Fabrication of the Dialysis Base Plate Device	39
2.3.2 Print-Pause-Print for Integrating Membranes into 3D-printed Devices	41
2.3.3 Sample Preparation	42
2.4 Experiment	43
2.4.1 Fluorescein Binding to BSA	43
2.4.2 Characterizing Incubation Time for Equilibrium Dialysis Experiments	44
2.4.3 Automated Equilibrium Dialysis Experiments	45
2.4.4 Calculations and Data Analysis	46
2.4.5 Zn <sup>2+</sup> Binding to HSA Sample Preparation	46
2.4.6 Characterization of Incubation-Time Studies for Zinc	47
2.4.7 Quantitation of <sup>65</sup> Zn <sup>2+</sup> via Liquid Scintillation Counting	47
2.4.8 Calculations and Data Analysis.	48
2.4.9 Impact of C-peptide on Zn <sup>2+</sup> Binding to HSA	48
2.4.10 Characterization of Incubation-Time Studies for C-peptide	49
2.5 Results	50
2.5.1 Direct Quantitation of Fluorescent Analyte-Ligand in an Equilibrium Dia	llysis
Device	50
2.5.2 Albumin-Free Equilibration Experiment	51
2.5.3 Fluorescein Binding to BSA Measurement	51
2.5.4 Automated Equilibrium Dialysis Technique	53
2.5.5 Zn <sup>2+</sup> Binding to HSA Equilibrium Time Measurement	54
2.5.6 Zn <sup>2+</sup> to HSA Saturation Binding Curve	55
2.5.7 Assessment of Competitive Binding by C-peptide	56

2.5.8 C-peptide Diffusion Time Studies	57
2.6 Discussion	58
REFERENCES	60
Chapter 3: Measuring C-peptide and Zinc Binding to Glycated Human Serum Albumir	ı via
3D-Printed Ultrafiltration Devices	63
3.1 Introduction	63
3.2 Methods	66
3.2.1 Membrane Preparation	66
3.2.2 Support-Free Printing for Direct Membrane Integration	66
3.2.3 Design and Fabrication of 3D-Printed Syringe Device for Ultrafiltration	67
3.2.4 3D-printed Centrifuge-Enabled Ultrafiltration Device	68
3.2.5 Sample Preparation	70
3.2.6 Syringe-Device Setup	72
3.2.7 Centrifuge Device Set Up	73
3.2.8 Sample Analysis of Zn <sup>2+</sup>	73
3.2.9 Sample Analysis for C-peptide	73
3.2.10 Calculations and Data Analysis	73
3.3 Results	75
3.3.1 Zn <sup>2+</sup> to HSA – Syringe Device	75
3.3.2 C-peptide to HSA – syringe device	77
3.3.3 C-peptide binding to HSA, with Zinc or Glucose – centrifuge device	79
3.4 Discussion	81
REFERENCES	83
Chapter 4: Analysis of Glycated Albumin and its Effect on the Interaction Between C-	
peptide, Zn <sup>2+</sup> , and Red Blood Cells	87
4.1 Introduction	87
4.2 Methods	90
4.2.1 Isolation of RBCs from Whole Blood	90
4.2.2 Isolation of HSA from Human Plasma	90
4.2.3 Electrospray Ionization-Time of Flight Mass Spectrometry	91
4.2.4 Preparation of C-peptide	92
4.2.5 Buffer Preparation	93
4.2.6 C-peptide Binding to RBCs	93
4.2.7 ATP Release	94
4.3 Results	95
4.3.1 Mass Spectrometry Analysis of Albumin Samples	95
4.3.2 C-peptide Uptake by RBCs	97
4.3.3 ATP Release from RBCs	98
4.4 Discussion	99
REFERENCES	102

Chapter 5: Conclusions and Future Directions	106
5.1 Conclusions	106
5.2 Receptor Studies	108
5.3 Future studies on in vivo glycated HSA	111
5.4 3D-printing Techniques and a Cell-Culture Permeability Device	112
REFERENCES	114

### LIST OF FIGURES

Figure 1.1 The human proinsulin molecule. Human proinsulin is comprised of the A-chain and B-chain of insulin (purple) connected by C-peptide (blue). When cleaved by specific enzymes, C-peptide is released from the A and B chains of insulin, leaving C-peptide and insulin in an equimolar ratio.

Figure 1.2 Typical fundus retina images: (a) Normal; (b) Mild non-proliferative diabetic retinopathy (NPDR); (c) Moderate NPDR; (d) Severe NPDR; (e) Prolific DR; (f) Macular edema. Borrowed from Mookiah, M. R. K.; et al. Computers in biology and medicine 2013, 43 (12), 2136-2155.

Figure 1.3 C-peptide Hype Curve: A graphical depiction of the number of research papers and meeting abstracts published between 1990 and March 2017 involving C-peptide and its role as an active biological substance. Data obtained using Thomson-Reuters Web of Science.

Figure 1.4. Cell to Cell Communication Device A. A 3D-printed fluidic device where RBCs are flowed in a channel beneath 3 transwell inserts. The device can be placed into a plate reader for direct quantitation of analytes in the transwell inserts. B. Schematic diagram of the device integrated with different cell types for inter-tissue communication studies, and a separate well for quantitation of ATP released the flowing from RBCs. C. Quantitation of NO in the third well from each channel. Channel 1 contained b-cells in the first well and endothelial cells in the third well, with a 7% solution of RBCs suspended in an albumin-containing buffer flowing underneath. Channel 2 contained the exact same set up as channel 1, except the RBCs were suspended in an albumin-free buffer. Channel 3 contained the exact same set up as channel 1, except without b-cells. Channel 4 contained the exact same set up as channel 1, except with the addition of a P2Y inhibitor to the endothelial cells. n = 5, error =SEM, \*represents values statistically different from channel 1, p < 0.01. Borrowed from Liu et al Integr. Biol. 2015, 7 (5), 534-543.

Figure 2.1 Equilibrium Dialysis. A schematic diagram of equilibrium-dialysis to measure protein-ligand binding affinity. Yellow ovals represent large proteins, and green triangles represent small lligands.

36

Figure 2.2 Diagram showing the exact dimensions of the 3D-printed device. All dimensions are in millimeters. The device is the same size and shape of a standard 96-well plate. The device is designed so that wells in the buffer and sample compartments are in the exact same location as wells in a standard 96-well plate.

40

Figure 2.3 Equilibrium Dialysis Device Left: A computer-aided design (CAD) file image of the device. Right: A picture of the final printed device with several membrane-holding inserts in place.

40

Figure 2.4 Print-Pause-Print for membrane integration. Left: A Connex 3D-printer was used to integrate membranes directly into a device. First, in A, a device containing a window was printed half-way. The printer was paused, and in B the operator laid down a porous membrane of choice over the window. In C, the printer resumes, laying polymer over the edges of the membrane to seamlessly seal it into the device. Right: CAD drawing of inserts designed to hold membranes with dimensions in millimeters.

Figure 2.5 Print-Pause-Print Flow Chart. In A, a model is drawn using Autodesk Inventor Professional CAD software. The model is saved as an .stl file and sent to the 3D-printer (B). The membrane holder is printed with multiple materials. In C, the operator places the membranes into the device halfway through the print process. Picture D shows the final product: a membrane holder with a membrane seamlessly sealed into the device. 42

Figure 2.6 A schematic diagram showing how the device is prepared for equilibrium dialysis. The wells in the black box contain 2.0  $\mu$ M fluorescein in buffer without BSA in the sample compartment, while the wells in the red box contain 2.0  $\mu$ M fluorescein in buffer with 42 mg/mL BSA in the sample compartment. The wells in the blue box contain standards. The white compartment represents a "buffer compartment", while the green compartment represents a "sample compartment." The black rectangles show where membrane-holding inserts are placed.

Figure 2.7 Plate Reader Settings A screenshot of the settings used to automate the plate-reader for automated equilibrium dialysis measurements.

45

Figure 2.8. Fluorescein Calibration Curve External standards calibration curve comparing the fluorescence intensity of fluorescein standards to their known concentrations. The standards were measured by placing the device directly in the plate reader. Error = s.d.

50

Figure 2.9 Fluorescein Binding and Equilibration Data. A: The samples contain 2.0  $\mu$ M fluorescein and no BSA. The concentration of fluorescein in the buffer-compartment of the well is monitored periodically. The concentration at 6.5 hours is not statistically different than at 9 hours (~ 1  $\mu$ M). In B, samples contain 42 mg/mL BSA and 2.0  $\mu$ M fluorescein. The concentration of fluorescein in the buffer-compartment becomes at 6.5 hours (0.16  $\pm$  0.02  $\mu$ M) is equal to that at 9 hours. n=3 \*The difference is not significant p>0.05. (error = s.d.)

Figure 2.10 Automated Fluorescein Binding. For the automated equilibrium dialysis technique, the concentration of fluorescein in the buffer-compartment at 12 hours was not statistically different than at 14 hours (0.17  $\pm$  0.01  $\mu$ M, n=3, p=0.42). (error = s.d.)

53

Figure 2.11 Zn<sup>2+</sup>-HSA Binding and Equilibration. A: Study of time needed to reach equilibrium as measured by the concentration of Zn<sup>2+</sup> in the buffer compartment becoming stable. \*values not statistically different (p=0.606).B: Saturation binding curve

created by placing seven samples containing 15  $\mu$ M HSA and varying concentrations of [Zn<sup>2+</sup>] (1-25  $\mu$ M). The samples were placed in separate wells of the device and incubated for 6 hours, (n = 3) error = std. dev. C: The mean free and bound [Zn<sup>2+</sup>] concentrations were analyzed using non-linear regression software (SigmaPlot 13.0), assuming a one-site binding model and accounting for non-specific binding, R<sup>2</sup> = 0.9985.

Figure 2.12 Investigation of C-peptide interference with  $Zn^{2+}$ -HSA binding. Results of equilibrium-dialysis study to measure the impact of C-peptide on  $Zn^{2+}$  binding to HSA. n= 3, Error = std. dev. 56

Figure 2.13 FITC-C-peptide Equilibration Time. A plot of FITC-C-peptide diffusion from the sample compartment into the buffer compartment over the course of several days by measuring the fluorescence intensity of the buffer compartment periodically. n=3 Error = std. dev.

Figure 3.1 ATP release from flowing RBCs treated with C-peptide, Zn<sup>2+</sup>, and albumin. Liu et al: Healthy RBCs were treated with different combinations C-peptide (CP), Zn<sup>2+</sup>, and albumin. The cells were then flowed through a 3D-printed device and the subsequent ATP release from the cells was quantified.

Figure 3.2 The Maillard Reaction of Protein Glycation. An open-chain molecule of glucose interacts with a terminal amine group on a protein to form a labile Schiff base. Over time, the Schiff base reconfigures into a more stable Amadori product. These glycation reactions can be followed by additional events to form irreversible advanced glycation end products (AGEs) such as carboxymethyl-lysine.

Figure 3.3 Membrane-Holding O-ring. Left: Diagram showing dimensions of the O-ring drawn in CAD software. Right: Membrane containing O-ring printed with and without support material. Note: The O-ring printed with support material is printed in TangoBlack and VeroClear, where the O-ring without support is in clear Tango+ and Veroclear. **67** 

Figure 3.4 3D-Printed Syringe-Enabled Ultrafiltration Device. A. A schematic diagram showing how all of the parts of the syringe-based device fit together. B. A photograph shows an orange-colored protein solution in the syringe which cannot pass through the membrane, and therefore a clear drop of buffer is eluted from the device 68

Figure 3.5 3D-printed Centrifuge-Enabled Ultrafiltration Device Left:. A CAD drawn schematic diagram showing the individual parts of the 3D-printed device, including both membranes. The numbers refer to the order in which each part was printed. Right: A photograph of the device ready to be used by being placed into a centrifuge tube. **69** 

Figure 3.6 Centrifuge-Device Speed and Time characterization. A graph showing the effect of different centrifuge speeds and times required to produce an ultrafiltrate sample. From

this data, an optimal centrifuge setting of 10,000g and 60 minutes was used for future studies. n=3, error = s.d. **70** 

Figure 3.7 Saturation Binding Curve between Zn2+ and HSA. A saturation binding curve was plotted from ultrafiltration data measured using Zn2+ and HSA. The data was analyzed using non-linear regression software (SigmaPlot 13.0) and the Kd and binding stoichiometry was calculated. The goodness of fit was calculated as R<sup>2</sup>= 0.9989. n=3-4. error = s.d.

Figure 3.8 Ultrafiltration data for  $Zn^{2+}$  binding to HSA with and without glucose or glycated HSA. The percentage of free  $Zn^{2+}$  in the sample containing glucose (n=5) was not statistically different than the control that contained no glucose (n=3). The glycated HSA sample (n=5) contained statistically more free- $Zn^{2+}$  \*(p<0.05) than both the control sample and the sample containing glucose., error = s.d.

Figure 3.9 Saturation binding Curve Between C-peptide and HSA and Comparison to Glycated HSA. A saturation binding curve was plotted from ultrafiltration data measured using C-peptide and nHSA. The data was analyzed using non-linear regression software (SigmaPlot 13.0) and the  $K_d$  and binding stoichiometry was calculated. The goodness of fit was calculated as R2= 0.992. n=3. error = s.d. The percentage of free C-peptide in the glycated HSA sample was not statistically different than the control

Figure 3.10 Binding between  $Zn^{2+}$  and HSA - Comparison Between Different Devices. A sample containing 10  $\mu$ M HSA and 5  $\mu$ M  $Zn^{2+}$  was made and the free  $Zn^{2+}$  in the sample was analyzed by measuring the  $Zn^{2+}$  in the ultrafiltrate using both the centrifuge-enabled device as well as the syringe-enabled device. There is no statistical difference in the results obtained from using either device.

Figure 3.11 Ultrafiltration Data Analyzing the Impact of Glucose,  $Zn^{2+}$ , and HSA-Glycation on the binding of C-peptide to HSA. Ultrafiltration was performed on samples containing C-peptide and HSA and the concentration of C-peptide in the ultrafiltrate was analyzed by ELISA. Neither the addition of glucose (p=0.14) or  $Zn^{2+}$  (p=0.21) affected the amount of C-peptide bound to HSA. The substitution of glycated human serum albumin for normal human serum albumin did not affect the binding of C-peptide (p=0.2). n=4 error = s.d. **80** 

Figure 3.12 Model of the high-affinity Zn<sup>2+</sup> binding site on HSA based on X-ray crystal structure. HSA is composed of three homologous domains. The primary Zn<sup>2+</sup> binding site is at the interface of domains I (orange) and II (blue). and is composed of two amino acids from domain I (His67 and Asn99), two amino acids from domain II (His247 and Asp249). This figure is borrowed from Lu *et al*.

Figure 4.1 Mass Spectra of Human Serum Albumin Samples. Time-of-flight mass spectra used to analyze the relative extent of glycation of four different human serum albumin samples. G=glycation (+162). C=cysteinylation (+119). SA = sulfinic acid (SO2H) (+31),

K=potassium. A: Purchased human serum albumin from Sigma, approximately 23% glycated. B: Purchased glycated human serum albumin from Sigma, approximately 67% glycated. C: Albumin isolated from plasma from a non-diabetic donor, approximately 15% glycated. D: Albumin isolated from plasma from a subject with Type-1 diabetes, approximately 41% glycated.

Figure 4.2 Uptake of C-peptide by 7% RBCs. The amount of C-peptide bound to RBCs in the presence of normal and glycated HSA. The RBCs in the sample containing nHSA bound 1.4  $\pm 0.1$  picomoles of C-peptide, while the samples containing gHSA bound 0.8  $\pm$  0.1 picomoles. p<0.05. n=3 blood draws, error = std error of the mean.

Figure 4.3 ATP release from RBCs treated with C-peptide,  $Zn^{2+}$ , and different forms of HSA. The ATP released from RBCs treated with C-peptide/ $Zn^{2+}$  and nHSA was higher than in the control sample which contained 7% RBCs and no C-peptide/ $Zn^{2+}$ . The ATP in the sample containing C-peptide/ $Zn^{2+}$ /gHSA was not statistically different than the control sample (p=0.48). n=4 blood draws. \*asterisks denote p<0.05. error = std. error of the mean **98** 

Figure 5.1 A schematic representation of the albumin-ligand complex receptor model proposed by Ockner.23 The diagram indicates that uptake of ligand (L) can happen by the specific interaction of the albumin-ligand complex with its putative receptor (predominant pathway), or result from direct uptake of unbound (free) ligand (conventional model, minor pathway).

Figure 5.2 An illustration of the principle of cell permeability assays. The blue triangles represent a drug or small molecule of interest

### <u>Chapter 1: Type 1 Diabetes History, Complications, and C-peptide</u>

### 1.1 Diabetes Mellitus

Diabetes mellitus (diabetes) is a disease characterized as a global epidemic by the World Health Organization. In 2017, it was approximated that 30.2 million adults in the United States and 424.9 million adults worldwide had diabetes. Scientists predict the number of adults with diabetes to increase to 35.6 million in the United States and 629 million worldwide by 2045. The global prevalence of the disease is up from 4.7% in 1980, to 8.5% of the total population in 2014. The estimated healthcare expenditure on diabetes has significantly increased from 232 billion dollars globally (USD) in 2007 to 727 billion dollars (USD) in 2017. The enormity of this epidemic has spurred researchers to invest their time and resources to study the disease and potential therapies for its associated complications.

Diabetes refers to a set of diseases distinguished by abnormally high glucose concentration in the bloodstream, caused by a variety of metabolic conditions. Accounts of diabetes date back several thousands of years, with Egyptian manuscripts from approximately 1500 B.C. as well as ancient Hindu writings describing a morbid and fatal disease highlighted by intense thirst, excessive urination, sweet urine, and deterioration of the body (extreme weight loss, and loss of hair and teeth); all of which are known today as markers of diabetes.<sup>3</sup> Between 500 and 600 AD, Indian physicians were first to characterize two different types of diabetes, one associated with youth and another associated with obesity.<sup>4</sup> These types of diabetes are what we now refer to as Type 1 (T1D) and Type 2 (T2D) diabetes, respectively. Though several other less-common types of diabetes exist, with similar complications, the focus of the research in this dissertation is T1D.

T1D is characterized as an autoimmune disease in which the patient's own immune system attacks certain cells in the pancreas that create the hormone needed to metabolize glucose, insulin. Without insulin, the body cannot convert the nutrients found in food into energy. Therefore, food and nutrients simply "pass through" the patient, as first described by the ancient Greeks (130-200 BC) who coined the name of the disease *diabetes*, or "to pass through." <sup>3-4</sup> This inability to metabolize nutrients in food results in uncontrollably high levels of glucose in the urine and bloodstream, as well as rapid deterioration of the patient's body. T2D is the most common type of diabetes and usually occurs in obese patients and is characterized by the body's inability to utilize insulin, as cells become "resistant" to its effects. In T2D, high glucose levels in the bloodstream cause the cells in the pancreas to over-produce insulin, and over time, the pancreatic cells cannot keep up with the high demand, causing glucose levels to increase uncontrollably. <sup>5</sup>

Today, both T1D and T2D are treated with insulin therapy as well as diet and exercise, with T2D patients also sometimes taking drugs such as sulfonylureas or metformin to help reduce complications. Despite therapies, both types of diabetes result in debilitating complications (many of which are believed to be related to the microvasculature), such as blindness, kidney failure, and nerve damage. The following section provides a brief history of research into diabetic therapies. leading up to current research and theories on diabetic microvascular complications.

### 1.2 A Brief History of Diabetes Research

In the 1800s the average life expectancy of a person with T1D was estimated to be 1.4 - 4.1 years after diagnosis. The main method of "treating" T1D was through severe caloric restriction, thus many many people with T1D not only died from starvation, due to the inability to utilize glucose, but also from severe infections and weakened immune systems causing them to be extremely vulnerable to pneumonia and tuberculosis. This problem led researchers worldwide to work fervently on therapies and cures for diabetes, including extreme fad diets and drugs, such as morphine. 10-12 One such therapy was made popular by French physician Pierre Priory in the late 1850s, who insisted that dramatically increasing the amount of raw glucose in the diet of diabetics would compensate for the glucose lost in the urine. 13 This therapy was later learned to cause more damage than good, as was proved by another French physician in the 1870s, Bouchardat, who noticed improvements in the conditions of his patients under opposite conditions, when he forced them to fast periodically and exercise vigorously.<sup>4, 13-14</sup> Later, in 1902, a German scientist, von Noorden announced his breakthrough cure of diabetes: the oatmeal diet.<sup>13, 15</sup> Von Noorden proclaimed that a steady diet of oatmeal alone reduced the amount of glucose in the urine of diabetics and therefore cured diabetes. In 1919, Frederick Madison Allen, an American physician, published his work "Total Dietary Regulation in The Treatment of Diabetes" and in 1921 opened the world's first clinic specifically for sufferers of diabetes mellitus, where he enforced strict low-carbohydrate diets of less than 400 calories per day. 10, 16 Dietaryrestricting therapies proved to prolong the life-span of diabetics to a mild degree and improve some health complications, but still resulted in death by starvation and undernourishment within a few years.9

In 1788, while performing an autopsy of a diabetic patient, Thomas Cawley made the discovery that the patient had a damaged pancreas.<sup>17</sup> It was confirmed by many throughout the mid-19<sup>th</sup> century that there was a strong correlation between the presence of diabetes and a damaged pancreas upon autopsy. This information was not very useful at the time, however, as the function of the pancreas was not understood. It was not until 1889 when, in an attempt to understand the pancreas' role in digestion, Oskar Minkowski and Joseph von Mering, at the University of Strasbourg, carefully removed the pancreas of a living dog and observed uncontrollable urination by the dog, as well as high glucose concentrations in the urine, the exact symptoms of diabetes.<sup>18</sup> Minkowski's discovery led researchers to the conclusion that removal or destruction of the pancreas was the cause of diabetes, and led many to hypothesize that readministering extracts of the pancreas may provide a treatment for diabetes.

Between 1889 and 1922, it is estimated that over 400 different researchers unsuccessfully attempted to re-administer pancreatic extracts to diabetic animals or patients, leading researchers to complain that the literature on the topic was exhaustively voluminous and filled with contradictory results. 19-21 Attempts to simply feed diabetics excised pancreas were almost always followed by negative results, including vomiting and sickness. This was extensively studied by the previously mentioned Frederick Allen, who claimed that pancreatic extracts had no clinical value. 16, 22 In 1901, Eugene L. Opie discovered that the damage to the pancreas in people with T1D was specific to a group of cells within the pancreas, the islets of Langerhans. 23 The islets of Langerhans were first identified in 1869 by a medical student in Berlin, Paul Langerhans, but their function was unknown at the time of discovery. 24 In 1907 the information from Opie led Scottish researchers Rennie and Fraser to feed four diabetic patients the islets of Langerhans of fish that

they isolated and boiled, however, this showed no improvement.<sup>22</sup> Rennie and Fraser also attempted to inject an aqueous extract of the islets intravenously into a fifth patient, and this appeared to be toxic and unhelpful.<sup>22</sup>

In 1906, Zuelzer started treating terminal patients with a unique formulation of pancreatic extracts obtained by alcohol extraction, followed by drying and subsequent dissolution in saline.<sup>19, 25</sup> Upon venous administration, the extract proved to abolish the characteristic trademarks of diabetes (glucose in the urine and hyperglycemia) in six different cases. However, the admistration of Zuelzer's extract was also always accompanied by nausea, severe fever, chills, and vomiting, leading researchers to believe it may do more harm than good.<sup>25</sup> Unfortunately, Zuelzer was forced to halt his research to go fight in World War I.<sup>19</sup>

In late 1920, another World War I physician, a London surgeon named Frederick Banting, was studying carbohydrate metabolism when he learned about the relationship between the islets of Langerhans and diabetes from an article printed in *Surgery, Gynecology, Obstetrics*. <sup>26</sup> Banting quickly hypothesized that the islets of Langerhans secreted the requisite hormone missing in T1D, but that the hormone would be destroyed in typical preparations by the powerful digestive enzymes secreted externally by the pancreas. <sup>26</sup> Banting hypothesized that the internal secretions from the islets of Langerhans within the pancreas could be isolated and re-administered to diabetics. Banting moved to the University of Toronto to conduct this research alongside research assistant Charles Best, and in 1922 successfully reported three different methods for isolating the potent extracts of the islets of Langerhans from the destructive enzyme-juices of the pancreas, the final method being an alcohol extraction similar to that created by Zuelzer. <sup>18</sup> Banting and Best administered their extract, named insulin, to a de-pancreatized dog every day and observed that

the dog was able to live healthily for more than 70 days (at which point it was euthanized), compared to a de-pancreatized dog without insulin would die after a maximum of 14 days. <sup>18</sup> The dog's blood and urine glucose levels always decreased after insulin administration to that of the control animal. <sup>18</sup> When incubating the isolated insulin with the secretions of the rest of the pancreas, the scientists observed complete destruction of the activity of insulin, thereby proving Banting's hypothesis that the extract of the islets must be separated from the digestive enzymes secreted externally by the pancreas. <sup>18</sup> By experimenting on rabbits, the researchers learned that administering too high of a concentration of insulin at once would cause extreme hypoglycemia (low-blood glucose), which caused seizures, convulsions, fevers, and other negative side-effects, similar to those observed in humans by Zuelzer. <sup>27-28</sup> The researchers learned through experimentation that the specific chemical preparation and purification of insulin was the key to its activity. Their superior experimental methodology in creating this preparation resulted in success on a project that 33 years of prior attempts had failed.

In less than one year, Banting and Best had discovered how to successfully isolate and dose insulin and began treating human subjects.<sup>29</sup> They successfully treated their first human T1D subject at the Toronto General Hospital in 1921, a 65-pound 14-year old boy with chronic fatigue whose teeth and hair were falling out, and saw him gain weight, strength, and achieve good health with daily insulin injections.<sup>18, 29</sup> The researchers at the University of Toronto began successfully treating more subjects as the world rapidly heard of their success, and were awarded the Nobel Prize in medicine in 1923 for their discovery of insulin. The pharmaceutical company Eli Lilly quickly began large-scale production of bovine insulin so that it could be available to the masses.<sup>19</sup>

The American Diabetes Association approximates that 7.4 million Americans are currently being treated with insulin, however, human insulin is now mass-produced by genetically engineered E. Coli bacteria.<sup>2</sup> The discovery of insulin in Toronto in 1922 is responsible for saving countless lives worldwide. The following section will discuss its biosynthesis and method of action.

### 1.3 Insulin Secretion and Action

Insulin is produced within a sub-type of cells housed within the islets of Langerhans in the pancreas, specifically, the  $\beta$ -cells. Within the  $\beta$ -cells, insulin is first formed by the ribosomes as preproinsulin, a 110 amino acid peptide.<sup>30</sup> As insulin crosses the rough endoplasmic reticulum, the signal sequence is cleaved to create the proinsulin molecule (Figure 1.1).<sup>31</sup>

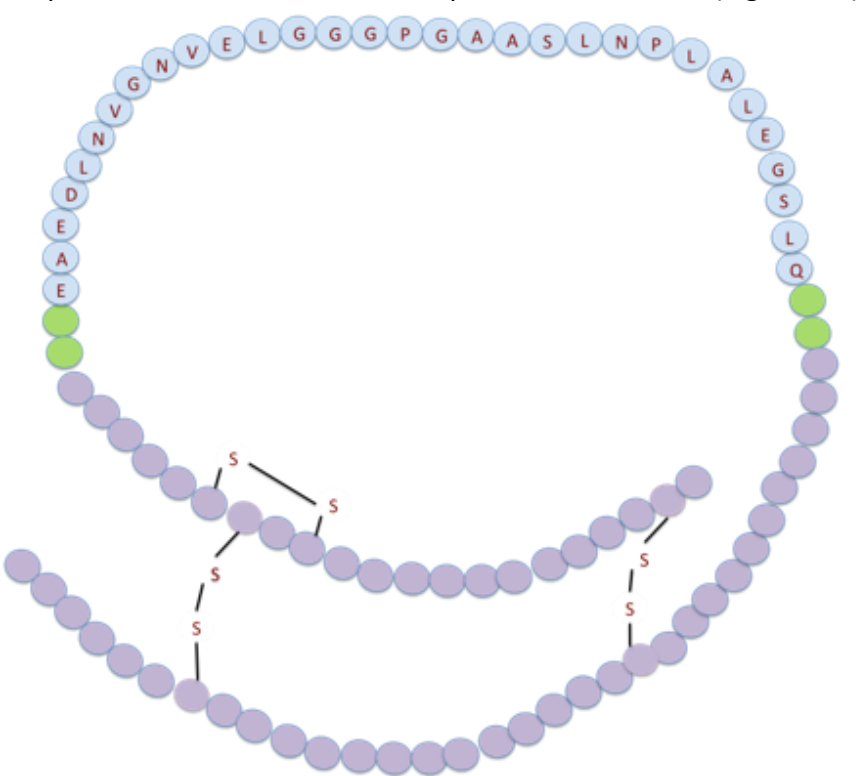


Figure 1.1 **The human proinsulin molecule**. Human proinsulin is comprised of the A-chain and B-chain of insulin (purple) connected by C-peptide (blue). When cleaved by specific enzymes, C-peptide is released from the A and B chains of insulin, leaving C-peptide and insulin in an equimolar ratio.

Proinsulin is made of the A and B chains of insulin, which are connected by C-peptide. <sup>32</sup> Proinsulin is folded into its native structure by three disulfide bridges in the endoplasmic reticulum, and is then transported to the Golgi apparatus, where it is packaged into secretory vesicles. <sup>31</sup> The vesicle membrane contains ATP dependent proton pumps, which regulate the internal pH of the vesicle. <sup>33</sup> At first, the proinsulin molecules are in a hexamer formation, but as the vesicles mature, the pH of the vesicle decreases to approximately 5.5, enabling pH dependent endopeptidases and carboxypeptidases to cleave C-peptide free from insulin, leaving the insulin in a hexamer formation that is held together by two zinc ions per hexamer. <sup>34-35</sup> Notably, zinc concentrations in the β-cells are amongst the highest in the body (~20 millimolar). Zinc enters the vesicle by the Zn-T8 transporter on the vesicle membrane. When blood-glucose levels increase after eating, the vesicle docks at the plasma membrane of the cell, the pH of the granules rapidly increases from 5.5 to 7.4 as the vesicle evacuates its contents out of the β-cells. The pH change causes the insulin hexamers to breakup into biologically active monomers. Insulin and C-peptide are released from the β-cells in an equimolar ratio along with a large amount of zinc. <sup>30</sup>

To secrete insulin from the  $\beta$ -cells, glucose first enters the pancreatic  $\beta$ -cells through the GLUT-2 transporter when levels of glucose rise from eating. The glucose is then phosphorylated and subjected to glycolysis, producing ATP in the cytosol. The increase in the ATP/ADP ratio results in ATP sensitive potassium channels (KATP channels) to close, causing an accumulation of intracellular potassium ions and membrane polarization.<sup>30</sup> The membrane polarization opens voltage-dependent calcium channels, allowing an influx of Ca<sup>2+</sup> ions into the cell via facilitated diffusion.<sup>30, 36</sup> The surge of Ca<sup>2+</sup> ions into the cell causes the secretory vesicles to fuse to the plasma membrane and exocytose C-peptide and insulin to enter the bloodstream in an equimolar

ratio. <sup>36</sup> Upon exocytosis, insulin interacts with fat and muscle cells, resulting in glucose uptake via facilitated diffusion and a decrease in blood-glucose levels. Until recently, it was believed that C-peptide was not biologically active in the bloodstream.<sup>37</sup>

Insulin increases cellular uptake of glucose by binding to an insulin receptor on the cell surface. The insulin receptor is a large transmembrane protein that functions as a tyrosine kinase receptor. The insulin receptor, insulin causes the autophosphorylation of tyrosine residues on subunits of the receptor. This addition of phosphate groups creates a binding site for insulin receptor substrate (IRS-1), which is then activated by phosphorylation, allowing it to bind to phosphoinositide 3-kinase (PI3K). Phosphoinositide 3-kinase adds a phosphate group to phosphatidylinositol 4,5-bisphosphate, converting it to phosphatidylinositol 3,4,5-triphosphate, or (PIP3), a secondary messenger, activating other kinases including protein kinase B (or Akt). Activation of Akt results in translocation of a glucose transporter (GLUT4) to the plasma membrane of the cell. 38-39 Therefore, by binding to certain cells, insulin is able to stimulate GLUT4 translocation to the cell surface, subsequently allowing glucose molecules to be transported into the cell, where they can be used for glycolysis and cellular respiration. 38 This process allows the cells to remove glucose from the bloodstream in order to use it for cellular processes.

Besides regulating glucose-metabolism, insulin is shown to have several other functions, such as regulation of lipid metabolism, uptake of triglycerides into muscle cells, increasing protein synthesis and decreasing protein degradation in muscle cells, and increasing fatty acid synthesis.  $^{40-42}$  In T1D, the pancreatic  $\beta$ -cells are destroyed, resulting in an insulin deficiency and thus uncontrolled glucose levels in the bloodstream. In order to survive, T1D patients administer themselves with insulin. However, even with insulin therapy along with diet and exercise, T1D

patients still experience many severe debilitating conditions. The following section will discuss research focused on T1D complications.

# 1.4 Diabetes Complications

The positive impact of exogenous insulin administration to T1D patients is undeniable, and along with proper diet and exercise, T1D patients can now lead normal, healthy lives. In fact, the combination of insulin administration along with proper diet and exercise has resulted in the difference in life expectancy between T1D patients and age-matched non-diabetics to be approximately 13 years in 2015, down from 27 years as reported in 1975. This is likely due to improvements in insulin dosing along with an increasingly better understanding of glucose management. However, despite improvements in life expectancy, T1D patients still suffer from severe, debilitating microvascular complications such as blindness, nerve damage, and kidney failure. Advanced to the complex of the compl

According to large-scale, long-term epidemiological studies in the United States, diabetic retinopathy, a condition that causes impaired vision, occurs in 97% of T1D patients that have been diagnosed with T1D for more than 25 years. <sup>45-46</sup> A more severe form of the condition known as proliferative diabetic retinopathy was shown to occur in 42%-53% of T1D patients 25 years after diagnosis. <sup>46</sup> Diabetic retinopathy and proliferative diabetic retinopathy are diagnosed by a physician observing images of the retina, taken by fundus photography, and looking for abnormalities such as retinal hemorrhages, vessel exudates, microaneurysms,

neovascularization, vitreous hemorrhages, and macular edema (retinal swelling), as seen in Figure 1.2.<sup>47-48</sup>

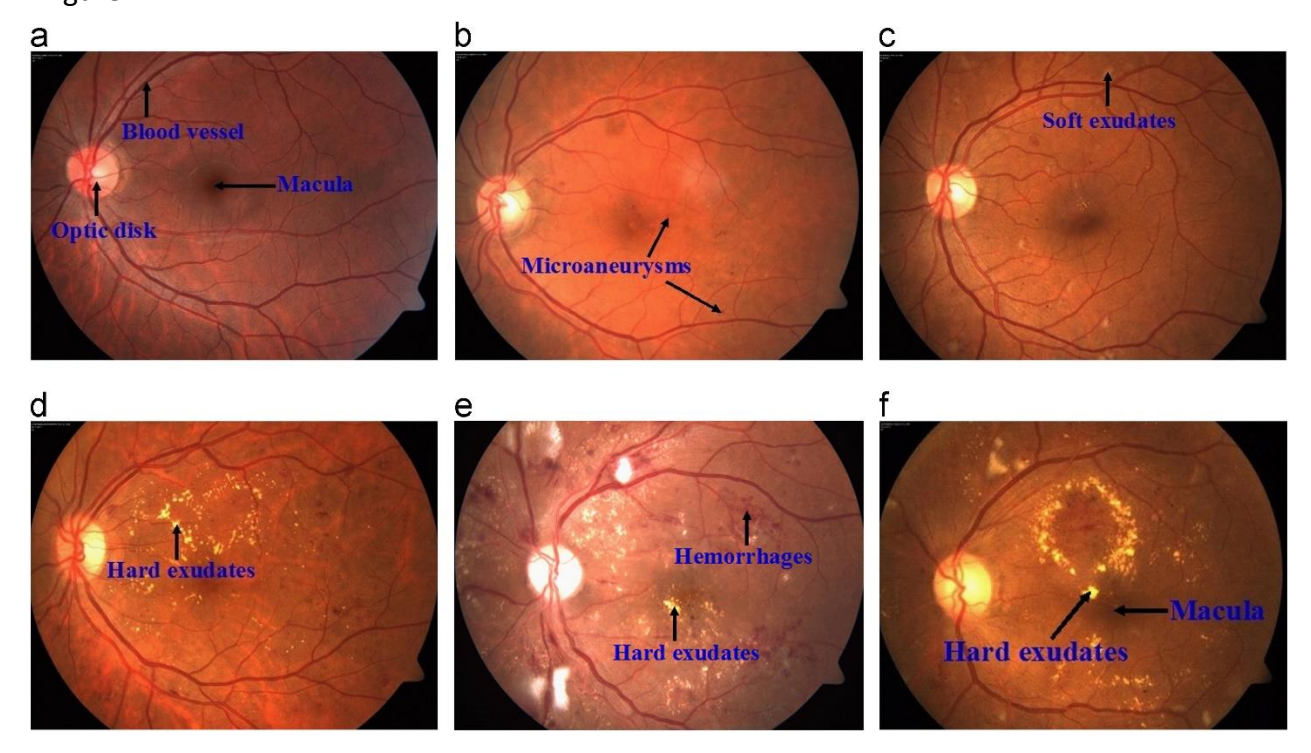


Figure 1.2 Typical fundus retina images: (a) Normal; (b) Mild non-proliferative diabetic retinopathy (NPDR); (c) Moderate NPDR; (d) Severe NPDR; (e) Prolific DR; (f) Macular edema. Borrowed from Mookiah, M. R. K.; *et al.* Computers in biology and medicine **2013**, 43 (12), 2136-2155.

Retinopathy is also detected by fluorescein angiopathy, which is considered the gold standard for studying the retinal vasculature.<sup>49-50</sup> In this procedure, the fluorescent molecule sodium fluorescein is injected intravenously before fluorescent images are taken of the eye. Sodium fluorescein is approximately 80% protein-bound in the bloodstream, allowing the 20% that is unbound to leak out of damaged blood vessels, thereby showing the breakdown of the bloodretinal barrier.<sup>50-51</sup>

Microaneurysms, the thickening of the basement membrane, and loss of pericytes all contribute to blindness in diabetic retinopathy.<sup>52</sup> The damage to the blood vessels may occur from increased polyol pathway flux, thus leading to increased sorbitol levels in the cells and

osmotic stress.<sup>53</sup> High levels of glucose might also cause oxidative stress to the cells, and advanced glycation end products (AGEs) are hypothesized to damage blood vessels.<sup>54</sup> Vascular Endothelial Growth Factor (VEGF) is responsible for forming new weak vessels in the retina, causing clouding of the vitreous and vision damage. VEGF-suppressants are commonly prescribed for diabetic retinopathy patients.<sup>55-56</sup>

Diabetics are observed to have poorly regulated blood flow in the microvasculature, which can cause hypoxia to certain tissues, as the red blood cells (RBCs) in the bloodstream which deliver oxygen are not able to efficiently travel through the vessels. 7-8, 57-58 Diabetic RBCs have been measured to be less deformable than RBCs from non-diabetics, which may impede blood flow in the microvasculature, where RBCs (5-8 micrometer) are larger in diameter than the blood vessels (<5 micrometer) through which they travel. 59-60 Under these conditions, the RBCs need to distort their shape in order to pass through the vessel to deliver oxygen to the tissues. Diabetic RBCs may cause hypoxia in the retina by being less deformable than healthy RBCs, thus limiting their ability to deliver oxygen to tissues. 61 Hypoxia is a stimulus of VEGF, which signals the formation of new blood vessels (neovascularization), which is a characteristic of proliferative retinopathy. 62

Diabetic nephropathy, or kidney disease, is the leading cause of kidney failure in the United States, responsible for >40% of the cases of end stage renal disease (ESRD).<sup>63</sup> Approximately 25% of T1D patients will develop overt diabetic nephropathy, which is diagnosed when the kidneys begin to fail by allowing >300 milligrams of albumin from the bloodstream into the urine in a 24-hour period.<sup>64</sup> The main function of the kidneys is to filter waste from the blood and direct it to be urinated out. The kidney is made of millions of nephrons and each nephron consists of a tiny

blood vessel called a glomeruli and a tubule. The glomeruli filter waste out of the blood, and the tubule carries away the waste to be excreted. Hypoxia and neovascularization in the nephron is hypothesized to cause damage to the glomeruli and be a major cause of progression of diabetic nephropathy.<sup>65</sup>

Approximately 7% of T1D patients develop nerve damage, or diabetic neuropathy, within one year after diagnosis, and 50% of T1D patients experience neuropathy at 25 years from diagnosis. <sup>66</sup> The Diabetes Control and Complications Trial (DCCT) studied T1D complications over a long period of time in 1,441 T1D patients. <sup>67</sup> The DCCT monitored two groups of T1D patients, one whose average blood glucose levels were intensively controlled by administering insulin 3-or-more times per day or undergoing continuous subcutaneous insulin infusion with the intent of maintaining glucose levels to that of healthy controls, and another group that underwent conventional therapy of one or two daily insulin injections. The average glucose levels were measured by hemoglobin A1c levels. Hemoglobin A1c measurements provide an average blood glucose level over the duration of 3 months. The intensively controlled group had an average A1c level of 7.2%, compared to 9.1% in the conventional therapy group (a healthy A1c level is approximately <5.7%). The DCCT found that a 5-year therapy consisting of intensive glucose control and regular insulin administration was able to reduce the risk of developing diabetic neuropathy by 60% when the patients did not have confirmed clinical neuropathy at baseline. <sup>67</sup>

Interestingly, the DCCT found an incidence of neuropathy of 15-21% after 5-years of intensive glucose control, and 40-52% of the intensively controlled group reported abnormal nerve conduction.<sup>68</sup> The results of the DCCT show that a therapy of regulating blood glucose by insulin and diet alone, though effective at reducing complications, does not abolish the chance of

developing neuropathy or nerve damage. Paired with this information, a retrospective study of the DCCT found a significant correlation between T1D patients who had residual  $\beta$ -cell activity, as measured by levels of C-peptide in the bloodstream, and reduced complications, in both the conventional and intensively controlled groups. <sup>69</sup> In fact, statistical analysis of the patient data showed a strong linear relationship between risk of retinopathy and log(C-peptide) concentrations in the bloodstream. <sup>69</sup> This information provides convincing evidence that administering insulin alone, along with diet and exercise, is not sufficient for preventing diabetic microvascular complications. Therefore, some hypothesize that administering other molecules normally secreted from the pancreatic  $\beta$ -cells, such as C-peptide, along with insulin may be necessary for treating T1D. <sup>70-72</sup>

# 1.5 C-peptide

In 1967, Steiner reported in *Science* the discovery of the C-peptide molecule, the 31-amino acid peptide chain in the proinsulin molecule that helps insulin fold into its native form. <sup>32</sup> As mentioned earlier, C-peptide is co-secreted in equimolar amounts with insulin from the pancreatic  $\beta$ -cells. Twenty years of research following its discovery suggested C-peptide had no biological activity after secretion from the  $\beta$ -cells. <sup>73</sup> However, due to C-peptide's ~30 minute half-life in the bloodstream, it was found that its quantitative assessment by enzyme-linked immunosorbent assay (ELISA) was a very powerful biomarker for  $\beta$ -cells activity, compared to insulin and its 4-minute half-life. <sup>74</sup>

In the late 1980s, it was reported that T1D patients with some lingering  $\beta$ -cell activity (as measured by plasma C-peptide levels) experienced fewer complications than T1D patients with no C-peptide in their bloodstream.<sup>75</sup> This important discovery inspired a surge of C-peptide research publications between 1990 and 2001 (Figure 1.3), when 136 peer-reviewed research articles were published concerning the therapeutic potential and bioactive capabilities of C-peptide.

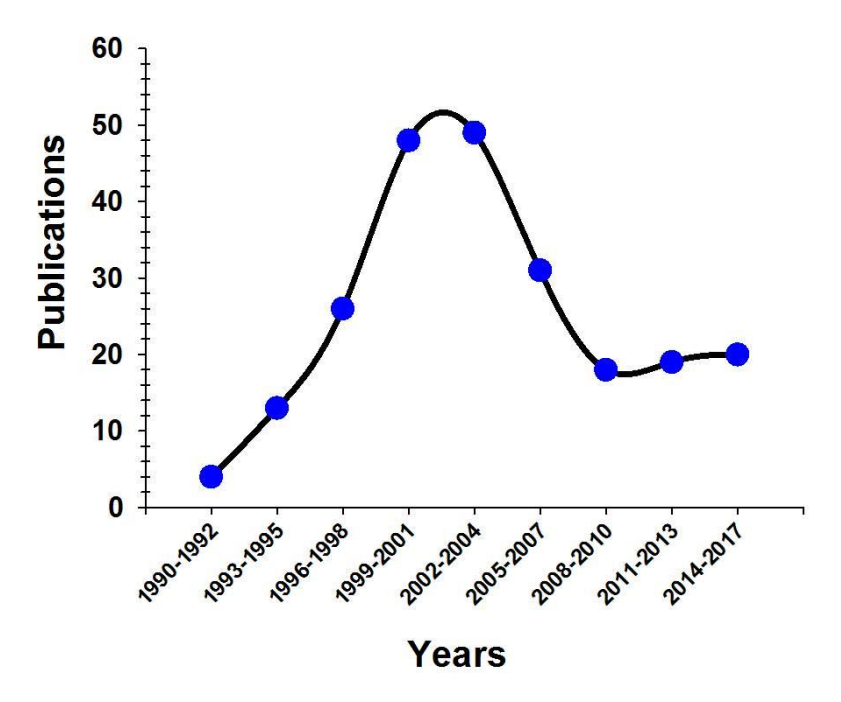


Figure 1.3 **C-peptide Hype Curve**: A graphical depiction of the number of research papers and meeting abstracts published between 1990 and March 2017 involving C-peptide and its role as an active biological substance. This data was obtained using Thomson-Reuters Web of Science.

Among the papers published in the early 1990s was a report of C-peptide being intravenously infused into exercising T1D patients, followed by measurement of blood flow as compared to controls (healthy and T1D patients infused with saline). A 27  $\pm$  4% improvement in blood flow and a 52  $\pm$  9% improvement in capillary diffusion capacity was measured by an indicator diffusion technique. The results of the study were seminal, as the authors concluded that C-peptide

infusion restored blood flow and capillary diffusion capacity to levels similar to healthy subjects. The authors hypothesized that C-peptide may play a key role in microvascular function, therefore suggesting that microvascular complications measured in T1D patients may be caused by a lack of C-peptide in their bloodstream. The same authors also demonstrated that C-peptide acts to improve renal function by reducing glomerular hyperfiltration and excessive albumin urinary excretion while improving A1c levels.<sup>77-78</sup>

Following these findings, German scientists Forst et al performed similar experiments and found that C-peptide improved blood flow in the skin of T1D patients.<sup>79</sup> In seeking an etiology of how the blood flow was improved, the scientists studied the impact of C-peptide on the deformability of RBCs. It was found that RBCs from T1D patients were less deformable than those from healthy subjects, and that incubating RBCs with nanomolar levels of C-peptide (in a phosphate buffer containing 0.2% bovine serum albumin) improved the deformability of T1D RBCs to values approaching those of healthy subjects. 80 No improvement in deformability of RBCs from healthy subjects was measured when subjected to C-peptide. Furthermore, the researchers experimented with adding different fragments of C-peptide to RBCs, and found that the Cterminus fragment, including the glutamic acid residue at position 27, must be present for bioactivity of the peptide. 60, 81 It was also reported that the T1D cells incubated with C-peptide displayed increased Na-K-ATPase activity, and they hypothesize this activity to be responsible for downstream effects resulting in the improved deformability of the cells.<sup>82</sup> Additional experiments showed abolished effects of C-peptide on T1D RBCs when the cells were co-incubated with EDTA, leading to their hypothesis that EDTA was binding intracellular Ca2+ reserves required for stimulation of Na-K-ATPase. 60 However, EDTA is a charged molecule at physiological pH,

therefore it is unlikely that it would be able to cross the cell-membrane to bind the intracellular Ca<sup>2+</sup>.

# 1.6 Effect of C-peptide on ATP Release from Red Blood Cells

In 2006, the Spence group reported that RBCs obtained from people with T2D secrete less than half as much adenosine triphosphate (ATP) as healthy controls when the cells were subjected to flow induced deformation through microbore tubing with interior diameters similar to microcirculation vessels (~50 micron diameter).<sup>83</sup> This was an important finding, as RBC-derived ATP is an indirect regulator of vascular resistance in the microcirculation because it stimulates the vessel dilator nitric oxide (NO) synthesis in endothelial cells.<sup>84-86</sup> Sprague, *et al.* have shown that infusing ATP at a minimum concentration of 300 nanomolar into an isolated rabbit lung decreased vascular resistance.<sup>87</sup> However, infusing 10 and 100 nanomolar ATP did not alter the vascular resistance, leading to the conclusion that nanomolar differences in available extracellular ATP in the microcirculation can result in significant physiological effects *in vivo*. In accordance, our group hypothesized that decreased ATP release from RBCs obtained from people with diabetes may contribute to microvascular complications in diabetes, as these complications are hypothesized to be derived from problematic microvascular blood flow.<sup>83</sup>

Based on the work of Forst *et al*, Spence hypothesized that the addition of C-peptide would also normalize ATP release from RBCs obtained from diabetic patients.<sup>60, 79-80, 82</sup> Initial experiments conducted by adding C-peptide to RBCs and measuring the resultant ATP release were successful, but not always reproducible.<sup>71</sup> It was discovered that after purifying C-peptide by high performance liquid chromatography (HPLC), its addition to RBCs yielded no increase in

ATP release from RBCs. <sup>88</sup> Mass spectrometric analysis found that when purchased commercially, the C-peptide is often contaminated by a transition-metal adduct, which can be removed by HPLC. ATP release from RBCs is increased upon incubation with C-peptide, but only when the C-peptide is first prepared with a transition metal. <sup>89</sup> As stated earlier, in the secretory vesicles of the pancreatic  $\beta$ -cells, C-peptide is in solution with high concentrations of Zn<sup>2+</sup>. Ensuing experiments suggested that combining C-peptide with Zn<sup>2+</sup> yields reproducible increases in ATP release from RBCs. <sup>34, 89-91</sup> By treating diabetic RBCs with a combination of C-peptide/Zn<sup>2+</sup>, deformation induced ATP release was normalized to that of controls. <sup>89</sup>

In all of the aforementioned ATP release experiments, the RBC samples were prepared in a physiological salt solution buffer (PSS) containing either 0.25, 0.5, or 5.0% bovine serum albumin. Later experiments showed that when the buffer was void of albumin, the addition of C-peptide and Zn<sup>2+</sup> to RBCs did not result in an increase in ATP release from the cells. <sup>92</sup> An investigation of binding by isothermal titration calorimetry (ITC) revealed that human serum albumin is capable of binding C-peptide and Zn<sup>2+</sup> with moderate and high affinities ( $K_a = 2.66 \pm 0.25 \times 10^5 \, M^{-1}$ ,  $K_a = 5.08 \pm 0.98 \times 10^7 \, M^{-1}$ , respectively). <sup>92</sup> The ITC results revealed that the binding of C-peptide to albumin is abolished when the glutamic acid residue at position 27 is replaced with an alanine. The binding of C-peptide to RBCs in the presence and absence of albumin was analyzed by combining C-peptide with RBCs in buffer, incubating the solution for 2 hours, then centrifuging and measuring the amount of C-peptide left in the supernatant by enzyme-linked immunosorbent assay (ELISA), a useful measurement technique for quantifying specific analytes. The resulting saturation-binding curve showed saturation at approximately 1800 molecules of C-peptide per cell, <sup>92</sup> but only when albumin is present in the buffer. Therefore, the interaction of

C-peptide with RBCs is dependent on the presence of albumin, a known carrier protein found in high concentrations in the bloodstream. <sup>93</sup>This important discovery may explain why a receptor for C-peptide has yet to be confirmed.

# 1.7 Fluidic Device for Advanced in vitro Studies of C-peptide

To further investigate the effect of  $\beta$ -cell secretions on the bloodstream, a 3D-printed device was created for studying the cell-to-cell communication between a pancreatic  $\beta$ -cell mimic (INS-1 cells), flowing RBCs, and endothelial cells (bovine pulmonary aortic endothelial cells). The device, seen in Figure 1.4, was the same size and shape as a standard 96-well plate, allowing it to be placed into a plate reader for direct analyte quantitation. It also incorporated a channel for

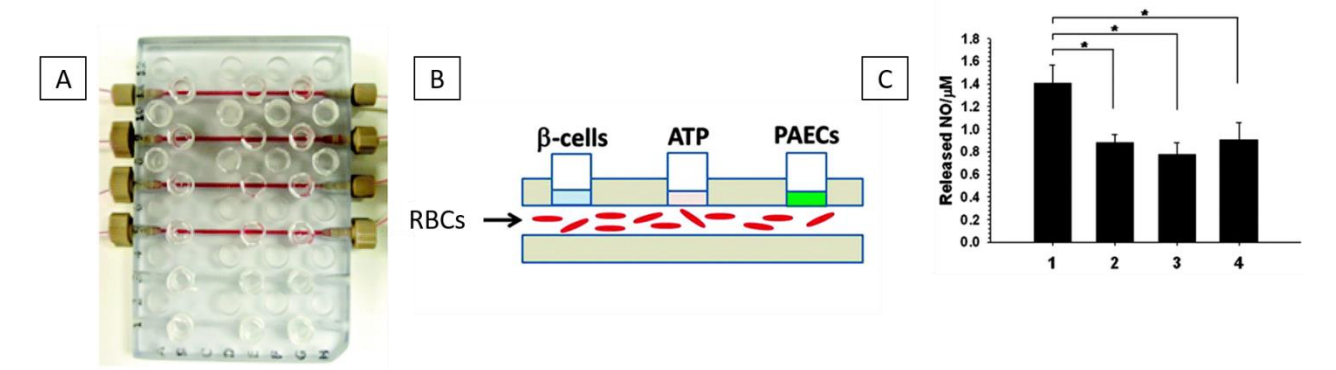


Figure 1.4. **Cell to Cell Communication Device A**. A 3D-printed fluidic device where RBCs are flowed in a channel beneath 3 transwell inserts. The device can be placed into a plate reader for direct quantitation of analytes in the transwell inserts. **B**. Schematic diagram of the device integrated with different cell types for inter-tissue communication studies, and a separate well for quantitation of ATP released the flowing from RBCs. **C**. Quantitation of NO in the third well from each channel. Channel 1 contained  $\beta$ -cells in the first well and endothelial cells in the third well, with a 7% solution of RBCs suspended in an albumin-containing buffer flowing underneath. Channel 2 contained the exact same set up as channel 1, except the RBCs were suspended in an albumin-free buffer. Channel 3 contained the exact same set up as channel 1, except without  $\beta$ -cells. Channel 4 contained the exact same set up as channel 1, except with the addition of a P2Y inhibitor to the endothelial cells. n = 5, error =SEM, \*represents values statistically different from channel 1, p < 0.01. Borrowed from Liu *et al* Integr. Biol. **2015**, 7 (5), 534-543.

flowing RBCs underneath several different wells that could hold cell culture inserts. The inserts allow the user to culture cells on top of a porous membrane, allowing molecules to diffuse across the membrane to interact with adjacent cells. The users treated the  $\beta$ -cells with a high glucose

solution to stimulate them to secrete the contents of the secretory vesicles (insulin, C-peptide, Zn<sup>2+</sup>, etc), which could then traverse the membrane and interact with the RBCs underneath. The RBCs, suspended in PSS buffer or albumin-free PSS buffer, were then flowed underneath the βcells for two hours.<sup>92</sup> In one of the wells above the membrane there were no cells, only buffer, to allow the ATP secreted from the RBCs to be quantified using the luciferin/luciferase chemiluminescence method. The ATP was also able to diffuse into another well containing endothelial cells. The production of NO from the endothelial cells as a result of ATP released from the RBCs was quantified (by using a fluorescent probe for NO) in both the presence and absence of a P2Y receptor inhibitor (PPADs). The purpose of the inhibitor was to investigate if the increase in NO from the endothelial cells was from ATP, as the P2Y receptor normally binds ATP and triggers NO synthase in endothelial cells. The results of the studies showed that β-cell secretions stimulated ATP release from RBCs, and that the resultant ATP release stimulated NO release from endothelial cells. The studies also showed that this effect was diminished when in the absence of albumin. Collectively, the researchers concluded that albumin is necessary for the beneficial interaction of β-cell secretions with RBCs.<sup>73, 92</sup>

The researchers also used the device to perform experiments to analyze the specific effect of C-peptide and  $Zn^{2+}$  on RBCs in the presence and absence of albumin. This experiment was performed systematically by incubating the RBCs with or without combinations of C-peptide,  $Zn^{2+}$ , or albumin, and then flowing the samples through the 3D-printed device to measure the resultant ATP release. The results of this experiment showed that C-peptide only increases the ATP released from RBCs when co-incubated with  $Zn^{2+}$  and albumin.

### 1.8 Successful-Rodent, Failed-Human Trials of C-peptide Replacement

The number of C-peptide publications per year peaked in the early 2000's and has considerably decreased in recent years. <sup>66</sup> This could be due to an important obstacle many have commented on in relation to C-peptide's candidacy as an active biological molecule: the lack of identification of a receptor. Though researchers have measured specific binding of C-peptide to a variety of cell types, a receptor has still not been identified and confirmed despite attempts by many. <sup>69-73</sup> A G-protein coupled receptor, GP146, was reported as a putative receptor by researchers at St. Louis University in 2015, however, a group from the University of Leicester showed convincing evidence of faults in the experiments from the group at St. Louis, and reported that the receptor is still unknown. <sup>72</sup> The inability to isolate a receptor has made many researchers and investors skeptical of C-peptide's bioactivity and potential as a therapeutic. However, many articles over the past 28 years have shown C-peptide to have activity *in vitro* on a variety of cell types, and also *in vivo* in a variety of animal and human models. <sup>74</sup>

In continuance with a decline in C-peptide research, in 2016, reports of a large-scale 12-month human clinical trial of a C-peptide analogue used to treat T1D neuropathy failed after phase-2b testing. The C-peptide analogue, called Ersatta, was a normal C-peptide molecule attached to a 40-kilodalton polyethelene glycol (PEG) residue to enhance the half-life of C-peptide in the bloodstream. The group previously published results of treating a common diabetic rodent model, the streptozotocin (STZ) mouse, with Ersatta. In this study, Ersatta prevented losses in sensory nerve conduction velocity, paw thermal response latency, and other characteristics of peripheral neuropathy. However, the 2016 human trial reported no

improvement in sural sensory nerve conduction velocity in T1D patients when compared to placebo. 94-95

Several publications have reported C-peptide replacement to be successful in ameliorating diabetic complications in rodent models, but follow up by reporting failure in human trials. For instance, C-peptide administration was successful in improving motor nerve conduction velocity (MNCV) (a metric of nerve damage) in multiple rodent models (STZ and BB/Wor rat). <sup>96-97</sup> However, in a later publication titled "Amelioration of Sensory Nerve Dysfunction by C-peptide in Patients with Type 1 Diabetes" the same authors report no improvement in MNCV in humans following 12 weeks of C-peptide treatment. <sup>98</sup> The stark inconsistencies between the diabetic animal model and diabetic humans have caused misperceptions about the efficacy of diabetic therapies. <sup>99</sup>

The failure of animal diabetes models to accurately mimic the human disease is of major concern due to the large amount of time and millions of dollars wasted on promising drug candidates. In the STZ rodent, a common model of diabetes, the rodents are administered either a large dose or several small doses of STZ, which has a cytotoxic effect on the pancreatic B-cells, therefore ceasing insulin secretions. Usually, the rodents begin insulin treatment soon thereafter. After STZ treatment, the rodents rapidly gain excess weight and are commonly very ill and under immense health-stress. The rodents also rapidly develop symptoms that mimic diabetic neuropathy, such as reduced sensory nerve conduction and latency to response to pain and thermal stimuli. Though these symptoms imitate those seen in diabetic humans, researchers argue that these features may be credited to the extreme ill health of the rodents, instead of genuine neuropathy. In these studies, the rodent experiences very little time with

deficiencies in pancreatic secretions before they begin treatment with insulin and/or C-peptide. This methodology is inconsistent with treating humans, where an adult T1D human may enter a clinical study without having had any C-peptide in their bloodstream for years or decades. During those years, the human experiences consistently high levels of glucose in their bloodstream. It is well studied in diabetes that these high levels of glucose in the bloodstream allows glucose to interact with proteins in a slow, time-dependent manner, causing protein-glycation and the formation of advanced-glycation end products. 101-104 The proteins impacted by glycation are reported to have altered functions and are hypothesized to be a cause of diabetic complications. 104-108 Protein glycation takes place on the order of months and the consequent effects could increase over the years during hyperglycemia. Therefore, prior to receiving C-peptide in a clinical trial, the diabetic animal model does not experience the same hyperglycemic time-period as an adult human. This discrepancy calls the validity of the diabetic animal model into question and may explain the conflicting results observed between human and rodent studies of C-peptide, as well as other diabetic drugs.

There have been many studies reporting benefits of replacing C-peptide in vivo in rodents, however, a large scale human clinical trial of C-peptide replacement has yet to be successful. T1, 109 Here, the author suggests that rigorously controlled *in vitro* studies should be performed under conditions that closely mimic those of the diabetic human. The benefits of insulin replacement therapy in humans were hypothesized for over 30 years before researchers discovered the appropriate chemical preparation of insulin through systematic and controlled experiments. Before these experiments, the experts in the field reported that replacement of pancreatic secretions was useless in treating diabetes. Similarly, the proper preparation and

administration of C-peptide needs to be studied more thoroughly under controlled conditions, and the molecular mechanisms by which it displays bioactivity need to be well understood before moving on to human trials. This dissertation reports new technologies and methods developed to better understand the interactions between C-peptide, human serum albumin, Zn<sup>2+</sup>, and RBCs, under conditions seen in diabetes. This dissertation also reports results of experiments that may be of importance in planning human trials of C-peptide replacement therapy in T1D.

**REFERENCES** 

#### REFERENCES

- 1. International Diabetes Federation Diabetes Atlas. International Diabetes Federation: 2017.
- 2. Association, A. D., Fast Facts Data and Statistics about Diabetes. **2017**.
- 3. Lakhtakia, R., The history of diabetes mellitus. *Sultan Qaboos University Medical Journal* **2013**, *13* (3), 368.
- 4. Pathak, A. K.; Sinha, P. K.; Sharma, J., Diabetes—A Historical review. *Journal of Drug Delivery and Therapeutics* **2013**, *3* (1).
- 5. Chatterjee, S.; Khunti, K.; Davies, M. J., Type 2 diabetes. *The Lancet* **2017,** *389* (10085), 2239-2251.
- 6. Holman, R. R.; Paul, S. K.; Bethel, M. A.; Matthews, D. R.; Neil, H. A. W., 10-year follow-up of intensive glucose control in type 2 diabetes. *New England Journal of Medicine* **2008**, *359* (15), 1577-1589.
- 7. Dugan, J.; Pfotenhauer, K.; Young, C.; Shubrook, J. H., Diabetes Microvascular Complications. *Primary Care Reports* **2017**, *23* (5).
- 8. Fowler, M. J., Microvascular and macrovascular complications of diabetes. *Clinical diabetes* **2008**, *26* (2), 77-82.
- 9. Brostoff, J.; Keen, H.; Brostoff, J., A diabetic life before and after the insulin era. *Diabetologia* **2007**, *50* (6), 1351-1353.
- 10. Allen, F. M.; Wishart, M. B., Experiments on carbohydrate metabolism and diabetes. II. The renal threshold for sugar and some factors modifying it. *J. Biol. Chem* **1920**, *43*, 129.
- 11. Tattersall, R., Pancreatic organotherapy for diabetes, 1889–1921. *Medical history* **1995,** *39* (3), 288-316.
- 12. Brunton, T. L., Lectures on the Pathology and Treatment of Diabetes Mellitus. *British medical journal* **1874,** *1* (686), 221.
- 13. Gacquin, M., Historical perspectives of dietary recommendations for diabetes. *Advanced Nutrition and Dietetics in Diabetes* **2015**, 15.
- 14. Karamanou, M.; Koutsilieris, M.; Laios, K.; Marineli, F.; Androutsos, G., Apollinaire Bouchardat (1806-1886): founder of modern Diabetology. *Hormones* **2014**, *13* (2), 296-300.
- 15. Herrick, J. B., THE OATMEAL DIET IN THE TREATMENT OF DIABETES MELLITUS. *Journal of the American Medical Association* **1908**, *50* (11), 861-865.

- 16. Allen, F. M.; Stillman, E.; Fitz, R., *Total dietary regulation in the treatment of diabetes*. Rockefeller Institute for Medical Research: 1919.
- 17. King, K. M.; Rubin, G., A history of diabetes: from antiquity to discovering insulin. *British journal of nursing* **2003**, *12* (18), 1091-1095.
- 18. Banting, F. G.; Best, C. H.; Collip, J. B.; Campbell, W. R.; Fletcher, A. A., Pancreatic extracts in the treatment of diabetes mellitus. *Canadian Medical Association Journal* **1922**, *12* (3), 141.
- 19. Bliss, M., *The discovery of insulin*. University of Chicago Press: 2013.
- 20. Dewitt, L. M., Morphology and physiology of areas of Langerhans in some vertebrates. *The Journal of experimental medicine* **1906**, *8* (2), 193.
- 21. Opie, E. L., *Disease of the pancreas: its cause and nature*. JB Lippincott: 1910.
- 22. Banting, F. G.; Best, C.; Collip, J.; Campbell, W.; Fletcher, A., Pancreatic extracts in the treatment of diabetes mellitus: preliminary report. *Canadian Medical Association journal* **1962**, *87* (20), 1062.
- 23. Opie, E. L., On the relation of chronic interstitial pancreatitis to the islands of Langerhans and to diabetes melutus. *Journal of Experimental Medicine* **1901**, *5* (4), 397-428.
- 24. Sakula, A., Paul Langerhans (1847–1888): a centenary tribute. *Journal of the Royal Society of Medicine* **1988**, *8*1 (7), 414-415.
- 25. Banting, F.; Campbell, W.; Fletcher, A., Further clinical experience with insulin (pancreatic extracts) in the treatment of diabetes mellitus. *Br Med J.* **1923**, *1* (3236), 8.
- 26. Banting, F. G., The history of insulin. Edinburgh Medical Journal 1929, 36 (1), 1.
- 27. Banting, F. G.; Best, C.; Collip, J.; Macleod, J.; Noble, E., The effect of pancreatic extract (insulin) on normal rabbits. *American Journal of Physiology-Legacy Content* **1922**, *62* (1), 162-176.
- 28. Banting, F. G.; Best, C.; Collip, J.; Macleod, J.; Noble, E., The effects of insulin on experimental hyperglycemia in rabbits. *American Journal of Physiology-Legacy Content* **1922**, *62* (3), 559-580.
- 29. Best, C. H., Nineteen hundred twenty-one in Toronto. *Diabetes* **1972**, *21* (Supplement 2), 385-395.
- 30. Rorsman, P.; Renström, E., Insulin granule dynamics in pancreatic beta cells. *Diabetologia* **2003**, *46* (8), 1029-1045.
- 31. Kitabchi, A. E., Proinsulin and C-peptide: A review. *Metabolism* **1977**, *26* (5), 547-587.
- 32. Steiner, D. F.; Cunningham, D.; Spigelman, L.; Aten, B., Insulin biosynthesis: evidence for a precursor. *Science* **1967**, *157* (3789), 697-700.
- 33. Hutton, J., The insulin secretory granule. *Diabetologia* **1989**, *32* (5), 271-281.

- 34. Medawala, W.; McCahill, P.; Giebink, A.; Meyer, J.; Ku, C.-J.; Spence, D. M., A molecular level understanding of zinc activation of C-peptide and its effects on cellular communication in the bloodstream. *Rev Diabet Stud* **2009**, *6* (3), 148.
- 35. Hutton, J. C., Insulin secretory granule biogenesis and the proinsulin-processing endopeptidases. *Diabetologia* **1994**, *37* (2), S48-S56.
- 36. Chapman, E. R., Synaptotagmin: A Ca 2+ sensor that triggers exocytosis? *Nature Reviews Molecular Cell Biology* **2002**, *3* (7), 498.
- 37. Hoogwerf, B. J.; Bantle, J. P.; Gaenslen, H. E.; Greenberg, B. Z.; Senske, B. J.; Francis, R.; Goetz, F. C., Infusion of synthetic human C-peptide does not affect plasma glucose, serum insulin, or plasma glucagon in healthy subjects. *Metabolism* **1986**, *35* (2), 122-125.
- 38. Lee, J.; Pilch, P. F., The insulin receptor: structure, function, and signaling. *American Journal of Physiology-Cell Physiology* **1994**, *266* (2), C319-C334.
- 39. Downward, J., Mechanisms and consequences of activation of protein kinase B/Akt. *Current opinion in cell biology* **1998,** *10* (2), 262-267.
- 40. Dimitriadis, G.; Mitrou, P.; Lambadiari, V.; Maratou, E.; Raptis, S. A., Insulin effects in muscle and adipose tissue. *Diabetes research and clinical practice* **2011**, *93*, S52-S59.
- 41. Randle, P. J., Regulatory interactions between lipids and carbohydrates: the glucose fatty acid cycle after 35 years. *Diabetes/metabolism reviews* **1998**, *14* (4), 263-283.
- 42. Horton, J. D.; Goldstein, J. L.; Brown, M. S., SREBPs: activators of the complete program of cholesterol and fatty acid synthesis in the liver. *The Journal of clinical investigation* **2002**, *109* (9), 1125-1131.
- 43. Livingstone, S. J.; Levin, D.; Looker, H. C.; Lindsay, R. S.; Wild, S. H.; Joss, N.; Leese, G.; Leslie, P.; McCrimmon, R. J.; Metcalfe, W., Estimated life expectancy in a Scottish cohort with type 1 diabetes, 2008-2010. *Jama* **2015**, *313* (1), 37-44.
- 44. McMillan, D. E., Deterioration of the microcirculation in diabetes. *Diabetes* **1975**, *24* (10), 944-957.
- 45. Cheung, N.; Mitchell, P.; Wong, T. Y., Diabetic retinopathy. *The Lancet* **2010**, *376* (9735), 124-136.
- 46. Klein, R.; Knudtson, M. D.; Lee, K. E.; Gangnon, R.; Klein, B. E., The Wisconsin Epidemiologic Study of Diabetic Retinopathy XXII: the twenty-five-year progression of retinopathy in persons with type 1 diabetes. *Ophthalmology* **2008**, *115* (11), 1859-1868.
- 47. Mookiah, M. R. K.; Acharya, U. R.; Chua, C. K.; Lim, C. M.; Ng, E.; Laude, A., Computer-aided diagnosis of diabetic retinopathy: A review. *Computers in biology and medicine* **2013**, *43* (12), 2136-2155.

- 48. Mookiah, M. R. K.; Acharya, U. R.; Martis, R. J.; Chua, C. K.; Lim, C. M.; Ng, E.; Laude, A., Evolutionary algorithm based classifier parameter tuning for automatic diabetic retinopathy grading: A hybrid feature extraction approach. *Knowledge-based systems* **2013**, *39*, 9-22.
- 49. Spencer, T.; Phillips, R. P.; Sharp, P. F.; Forrester, J. V., Automated detection and quantification of microaneurysms in fluorescein angiograms. *Graefe's archive for clinical and experimental ophthalmology* **1992**, *230* (1), 36-41.
- 50. Salz, D. A.; Witkin, A. J., Imaging in diabetic retinopathy. *Middle East African journal of ophthalmology* **2015**, *22* (2), 145.
- 51. Nagataki, S.; Matsunaga, I., Binding of fluorescein monoglucuronide to human serum albumin. *Investigative ophthalmology & visual science* **1985**, *26* (8), 1175-1178.
- 52. Ciulla, T. A.; Amador, A. G.; Zinman, B., Diabetic retinopathy and diabetic macular edema: pathophysiology, screening, and novel therapies. *Diabetes care* **2003**, *26* (9), 2653-2664.
- 53. Lorenzi, M., The polyol pathway as a mechanism for diabetic retinopathy: attractive, elusive, and resilient. *Journal of Diabetes Research* **2007**, *2007*.
- 54. Hammes, H.-P.; Martin, S.; Federlin, K.; Geisen, K.; Brownlee, M., Aminoguanidine treatment inhibits the development of experimental diabetic retinopathy. *Proceedings of the National Academy of Sciences* **1991**, *88* (24), 11555-11558.
- 55. Aiello, L. P.; Pierce, E. A.; Foley, E. D.; Takagi, H.; Chen, H.; Riddle, L.; Ferrara, N.; King, G. L.; Smith, L., Suppression of retinal neovascularization in vivo by inhibition of vascular endothelial growth factor (VEGF) using soluble VEGF-receptor chimeric proteins. *Proceedings of the National Academy of Sciences* **1995**, *92* (23), 10457-10461.
- 56. Waisbourd, M.; Goldstein, M.; Loewenstein, A., Treatment of diabetic retinopathy with anti-VEGF drugs. *Acta ophthalmologica* **2011**, *89* (3), 203-207.
- 57. Brownlee, M., Biochemistry and molecular cell biology of diabetic complications. *Nature* **2001**, *414* (6865), 813.
- 58. Tuck, R.; Schmelzer, J.; Low, P., Endoneurial blood flow and oxygen tension in the sciatic nerves of rats with experimental diabetic neuropathy. *Brain* **1984**, *107* (3), 935-950.
- 59. McMillan, D. E.; Utterback, N. G.; La Puma, J., Reduced erythrocyte deformability in diabetes. *Diabetes* **1978**, *27* (9), 895-901.
- 60. Hach, T.; Forst, T.; Kunt, T.; Ekberg, K.; Pfützner, A.; Wahren, J., C-peptide and its C-terminal fragments improve erythrocyte deformability in type 1 diabetes patients. *Experimental diabetes research* **2008**, *2008*.
- 61. Parthasarathi, K.; Lipowsky, H. H., Capillary recruitment in response to tissue hypoxia and its dependence on red blood cell deformability. *American Journal of Physiology-Heart and Circulatory Physiology* **1999**, *277* (6), H2145-H2157.

- 62. Aiello, L. P.; Northrup, J. M.; Keyt, B. A.; Takagi, H.; Iwamoto, M. A., Hypoxic regulation of vascular endothelial growth factor in retinal cells. *Archives of ophthalmology* **1995**, *113* (12), 1538-1544.
- 63. Control, C. f. D.; Prevention, Incidence of end-stage renal disease attributed to diabetes among persons with diagnosed diabetes---United States and Puerto Rico, 1996-2007. *MMWR. Morbidity and mortality weekly report* **2010**, *59* (42), 1361.
- 64. Steinke, J. M.; Sinaiko, A. R.; Kramer, M. S.; Suissa, S.; Chavers, B. M.; Mauer, M., The early natural history of nephropathy in type 1 diabetes: III. Predictors of 5-year urinary albumin excretion rate patterns in initially normoalbuminuric patients. *Diabetes* **2005**, *54* (7), 2164-2171.
- 65. Dronavalli, S.; Duka, I.; Bakris, G. L., The pathogenesis of diabetic nephropathy. *Nature Reviews Endocrinology* **2008**, *4* (8), 444.
- 66. Vinik, A., Diabetes: Clinical Science in Practice. Cambridge University Press: Cambridge, UK, 1995.
- 67. Control, D.; Group, C. T. R., The effect of intensive treatment of diabetes on the development and progression of long-term complications in insulin-dependent diabetes mellitus. *New England journal of medicine* **1993**, *329* (14), 977-986.
- 68. Tesfaye, S.; Chaturvedi, N.; Eaton, S. E.; Ward, J. D.; Manes, C.; Ionescu-Tirgoviste, C.; Witte, D. R.; Fuller, J. H., Vascular risk factors and diabetic neuropathy. *New England Journal of Medicine* **2005**, *352* (4), 341-350.
- 69. Lachin, J. M.; McGee, P.; Palmer, J. P., Impact of C-peptide preservation on metabolic and clinical outcomes in the Diabetes Control and Complications Trial. *Diabetes* **2013**, DB\_130881.
- 70. Wahren, J., C-peptide and the pathophysiology of microvascular complications of diabetes. *Journal of Internal Medicine* **2017**, *281* (1), 3-6.
- 71. Sima, A. A., *Diabetes & C-peptide: Scientific and Clinical Aspects*. Springer Science & Business Media: 2011.
- 72. Wahren, J., C-peptide: new findings and therapeutic implications in diabetes. *Clinical physiology and functional imaging* **2004**, *24* (4), 180-189.
- 73. Pinger, C. W.; Entwistle, K.; Bell, T.; Liu, Y.; Spence, D., C-Peptide replacement therapy in type 1 diabetes: are we in the trough of disillusionment? *Mol Biosyst* **2017**, *13* (8), 1432-1437.
- 74. Melani, F.; Rubenstein, A. H.; Oyer, P. E.; Steiner, D. F., Identification of proinsulin and C-peptide in human serum by a specific immunoassay. *Proceedings of the National Academy of Sciences* **1970**, *67* (1), 148-155.
- 75. Sjöberg, S.; Gunnarsson, R.; Gjötterberg, M.; Lefvert, A.; Persson, A.; Östman, J., Residual insulin production, glycaemic control and prevalence of microvascular lesions and polyneuropathy in long-term type 1 (insulin-dependent) diabetes mellitus. *Diabetologia* **1987**, *30* (4), 208-213.

- 76. Johansson, B.-L.; Linde, B.; Wahren, J., Effects of C-peptide on blood flow, capillary diffusion capacity and glucose utilization in the exercising forearm of type 1 (insulin-dependent) diabetic patients. *Diabetologia* **1992**, *35* (12), 1151-1158.
- 77. Johansson, B. L.; Borg, K.; Fernqvist-Forbes, E.; Kernell, A.; Odergren, T.; Wahren, J., Beneficial effects of C-peptide on incipient nephropathy and neuropathy in patients with Type 1 diabetes mellitus. *Diabetic medicine* **2000**, *17* (3), 181-189.
- 78. Wahren, J.; Ekberg, K.; Johansson, J.; Henriksson, M.; Pramanik, A.; Johansson, B.-L.; Rigler, R.; Jörnvall, H., Role of C-peptide in human physiology. *American Journal of Physiology-Endocrinology And Metabolism* **2000**, *278* (5), E759-E768.
- 79. Forst, T.; Kunt, T.; Pohlmann, T.; Goitom, K.; Engelbach, M.; Beyer, J.; Pfützner, A., Biological activity of C-peptide on the skin microcirculation in patients with insulin-dependent diabetes mellitus. *The Journal of clinical investigation* **1998**, *101* (10), 2036-2041.
- 80. Kunt, T.; Schneider, S.; Pfützner, A.; Goitum, K.; Engelbach, M.; Schauf, B.; Beyer, J.; Forst, T., The effect of human proinsulin C-peptide on erythrocyte deformability in patients with type I diabetes mellitus. *Diabetologia* **1999**, *42* (4), 465-471.
- 81. Rigler, R.; Pramanik, A.; Jonasson, P.; Kratz, G.; Jansson, O.; Nygren, P.-Å.; Ståhl, S.; Ekberg, K.; Johansson, B.-L.; Uhlen, S., Specific binding of proinsulin C-peptide to human cell membranes. *Proceedings of the National Academy of Sciences* **1999**, *96* (23), 13318-13323.
- 82. Forst, T.; Kunt, T., Effects of C-peptide on microvascular blood flow and blood hemorheology. *Journal of Diabetes Research* **2004**, *5* (1), 51-64.
- 83. Carroll, J.; Raththagala, M.; Subasinghe, W.; Baguzis, S.; Oblak, T. D. a.; Root, P.; Spence, D., An altered oxidant defense system in red blood cells affects their ability to release nitric oxide-stimulating ATP. *Molecular BioSystems* **2006**, *2* (6-7), 305-311.
- 84. Sprague, R. S.; Stephenson, A. H.; Ellsworth, M. L., Red not dead: signaling in and from erythrocytes. *Trends in Endocrinology & Metabolism* **2007**, *18* (9), 350-355.
- 85. Ellsworth, M. L.; Ellis, C. G.; Goldman, D.; Stephenson, A. H.; Dietrich, H. H.; Sprague, R. S., Erythrocytes: oxygen sensors and modulators of vascular tone. *Physiology* **2009**, *24* (2), 107-116.
- 86. González-Alonso, J.; Olsen, D. B.; Saltin, B., Erythrocyte and the regulation of human skeletal muscle blood flow and oxygen delivery: role of circulating ATP. *Circulation research* **2002**, *91* (11), 1046-1055.
- 87. Sprague, R. S.; Olearczyk, J. J.; Spence, D. M.; Stephenson, A. H.; Sprung, R. W.; Lonigro, A. J., Extracellular ATP signaling in the rabbit lung: erythrocytes as determinants of vascular resistance. *American Journal of Physiology-Heart and Circulatory Physiology* **2003**, *285* (2), H693-H700.
- 88. Meyer, J., *Successful and reproducible bioactivity with C-peptide via activation with zinc.* MICHIGAN STATE UNIVERSITY: 2009.

- 89. Meyer, J. A.; Froelich, J. M.; Reid, G. E.; Karunarathne, W. K.; Spence, D. M., Metal-activated C-peptide facilitates glucose clearance and the release of a nitric oxide stimulus via the GLUT1 transporter. *Diabetologia* **2008**, *51* (1), 175-182.
- 90. Keltner, Z.; Meyer, J. A.; Johnson, E. M.; Palumbo, A. M.; Spence, D. M.; Reid, G. E., Mass spectrometric characterization and activity of zinc-activated proinsulin C-peptide and C-peptide mutants. *Analyst* **2010**, *135* (2), 278-288.
- 91. Meyer, J. A.; Spence, D. M., A perspective on the role of metals in diabetes: past findings and possible future directions. *Metallomics* **2009**, *1* (1), 32-41.
- 92. Liu, Y.; Chen, C.; Summers, S.; Medawala, W.; Spence, D. M., C-peptide and zinc delivery to erythrocytes requires the presence of albumin: implications in diabetes explored with a 3D-printed fluidic device. *Integr. Biol.* **2015**, *7* (5), 534-543.
- 93. Peters Jr, T., *All about albumin: biochemistry, genetics, and medical applications*. Academic press: 1995.
- 94. Wahren, J.; Foyt, H.; Daniels, M.; Arezzo, J. C., Long-acting C-peptide and neuropathy in type 1 diabetes: a 12-month clinical trial. *Diabetes care* **2016**, *39* (4), 596-602.
- 95. Jolivalt, C.; Rodriguez, M.; Wahren, J.; Calcutt, N., Efficacy of a long-acting C-peptide analogue against peripheral neuropathy in streptozotocin-diabetic mice. *Diabetes, Obesity and Metabolism* **2015**, *17* (8), 781-788.
- 96. Cotter, M. A.; Cameron, N. E., C-peptide effects on nerve conduction and blood flow in streptozotocin-induced diabetic rats: modulation by nitric oxide synthase inhibition. *Diabetes* **2001**, *50*, A184.
- 97. Sima, A. A. F.; Zhang, W.; Sugimoto, K.; Henry, D.; Li, Z.; Wahren, J.; Grunberger, G., C-peptide prevents and improves chronic Type I diabetic polyneuropathy in the BB/Wor rat. *Diabetologia* **2001**, *44* (7), 889-897.
- 98. Ekberg, K.; Brismar, T.; Johansson, B.-L.; Jonsson, B.; Lindström, P.; Wahren, J., Amelioration of Sensory Nerve Dysfunction by C-Peptide in Patients With Type 1 Diabetes. *Diabetes* **2003**, *52* (2), 536-541.
- 99. Fox, A.; Eastwood, C.; Gentry, C.; Manning, D.; Urban, L., Critical evaluation of the streptozotocin model of painful diabetic neuropathy in the rat. *Pain* **1999**, *81* (3), 307-316.
- 100. Apfel, S. C., Diabetic neuropathy models: Are they relevant? *Drug Discovery Today: Disease Models* **2007**, *3* (4), 397-402.
- 101. Barnaby, O. S.; Cerny, R. L.; Clarke, W.; Hage, D. S., Comparison of modification sites formed on human serum albumin at various stages of glycation. *Clin. Chim. Acta* **2011**, *412* (3–4), 277-285.
- 102. Barnaby, O. S.; Cerny, R. L.; Clarke, W.; Hage, D. S., Quantitative analysis of glycation patterns in human serum albumin using 16O/18O-labeling and MALDI–TOF MS. *Clin. Chim. Acta* **2011**, *412* (17–18), 1606-1615.

- 103. Anguizola, J.; Matsuda, R.; Barnaby, O. S.; Hoy, K. S.; Wa, C.; DeBolt, E.; Koke, M.; Hage, D. S., Review: Glycation of human serum albumin. *Clin. Chim. Acta* **2013**, *425*, 64-76.
- 104. Rondeau, P.; Bourdon, E., The glycation of albumin: structural and functional impacts. *Biochimie* **2011,** *93* (4), 645-658.
- 105. Hage, D. S., Analysis of Biological Interactions by Affinity Chromatography: Clinical and Pharmaceutical Applications. *Clin. Chem.* **2017**.
- 106. Hage, D. S.; Jackson, A.; Sobansky, M. R.; Schiel, J. E.; Yoo, M. J.; Joseph, K., Characterization of drug–protein interactions in blood using high-performance affinity chromatography. *J. Sep. Sci.* **2009**, *32* (5-6), 835-853.
- 107. Matsuda, R.; Anguizola, J.; Joseph, K.; Hage, D. S., High-performance affinity chromatography and the analysis of drug interactions with modified proteins: binding of gliclazide with glycated human serum albumin. *Anal. Bioanal. Chem.* **2011**, *401* (9), 2811.
- 108. Baraka-Vidot, J.; Guerin-Dubourg, A.; Bourdon, E.; Rondeau, P., Impaired drug-binding capacities of in vitro and in vivo glycated albumin. *Biochimie* **2012**, *94* (9), 1960-1967.
- 109. Luzi, L.; Zerbini, G.; Caumo, A., C-peptide: a redundant relative of insulin? *Diabetologia* **2007**, *50* (3), 500-502.

## Chapter 2: A 3D-Printed Device for Enhanced Equilibrium Dialysis Binding Measurements

## 2.1 Prologue

In 2008, the Spence group published results showing that treatment with C-peptide causes red blood cells (RBCs) to release increased levels of ATP, but only when the peptide is first combined with a transition metal.<sup>1</sup> Ensuing experiments over the next seven years focused on measuring specific binding between Zn<sup>2+</sup> and C-peptide using techniques such as circular dichroism, fluorescence spectroscopy, mass spectrometry, etc., however, only weak non-specific interactions were measured.<sup>2</sup> In early 2015, the Spence group published results from isothermal titration calorimetry (ITC) binding experiments showing that C-peptide and Zn<sup>2+</sup> do not exhibit specific binding to each other, but they each bind specifically to albumin.<sup>3</sup> This interaction between C-peptide, Zn<sup>2+</sup>, and albumin was found to be necessary in order for C-peptide to interact with RBCs.

Also in early 2015, I joined the Spence group and decided to further study the molecular interactions between C-peptide, Zn<sup>2+</sup>, and albumin under diabetic conditions (i.e. high glucose). Initial attempts at binding experiments were hindered by limited access to the ITC instrument on campus, which was regularly out-of-commission or being used by other scientists. Purchasing our own ITC instrument was not an option, as they can be very expensive. Further, the experiments needed to be performed under a variety of physiological conditions which would be difficult to imitate using ITC experiments (temperature, wide concentration ranges, competitive binding, etc). Lastly, the albumin samples being studied were heterogeneous mixtures (due to the microheterogeneity of plasma albumin), which would make accurate ITC binding analysis tedious and difficult. Therefore, it was decided to perform the experiments using equilibrium dialysis, a

traditional binding technique that I could perform in our own lab. The nature of equilibrium-dialysis experiments (explained below in section 2.1.2) allows protein-ligand binding measurements to be made under conditions of the user's choice, therefore allowing me to analyze the heterogeneous albumin samples.

Initially, I used a commercially purchased equilibrium dialysis device to try to measure the binding affinity between human serum albumin (HSA) and Zn<sup>2+</sup>. However, I found that the purchased devices were pre-contaminated with Zn<sup>2+</sup> at a level that would significantly alter the experiments (approximately 269.6 ± 16.7 picomoles per well in the device, as determined by inductively-coupled plasma optical emission spectroscopy (ICP-OES)). Meanwhile, the Spence group had recently started using 3D-printing to create customizable lab tools. Dr. Spence suggested using 3D-printing to create our own equilibrium-dialysis devices that we could customize to specifically study the binding interactions we were interested in. This suggestion led directly to the work performed in this Chapter.

#### 2.2 Introduction

A quantitative determination of molecular binding interactions between C-peptide, Zn<sup>2+</sup>, and albumin could provide insight into the unknown mechanism by which they interact with red blood cells (RBCs). Liu *et al.* demonstrated that C-peptide interacts with RBCs and increases the amount of ATP released from these cells, but only when in the presence of Zn<sup>2+</sup> and albumin.<sup>3</sup> It was also reported by these same authors that RBCs uptake Zn<sup>2+</sup> in an equimolar ratio with C-peptide, and that C-peptide only binds to RBCs when in the presence of albumin. Finally, their data suggested that C-peptide and albumin facilitate specific binding of Zn<sup>2+</sup> to RBCs. Human serum albumin (HSA) is the most common protein found in the blood plasma and is a well-

documented carrier protein, as it binds a variety of ligands (drugs, peptides, ions, etc.) and distributes ligands throughout the body via the bloodstream.<sup>4-5</sup> The work featured in this chapter reports new technologies developed to improve protein-ligand binding measurements. In this chapter, we test the hypothesis that C-peptide assists the uptake of Zn<sup>2+</sup> to RBCs by decreasing the binding affinity of Zn<sup>2+</sup> to HSA.

There are many analytical techniques reported for measuring the binding affinity of a ligand to a protein, including but not limited to isothermal titration calorimetry (ITC), surface plasmon resonance, 6-7 mass spectrometry, 8 equilibrium dialysis, 7 ultrafiltration, 9 ultracentrifugation, 10 and ultrafast affinity extraction chromatography. 11-12 Each technique has unique advantages and disadvantages, and the user must decide which is most appropriate and practical for their needs. Equilibrium dialysis is a simple binding technique used for many years that provides highly precise, reproducible, and cost effective analyses of binding constants, and can be performed

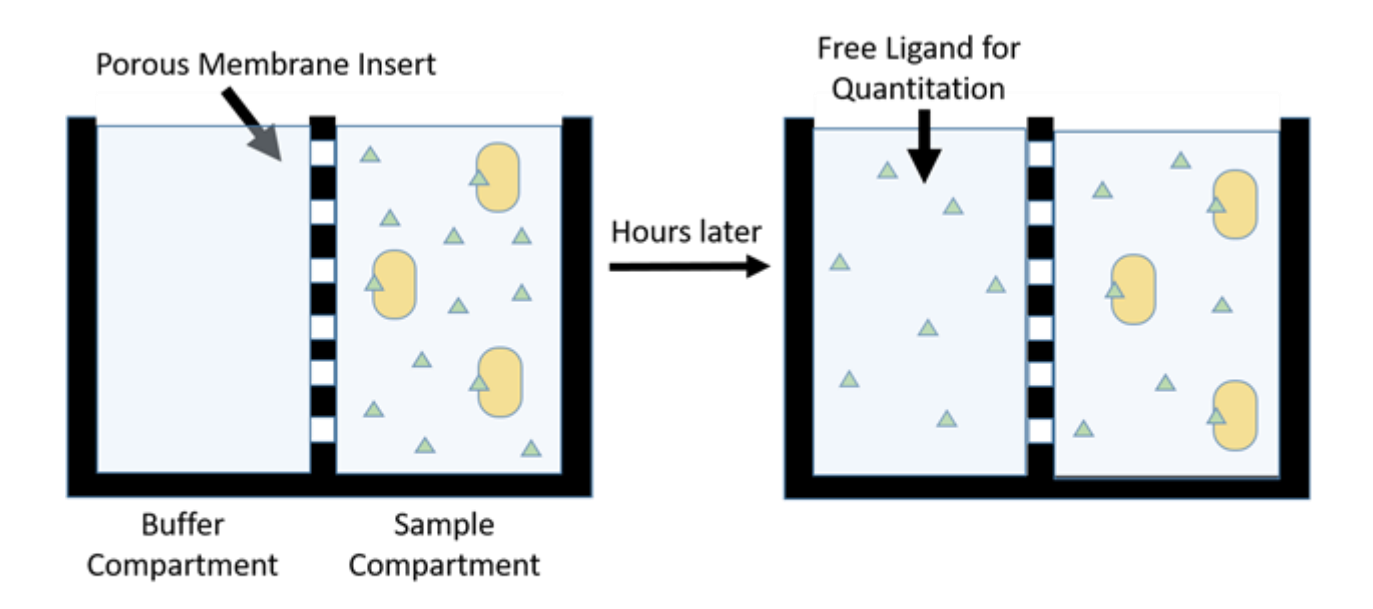


Figure 2.1 Equilibrium Dialysis. A schematic diagram of equilibrium-dialysis to measure protein-ligand binding affinity. Yellow ovals represent large proteins, and green triangles represent small lligands.

when the ligand and protein of interest have large enough differences in molecular weight (at least 5x difference). <sup>13-15</sup> In equilibrium dialysis experiments, a protein and ligand are combined in solution and transferred into a compartment on one side of a porous membrane with only buffer solution on the opposite side of the membrane (See Figure 2.1 above). The membrane has pores large enough to allow the ligand to diffuse through, but small enough to retain the protein/ligand complex in the original sample-compartment. The equilibrium dialysis device is incubated on a shaker for several hours until the concentration of free-ligand is equal on both sides of the membrane, as indicated by the concentration of analyte-ligand ceasing to increase in the buffer compartment. At this point, the concentration of analyte-ligand be quantified and used in the equations below as the free-ligand. This information can then be used to calculate a single-point affinity constant, create a saturation binding curve, Hill plot, or Scatchard plot to analyze the characteristics of the binding interaction.<sup>7</sup>

Eq. 2.1: [Bound Ligand] = 
$$\frac{\text{Total ligand (moles)} - \text{Free ligand (moles)}}{\text{Volume in Sample Compartment}}$$

Eq. 2.2: 
$$% Protein Bound = \frac{Bound \ ligand \ (moles)}{Total \ ligand \ (moles)} * 100\%$$

Eq. 2.3: 
$$K_a = \frac{[Bound\ ligand]}{[Free\ ligand]*([Total\ Receptor] - [Bound\ Ligand])}$$

Plasma-protein binding measurements, such as equilibrium dialysis, are an important aspect of pharmacology because they provide pharmacokinetic information about the ligand being studied.<sup>4</sup> It is commonly believed by pharmacologists that only the unbound, or free, fraction of the ligand is available to cells and tissues. This is not always true however, as there are several

cases reported in the literature where cells only uptake ligands that are bound to carrier-proteins. <sup>16-17</sup> In this construct, it is valuable to measure the binding constants between the ligands and proteins when studying either situation.

Despite the many advantages of equilibrium dialysis methods, a shortcoming is the long incubation times required for the free-ligand to reach equal concentrations on both sides of the membrane, which can range from 6-24 hours. <sup>18</sup> If the system is not given enough time to establish equilibrium, then the concentration of free-ligand will not be able to reach equal concentrations in the sample and buffer compartment, which will lead to deceptively low approximations of free-ligand, and inaccurately low K<sub>d</sub> measurements (erroneously strong affinity). This drawback often precludes equilibrium dialysis methods from being used for many applications.

To overcome the throughput issue, commercially available equilibrium-dialysis devices have been as adapted to 96-well plate technologies to enable high-throughput binding measurements by permitting the use of multi-channel pippetors and automated liquid handling systems. However, there are shortcomings associated with the commercially available systems, such as limited membrane options (such as molecular weight cutoff and material types), and reported membrane characteristics (such as percent porosity). Not knowing the percent porosity of the membrane makes mathematical predictive modelling of equilibration times difficult, requiring the user to "guess and check" equilibration times prior to performing the desired measurement.

In this chapter, the fabrication and characterization of a 3D-printed equilibrium dialysis device that fits into a plate reader or scintillation counter for direct quantitation of analyte-ligands is

described. The fabrication of this device is made possible by the novel 3D-printing technique known as *Print-Pause-Print*. *Print-Pause-Print* allows the user to integrate any membrane of their choice directly, and without leakage, into Polyjet 3D-printed devices.<sup>19</sup> Membrane integration into analytical fluidic devices is useful for many applications; however, it is often difficult and usually involves O-rings or adhesives to prevent leakage.<sup>20-22</sup> The device was characterized by measuring the binding of fluorescein to bovine serum albumin (BSA), as these are inexpensive and commonly available reagents and the binding affinity between the two reagents is thoroughly documented in the literature due to its use in studying blood-retina and blood-brain barriers.<sup>23-26</sup> Once established, the device was used for measuring the affinity of Zn<sup>2+</sup> for HSA, and the impact of C-peptide on the affinity of Zn<sup>2+</sup>/HSA binding.

#### 2.3 Fabrication and Preparation Methods

### 2.3.1 Fabrication of the Dialysis Base Plate Device

The device base is the same size and shape of a 96-well plate, as seen in Figure 2.2. The device was created by an additive manufacturing technique using an Objet Connex 350 3D printer. This Polyjet printer is capable of 16  $\mu$ m resolution in the Z-axis and 600 dpi in the XY plane. The .stl file was created using CAD software (Autodesk Inventor Professional, 2016) to create the blueprints of the device. Then, the .stl file was submitted to the printer. The printer interprets the .stl file and deposits  $\sim$ 30  $\mu$ m layers of a chosen liquid polymer, followed by curing of the polymer via UV light to create a rigid object according to the specifications of the .stl file. This 3D printer is capable of printing multiple materials with different properties into the same device for added functionality. In this way, a dialysis base plate (Figure 2.3) was printed in a rigid

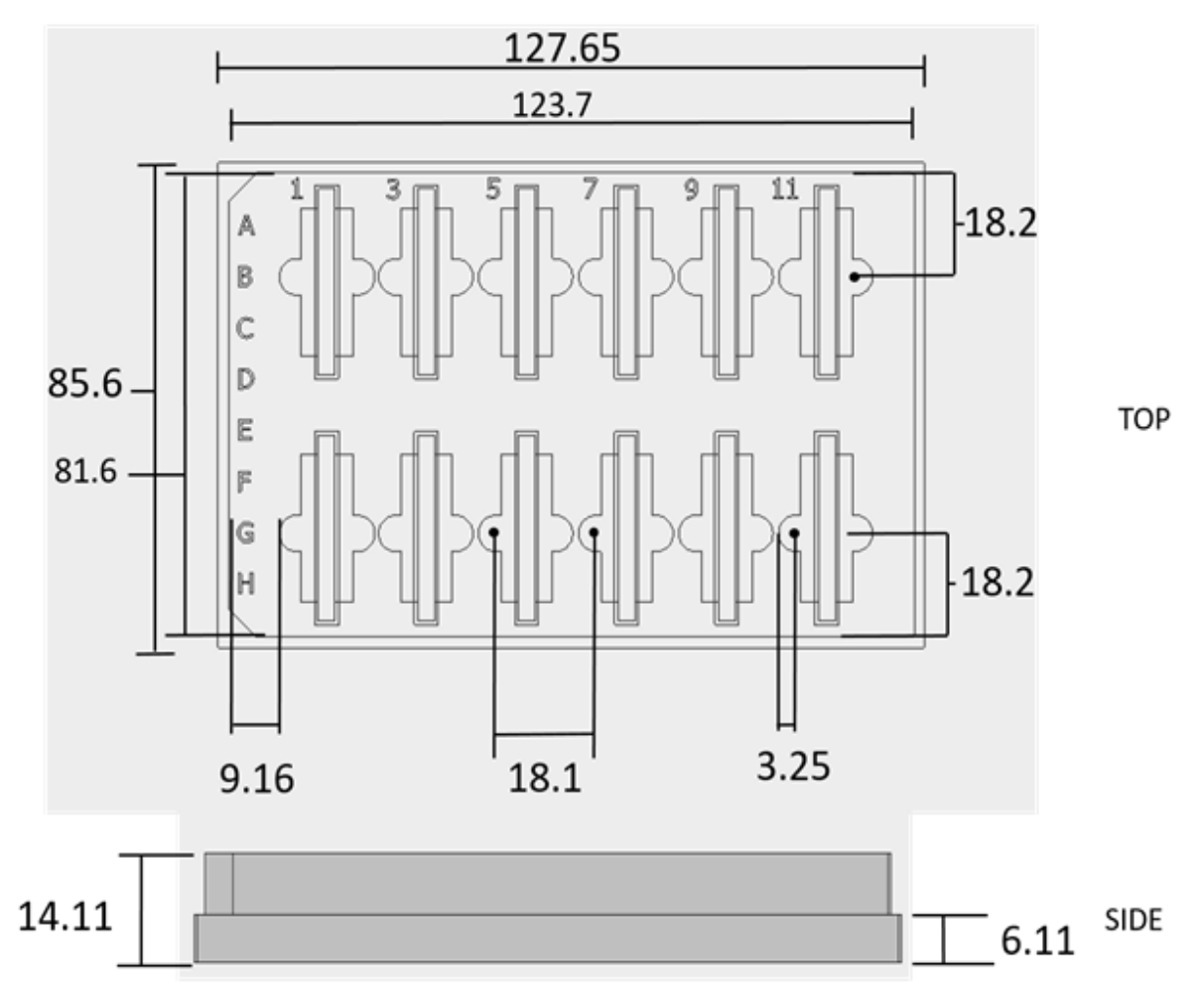


Figure 2.2 Diagram showing the exact dimensions of the 3D-printed device. All dimensions are in millimeters. The device is the same size and shape of a standard 96-well plate. The device is designed so that wells in the buffer and sample compartments are in the exact same location as wells in a standard 96-well plate.

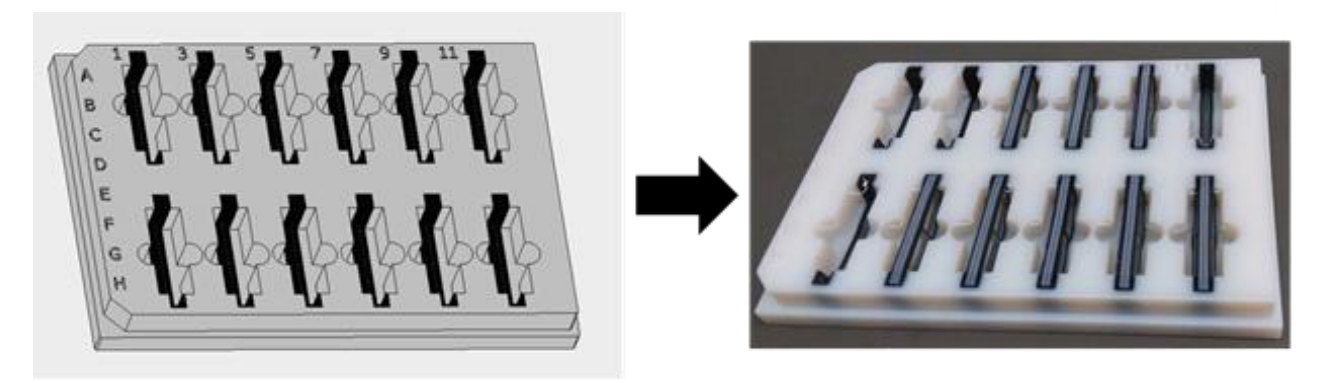


Figure 2.3 Equilibrium Dialysis Device Left: A computer-aided design (CAD) file image of the device. Right: A picture of the final printed device with several mebrane-holding inserts in place.

material (VeroClear, Stratasys, Ltd., Eden Prairie, MN) containing 12 wells that were lined with 0.6 mm of a rubberlike material (Tangoblack, Stratasys, Ltd.). Two different versions of the base plate were printed. The first device has circular wells that are in the exact location of wells of a

normal 96-well plate to be used for direct quantitation of the analyte-ligand in a plate reader. The other version of the device is printed without circular wells and was used for experiments where the analyte-ligand needed to be removed from the device for measurement.

### 2.3.2 Print-Pause-Print for Integrating Membranes into 3D-printed Devices

A *Print-Pause-Print* technique was invented to incorporate size-exclusion dialysis membranes into printed membrane-holding inserts, as seen in Figure 2.4A. The inserts were designed as assembly files to include a thin layer of TangoBlack on both of the outside surfaces of the insert, and a thin (0.55 mm) layer exactly in the middle of the insert. This rubbery material is able to slightly compress, much like a rubber gasket, in order to create a water-tight seal. The exact

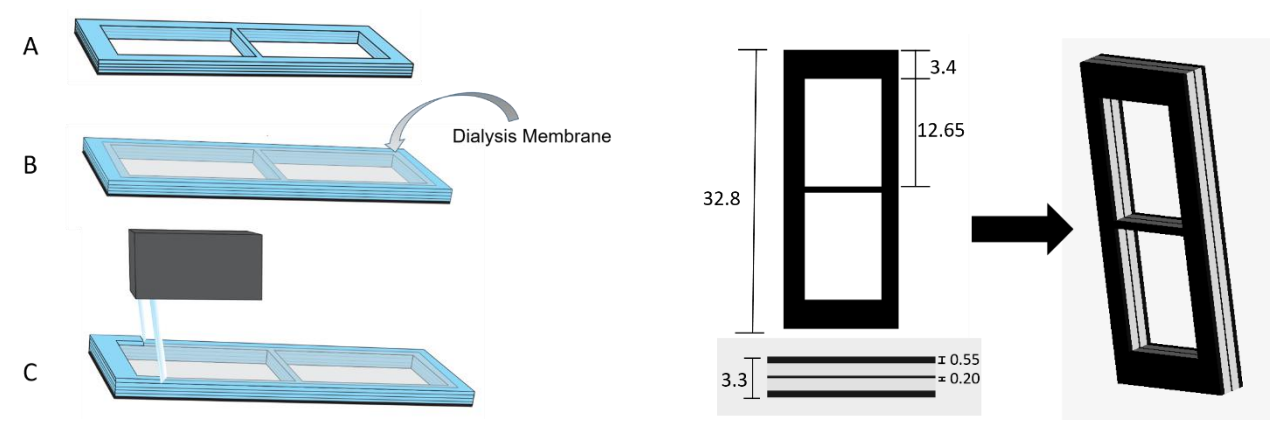


Figure 2.4 Print-Pause-Print for membrane integration. Left: A Connex 3D-printer was used to integrate membranes directly into a device. First, in **A**, a device containing a window was printed half-way. The printer was paused, and in **B** the operator laid down a porous membrane of choice over the window. In **C**, the printer resumes, laying polymer over the edges of the membrane to seamlessly seal it into the device. **Right:** CAD drawing of inserts designed to hold membranes with dimensions in millimeters.

dimensions of the inserts can be seen in Figure 2.4B. After submission of the .stl file to the 3D printer, the print process was started and then paused at the halfway point of the print job. Precut dialysis membranes with 3.5 kDa molecular weight cut-off (MWCO) (Spectrum Laboratories Inc, Rancho Dominguex, CA) were placed onto the TangoBlack surface, which has slightly adhesive properties to help attach the membrane, and the printing process was resumed, adding

layers of VeroWhite material on top of the edges of the membrane, sealing it into the device. The membrane-inserts were then cleaned with distilled and deionized  $H_2O$  (DDW, 18  $M\Omega$ ) and inserted into the wells in the main device. A flow-chart for the *Print-Pause-Print* process can be seen in Figure 2.5.

The primary challenge in fabricating this device was designing it so that undesired leakage did not occur between the two compartments. This was achieved by the incorporation of multiple materials with different properties into the same device, rubbery TangoBlack and rigid VeroWhite, to create a tight seal around the membrane insert. Leakage was assessed by placing water into each sample compartment with nothing in the buffer compartment and shaking the device for approximately 5 minutes, while simultaneously observing to see if any water leaked into the buffer compartment. Once the device passed this test, it was ready to be used for binding experiments.

#### 2.3.3 Sample Preparation

Bovine serum albumin (BSA, lyophilized powder, ≥ 98%) was commercially purchased (Sigma Chemical, St. Louis, MO). Fluorescein sodium salt (Sigma) was diluted in DDW to create a 300 μM stock solution of fluorescein. Albumin from human serum (HSA; lyophilized powder, free of fatty

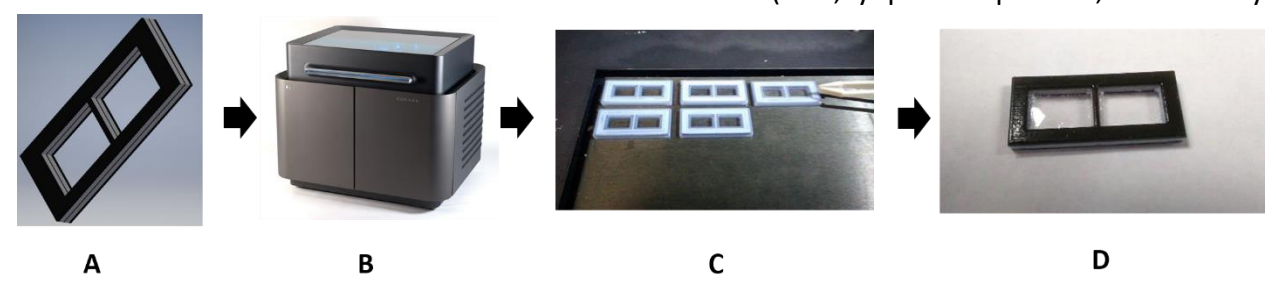


Figure 2.5 **Print-Pause-Print Flow Chart**. In **A**, a model is drawn using Autodesk Inventor Professional CAD software. The model is saved as an .stl file and sent to the 3D-printer (**B**). The membrane holder is printed with multiple materials. In **C**, the operator places the membranes into the device halfway through the print process. Picture **D** shows the final product: a membrane holder with a membrane seamlessly sealed into the device.

acid and globulin,  $\geq$ 99% pure, via agarose gel electrophoresis, Sigma). The Pierce bicinchoninic acid (BCA) protein assay kit was (ThermoScientific) was used for all protein assays, using BSA as a reference. Radio-labeled Zn<sup>2+</sup> (purchased as <sup>65</sup>ZnCl<sub>2</sub>, PerkinElmer) (half-life = 244 days) was diluted in DDW to prepare an 80  $\mu$ M stock solution of Zn<sup>2+</sup>. FITC-labelled C-peptide (Peptide2.0 ,Chantilly, VA) was prepared as a 6.3  $\mu$ M stock solution in DDW.

### 2.4 Experiment

## 2.4.1 Fluorescein Binding to BSA

First, a stock solution of BSA was prepared daily by diluting the lyophilized BSA with phosphate dialysis buffer (200 mM phosphate buffer in DDW, pH 7.40, sterile filtered through 0.22  $\mu$ m filters, Sigma) to make a working solution of 50 mg/mL BSA. From this stock solution, samples were made (10 mL total) to contain 42 mg/mL BSA (approx. 640  $\mu$ M, to mimic albumin concentrations found in blood plasma) and 2  $\mu$ M fluorescein. A separate sample containing no BSA was prepared in the exact same manner to contain 2  $\mu$ M fluorescein in dialysis buffer. Standards (3 mL total) containing known concentrations of fluorescein were made in buffer, ranging in concentration from 0.125 to 1.0  $\mu$ M, including a blank.

#### 2.4.2 Characterizing Incubation Time for Equilibrium Dialysis Experiments

The cleaned membrane holders were inserted into the device, as shown in Figure 2.6. Then, a 1.1 mL aliquot of sample containing 42 mg/mL BSA and 2  $\mu$ M fluorescein in dialysis buffer was pipetted into the sample compartment of the first 3 wells, followed by 1.1 mL of dialysis buffer into the corresponding buffer wells on the adjacent side of the membrane. This was repeated in the next 3 wells with sample containing 0 mg/mL BSA and 2  $\mu$ M fluorescein. Five of the other wells contained standards in both the sample and buffer compartments. For instance, 1.1 mL of

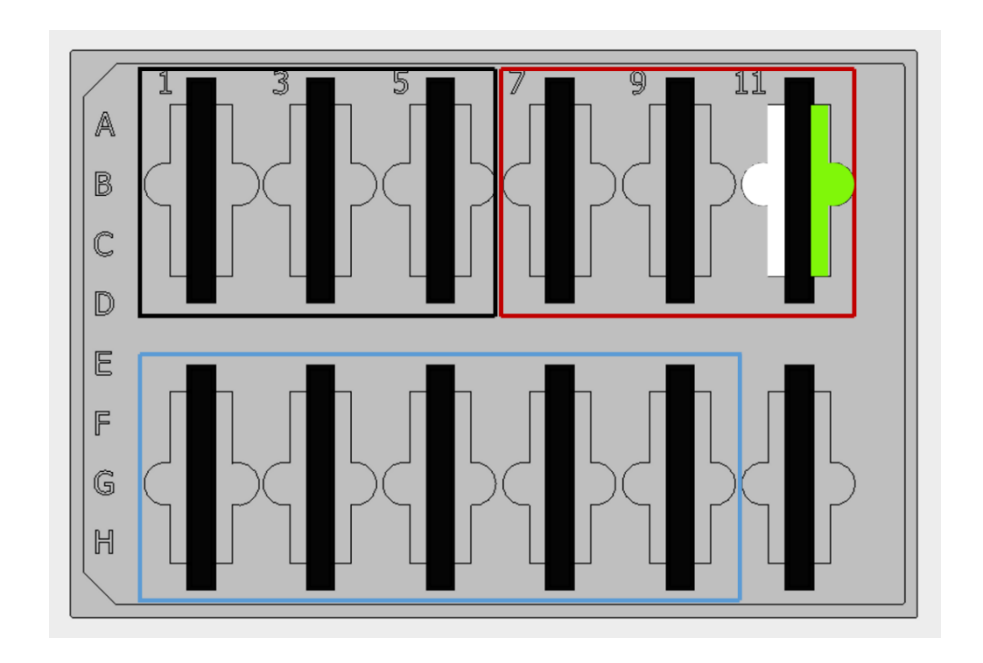


Figure 2.6 A schematic diagram showing how the device is prepared for equilibrium dialysis. The wells in the black box contain 2.0  $\mu$ M fluorescein in buffer without BSA in the sample compartment, while the wells in the red box contain 2.0  $\mu$ M fluorescein in buffer with 42 mg/mL BSA in the sample compartment. The wells in the blue box contain standards. The white compartment represents a "buffer compartment", while the green compartment represents a "sample compartment." The black rectangles show where membrane-holding inserts are placed.

1  $\mu$ M fluorescein standard was pipetted into both the sample and buffer compartments of the same well, and this was repeated for the other four standards in four other wells. A layout of the samples and standards in the device can be seen in Figure 2.6. The entire device was agitated at 220 rpm at 37 °C on an orbital shaker (Talboys) to provide constant mixing at physiological

temperature. The device was removed from the shaker and placed directly into a plate reader (FlexStation 3, Molecular Devices) for free ligand quantitation at 2, 4, 5.5, 6.5, 7.5, 8, 8.5, and 9 hours. This was performed by measuring the fluorescence (excitation wavelength: 485 nm, emission wavelength: 512 nm, cut-off: 495 nm) in the buffer-compartment of each sample well, including the wells containing standards. The data was then exported to a separate spreadsheet (Microsoft Excel) for data analysis.

### 2.4.3 Automated Equilibrium Dialysis Experiments

The device was set up with samples and standards exactly as described in the previous section and in Figure 2.6. After addition of samples and standards, the device was immediately placed into the plate reader instead of the orbital shaker. Using the settings in the instrument software,

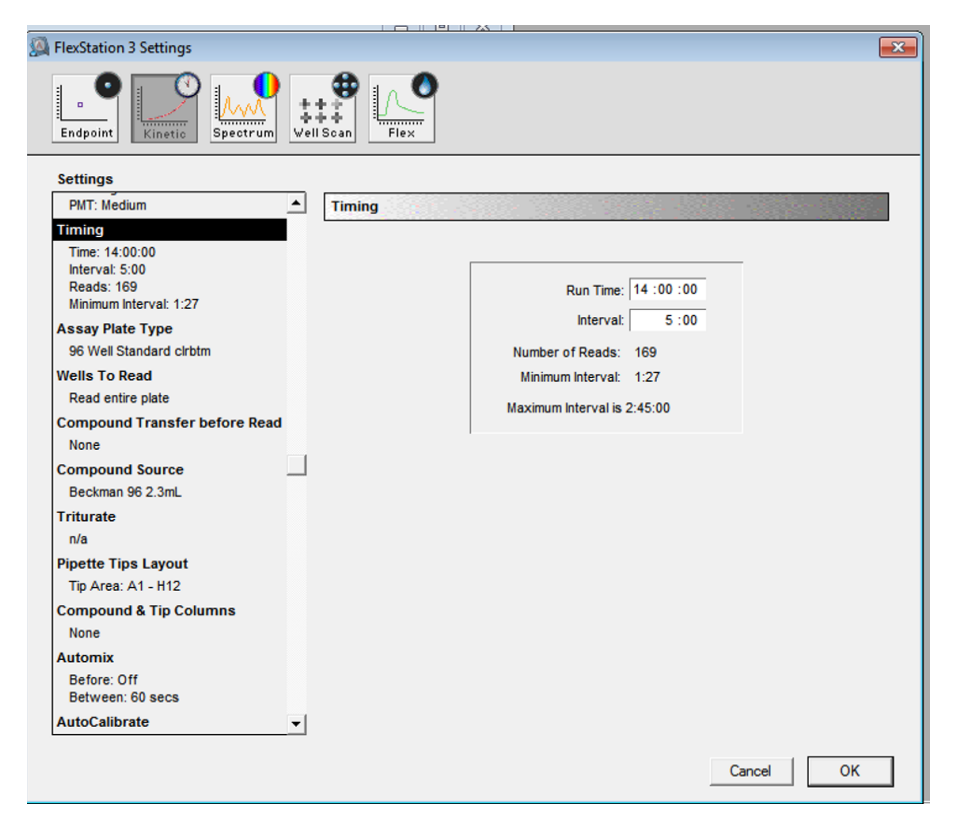


Figure 2.7 Plate Reader Settings A screenshot of the settings used to automate the plate-reader for automated equilibrium dialysis measurements.

the instrument was programmed to measure the fluorescence of the samples (as described previously) every 5 minutes for the next 14 hours, while shaking for one full minute prior to the reading, as seen in Figure 2.7. Once the user clicked "start", they were able to leave until the next day to export, analyze, and interpret the data.

### 2.4.4 Calculations and Data Analysis

For the fluorescein experiments, the fluorescence intensity values measured on the device by the plate reader were exported to a Microsoft Excel spreadsheet for data analysis. The fluorescence intensities of the standards were used to make an external-standards calibration curve. This calibration curve was used to quantify the concentration of free-fluorescein in the buffer compartments of the sample wells. The free concentration of fluorescein was then used in equations 2.1, 2.2, and 2.3 to calculate the percent protein bound and global equilibrium constant  $nK_a$  of the system.

# 2.4.5 Zn<sup>2+</sup> Binding to HSA sample preparation

A stock solution of HSA was prepared fresh daily by dissolving the lyophilized HSA powder in dialysis-buffer (150 mM NaCl, 21 mM Tris, pH 7.40 in DDW, sterile filtered through 0.22  $\mu$ m filters) to make a 5 mg/mL HSA solution as confirmed by the BCA assay. From this stock solution, samples (each 750  $\mu$ L total) were prepared in dialysis-buffer to contain 15.0  $\mu$ M HSA and different concentrations of radioactive Zn<sup>2+</sup> ranging from 1 to 25  $\mu$ M.

#### 2.4.6 Characterization of Incubation-Time Studies for Zinc

First, the membrane-holders were placed into the dialysis base-plate. Then, the compartments and membranes were rinsed three times with DDW to remove any contamination or debris. Excess liquid was removed with a pipette. A 700  $\mu$ L aliquot of sample containing 15  $\mu$ M HSA and 5  $\mu$ M Zn<sup>2+</sup> was then pipetted into a sample compartment on the device. Subsequently, 700  $\mu$ L of dialysis-buffer were pipetted into the other compartment on the device. This exact procedure was repeated in 4 other wells on the device, followed by placement of a 96-well plate adhesive plate-sealer to prevent evaporation during incubation. The entire device was agitated at 220 rotations per minute at 37°C on an incubating orbital shaker to provide constant mixing and a physiological temperature. Lastly, 500  $\mu$ L of sample were removed from the buffer-compartment of an individual well following 2, 4, 5.5, 8, and 10 hours of incubation for quantitation of free Zn<sup>2+</sup>.

### 2.4.7 Quantitation of Free <sup>65</sup>Zn<sup>2+</sup> via Liquid Scintillation Counting

Samples containing 15.0  $\mu$ M HSA and different concentrations of Zn<sup>2+</sup> (1, 2.5, 5, 10, 16, 19, and 25  $\mu$ M Zn<sup>2+</sup>) were pipetted into separate sample-compartments of the device, as described in the previous section, with equal volumes of diluted dialysis-buffer in the adjacent buffer-compartments. The device was agitated/incubated at 37°C for 6 hours. Then, immediately following the 6-hour incubation, 500  $\mu$ L of sample from the buffer compartments were removed for quantitation of free Zn<sup>2+</sup> using a Perkin Elmer MicroBeta TriLux 1450 liquid scintillation counter to measure the beta decay of the radioactive <sup>65</sup>Zn<sup>2+</sup> tracer. A 90  $\mu$ L aliquot of sample was pipetted into a well of a 96-well plate followed by the addition of 90  $\mu$ L of scintillation cocktail

(OptiPhase Supermix, Perkin Elmer) to the sample-containing well. Standards of known Zn<sup>2+</sup> concentrations in dialysis-buffer were treated in the same manner to generate an external-standards calibration curve. The plate was placed into the instrument for counting following a 30-minute delay.

### 2.4.8 Calculations and Data Analysis

After the concentration of free  $Zn^{2+}$  was quantitatively determined, the concentration of bound  $Zn^{2+}$  was calculated by subtracting the moles of free  $Zn^{2+}$  from the total moles of  $Zn^{2+}$  originally added and accounting for the volume in the sample-compartment, as seen in Equation 2.1. The concentrations of free versus bound  $Zn^{2+}$  were plotted to create a saturation binding-curve. This curve was then analyzed by non-linear regression software (SigmaPlot 13.0) to calculate an equilibrium-dissociation constant ( $K_d$ ) and number of receptor binding sites ( $E_{max}$ ) for the system.

# 2.4.9 Impact of C-peptide on Zn<sup>2+</sup> Binding to HSA

To assess if C-peptide alters the binding of Zn<sup>2+</sup> to HSA, a competitive-binding experiment was designed and performed. The samples in the experiment contained C-peptide in excess to HSA, so that >99% of the HSA in the sample would be bound to C-peptide. Control samples were also made by adding DDW instead of C-peptide. Samples were prepared to contain 10  $\mu$ M HSA, 25  $\mu$ M C-peptide, and 5  $\mu$ M ZnCl<sub>2</sub> in dialysis buffer, or simply 10  $\mu$ M HSA with 5  $\mu$ M ZnCl<sub>2</sub>. Membrane inserts with dialysis membranes (3.5 kDa MWCO) were placed into eight wells in the device. Then, 950  $\mu$ L of sample were placed into the sample compartment of each well with an equal volume of dialysis buffer in the adjacent buffer compartment. Again, a plate-sticker was placed on top of

the device and the device was incubated and shaken for 6 hours at 37°C, then 400  $\mu$ L of sample from the buffer compartment were removed and analyzed by liquid scintillation counting exactly as described above.

### 2.4.10 Characterization of Incubation-Time Studies for C-peptide

An experiment was designed to quantitatively determine the incubation-time needed for an equilibrium-dialysis experiment to measure C-peptide binding to albumin. The experiment was performed in a similar manner to that explained for fluorescein binding. Membranes with 20kDa MWCO pores were removed from dialysis cassettes (Thermofisher) and integrated into membrane-inserts as described above. A fluorescent C-peptide analogue, modified with a single covalently attached fluorescein isothiocyanate molecule, was used to measure the time needed for the concentration C-peptide to equilibrate in both the buffer and sample compartments. This was accomplished by pipetting 1100 µL of a sample containing 569 nM FITC-C-peptide in dialysis buffer into the sample compartment of the device, followed by 1100 µL of dialysis buffer into the buffer compartment. The entire device was agitated at 220 rpm at 37 °C on an orbital shaker to provide constant mixing at physiological temperature. The printed device was removed from the shaker and placed directly into a plate reader periodically over 75 hours for measuring the fluorescence intensity (excitation wavelength: 485 nanometers, emission wavelength: 512 nanometers, cut-off: 495 nanometers) in the buffer-compartment of the sample well.

#### 2.5 Results

### 2.5.1 Direct Quantitation of Fluorescent Analyte-Ligand in an Equilibrium Dialysis Device

Standards of known analyte concentration were pipetted into separate wells of the device (in both the sample and buffer compartments) and then the device was placed directly into the plate reader for on-chip fluorescence intensity measurements of the buffer compartments to characterize the device's ability to be used for quantitative on-chip measurements. An external standards calibration curve was created from the data (as seen in Figure 2.8), and an R<sup>2</sup> value of 0.998 was measured, therefore demonstrating that increases in the fluorescence intensity in the buffer-compartments directly and linearly correlate with increases in analyte concentration. The

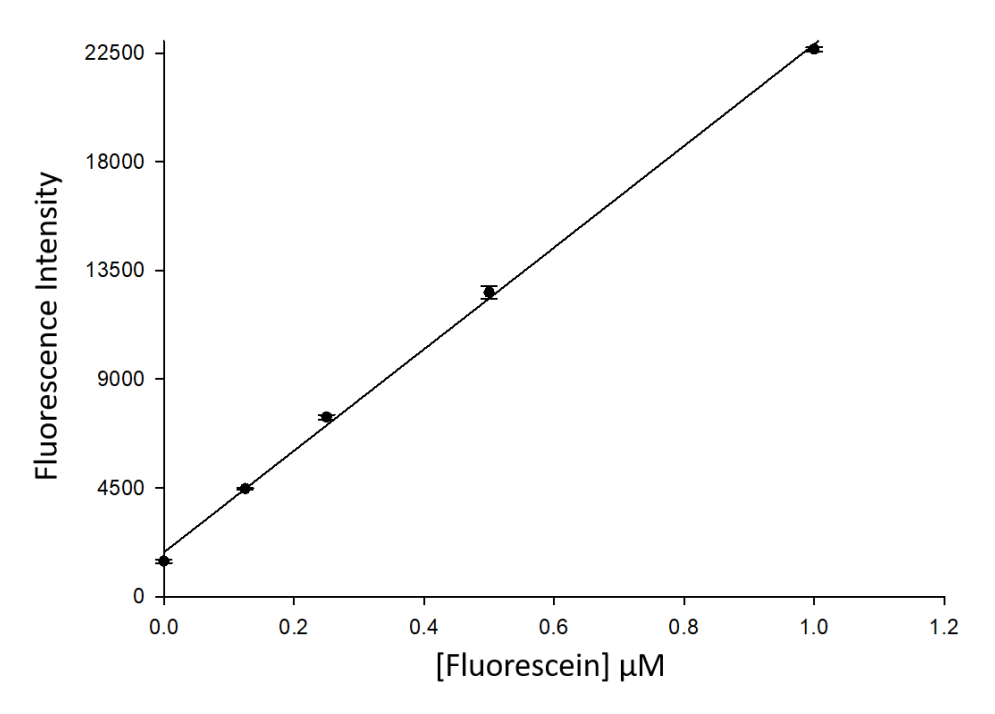


Figure 2.8. **Fluorescein Calibration Curve** External standards calibration curve comparing the fluorescence intensity of fluorescein standards to their known concentrations. The standards were measured by placing the device directly in the plate reader. (Error = std. dev.)

standards were removed from the device, rearranged into different wells, and measured again to ensure that there was no bias or error associated with different wells in the device.

#### 2.5.2 Albumin-Free Equilibration Experiment

Non-specific binding of analyte-ligand to the membrane is a major criticism of equilibrium dialysis, as this would lead to the calculation of a deceptively large binding-constant. Non-specific binding was, therefore, analyzed in the first experiment by pipetting 1.1 mL of 2  $\mu$ M fluorescein (no albumin) in the sample compartment of the first three wells, followed by adding an equal volume (1.1 mL) of buffer to the respective buffer compartments, and measuring the concentration of free fluorescein that diffused into the buffer compartment periodically over the course of 9 hours. Shown in Figure 2.9A, the concentration of fluorescein in the buffer compartment at 6.5 hours (1.04  $\pm$  0.05  $\mu$ M) was not statistically different from that measured at 9 hours (1.08  $\pm$  0.04  $\mu$ M, n =3, p=0.3), therefore the fluorescein concentration had equilibrated and 50% of the original 2  $\mu$ M sample was in each compartment. This result suggests that there is negligible non-specific binding of fluorescein to the membrane.

# 2.5.3 Fluorescein Binding to BSA Measurement

In order for equilibrium dialysis binding measurements to be accurate, samples must be incubated long enough for the free-ligand concentration to equilibrate between the two compartments. An inadequate incubation time will lead to a deceptively high K<sub>a</sub> approximation. An experiment was designed to evaluate the appropriate incubation time for the system, indicated by the time when the concentration of ligand in the buffer compartment ceased to increase. A 1.1 mL sample containing a physiological bloodstream concentration of albumin (42)

mg/mL, or  $^{\sim}632~\mu\text{M}$ ) and 2.0  $\mu\text{M}$  fluorescein was pipetted into the sample compartment of three separate wells, followed by 1.1 mL of dialysis buffer into the corresponding buffer compartments.

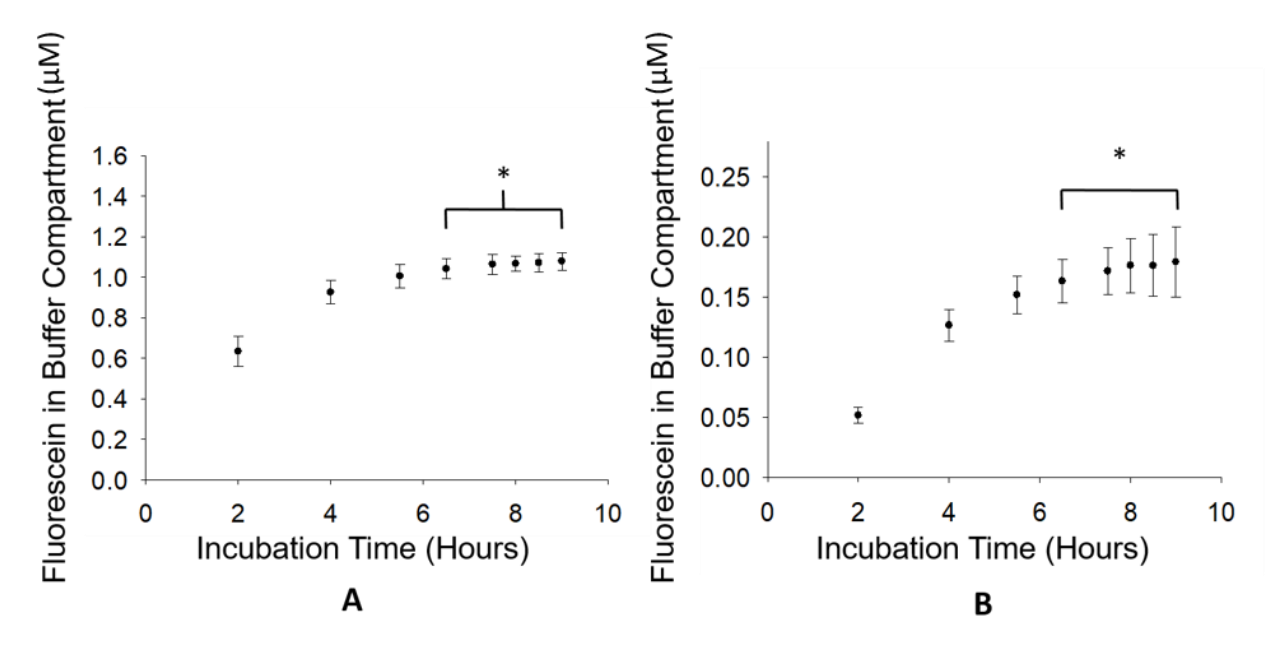


Figure 2.9 Fluorescein Binding and Equilibration Data. A: The samples contain 2.0  $\mu$ M fluorescein and no BSA. The concentration of fluorescein in the buffer-compartment of the well is monitored periodically. The concentration at 6.5 hours is not statistically different than at 9 hours (~ 1  $\mu$ M). In **B**, samples contain 42 mg/mL BSA and 2.0  $\mu$ M fluorescein. The concentration of fluorescein in the buffer-compartment becomes at 6.5 hours (0.16  $\pm$  0.02  $\mu$ M) is equal to that at 9 hours. n=3 \*The difference is not significant p>0.05. (error = std.dev.)

The free fluorescein in the buffer compartment reached a steady concentration after 6.5 hours  $(0.16\pm0.02~\mu\text{M})$ , indicated by a concentration not statistically different from that at 9 hours  $(0.18\pm0.03~\mu\text{M})$ , n=3, p=0.5), as displayed in Figure 2.9B. We can calculate the percentage of fluorescein bound to protein to be  $81\pm3$ % using equation 2.2, which is equal to values reported in the literature for HSA binding to fluorescein (53-83%). We can calculate an approximate global equilibrium constant, or  $n\text{K}_a$ , to be  $1.5\pm0.3\times10^4~\text{M}^{-1}$  using equation 2.3, where n is equal to the number of fluorescein molecules bound per molecule of albumin. This can be compared to values reported in the literature for BSA binding to fluorescein  $(\text{K}_a=2.8\times10^4~\text{M}^{-1})$  or  $n\text{K}_a=8.4\times10^4~\text{M}^{-1}$ ,  $n\text{K}_a=1.45\times10^5~\text{M}^{-1}$  no error was reported for either value).

#### 2.5.4 Automated Equilibrium Dialysis Technique

A 9-hour incubation requiring periodic attention from the user is not practical for many lab scenarios; therefore, an automated equilibrium dialysis technique was developed so that the device could be set up in under one hour and placed into the plate reader to run automatically overnight. The plate reader was simply programmed to make fluorescence measurements of the buffer compartments every 5 minutes for 14 hours, with shaking for one full minute prior to each reading, as seen in Figure 2.7. The binding system reached equilibrium at approximately 12 hours, as indicated by the free-fluorescein concentration at 12 hours (0.16  $\pm$  0.01  $\mu$ M, n=3) being statistically equal to that at 14 hours (0.17  $\pm$  0.01  $\mu$ M, n=3, p=0.42). The average concentration, including standard deviation, of the three wells was plotted in Figure 2.10. The data from this

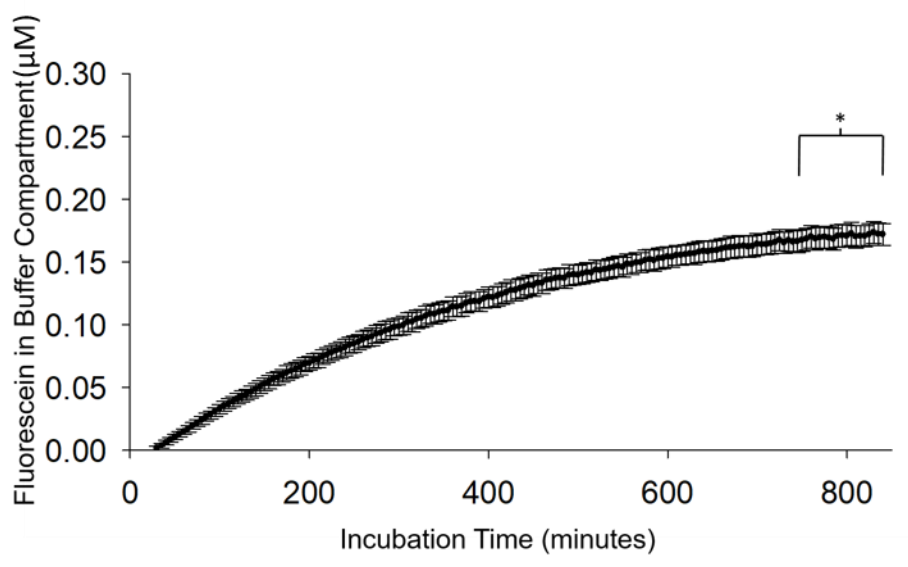


Figure 2.10 **Automated Fluorescein Binding**. For the automated equilibrium dialysis technique, the concentration of fluorescein in the buffer-compartment at 12 hours was not statistically different than at 14 hours (0.17  $\pm$  0.01  $\mu$ M, n=3, p=0.42). (error = std. dev.)

experiment agrees well with the previous experiment and also the values reported in the literature, confirming the device's ability to measure the binding affinity between small fluorescent molecules and large plasma proteins, in a time efficient manner. The time needed to

reach equilibrium for this experiment is longer than the previous experiment, likely because the device was not constantly mixing while in the plate reader as it was on the orbital shaker.

# 2.5.5 Zn<sup>2+</sup> Binding to HSA Equilibrium Time Measurement

The device was then used to analyze the binding affinity between HSA and Zn<sup>2+</sup>. Preliminary experiments were required to measure the time needed for the concentration of free Zn<sup>2+</sup> to reach equilibrium on both sides of the membrane. The incubation time needed to reach equilibrium was indicated by the time when the free concentration of Zn<sup>2+</sup> stopped increasing in the buffer-compartment. As seen in Figure 2.11A, the difference in the concentration of free Zn<sup>2+</sup> after 5.5 hours of incubation was not statistically different from the concentration at 8 or 10 hours, indicating a minimum incubation time of 5.5 hours to be sufficient for the system to reach equilibrium. Thus, future studies used a conservative incubation time of 6 hours.

# 2.5.6 Zn<sup>2+</sup> to HSA Saturation Binding Curve

Experiments were then performed in order to produce a saturation binding-curve between HSA and  $Zn^{2+}$  by holding the concentration of HSA constant and varying the concentration of  $Zn^{2+}$  so that the free concentration of  $Zn^{2+}$  was varied across three orders of magnitude. The experiment was replicated three times and the results can be seen in Figure 2.11B, showing a reproducible binding curve. The three data-points collected for each different concentration of  $Zn^{2+}$  were averaged, plotted, and analyzed by non-linear regression software (SigmaPlot 13.0), to produce the graph in Figure 2.11C. The data fit well to a one-site binding model accounting for non-specific binding with a goodness-of-fit  $R^2$  of 0.998. An equilibrium dissociation constant ( $K_d$ ) and binding stoichiometry (n) was calculated as (5.62  $\pm$  0.93)  $\times$  10<sup>-7</sup> molar and 1.6  $\pm$  0.2, respectively. The  $K_d$  can be converted to a log K value of 6.2  $\pm$  0.1, and can be compared to a previously reported log K value of 6.4  $\pm$  0.8, thus confirming the ability of this device and technique to measure the binding of  $Zn^{2+}$  to HSA.<sup>27</sup>

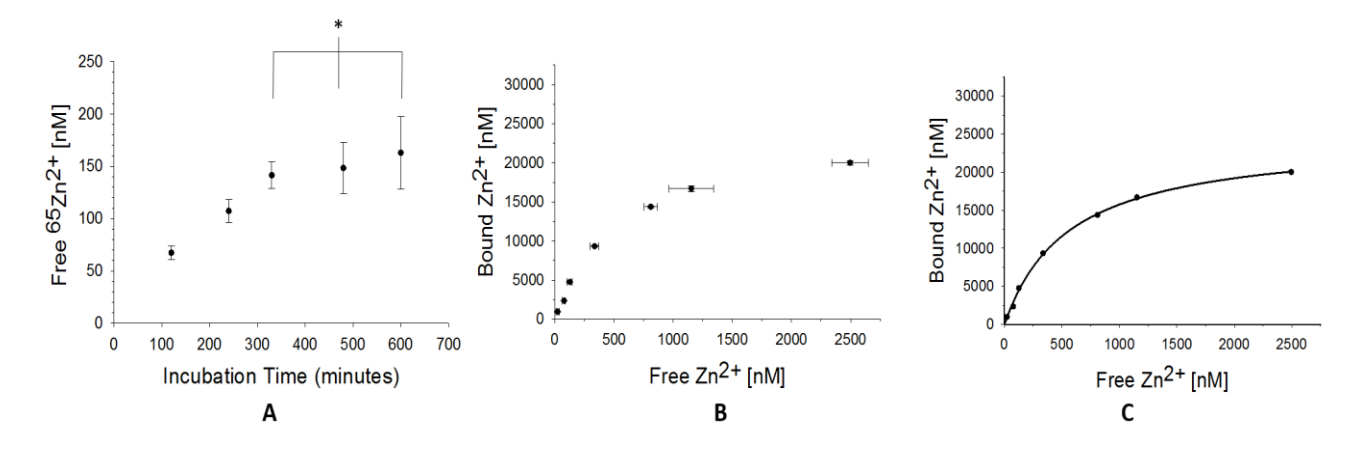


Figure 2.11  $Zn^{2+}$ -HSA Binding and Equilibration. A: Study of time needed to reach equilibrium as measured by the concentration of  $Zn^{2+}$  in the buffer compartment becoming stable. \*values not statistically different (p=0.606).**B**: Saturation binding curve created by placing seven samples containing 15  $\mu$ M HSA and varying concentrations of  $[Zn^{2+}]$  (1-25  $\mu$ M). The samples were placed in separate wells of the device and incubated for 6 hours, (n = 3) error = std. dev. **C**: The mean free and bound  $[Zn^{2+}]$  concentrations were analyzed using non-linear regression software (SigmaPlot 13.0), assuming a one-site binding model and accounting for non-specific binding,  $R^2 = 0.9985$ .

# 2.5.7 Assessment of Competitive Binding by C-peptide

I first hypothesized that C-peptide may alter the binding affinity of  $Zn^{2+}$  to HSA, therefore allowing RBCs to more readily uptake  $Zn^{2+}$  when in solution with C-peptide. To test this hypothesis, HSA was incubated with  $Zn^{2+}$  with or without excess C-peptide, placed in the sample compartment of the device, incubated for 6 hours, and the resulting free  $Zn^{2+}$  in the buffer

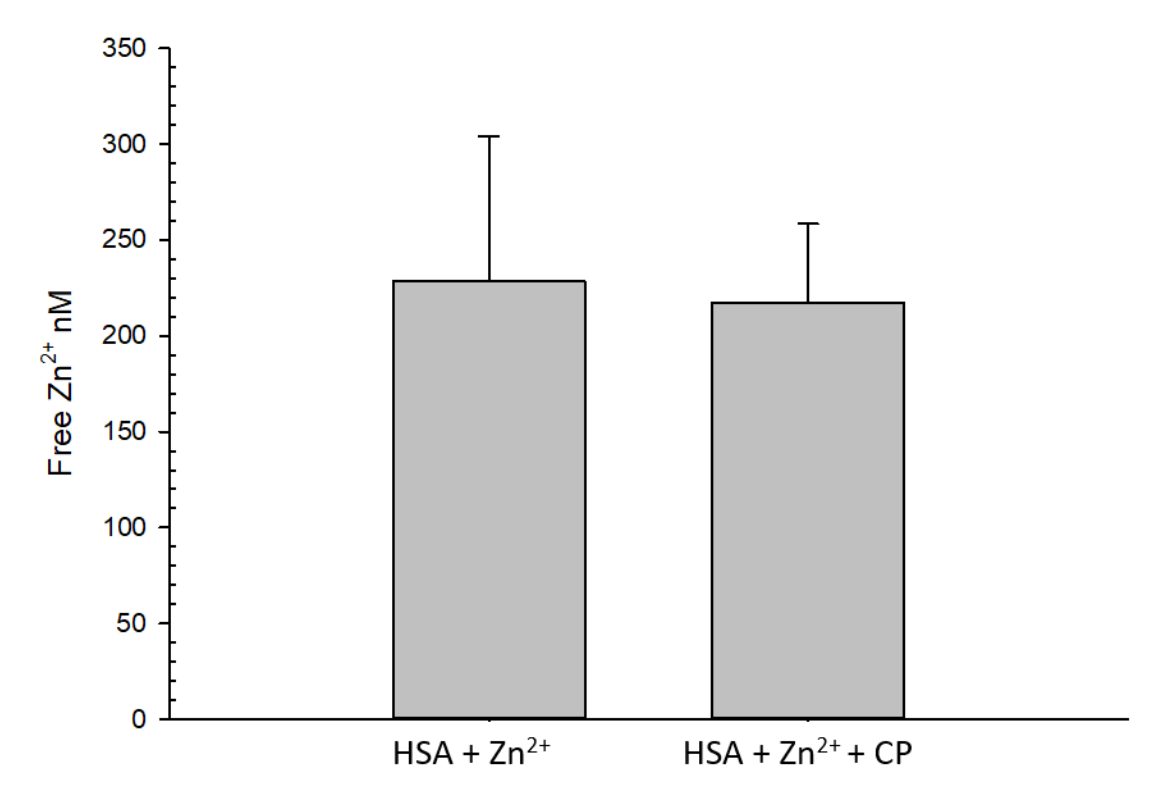


Figure 2.12 Investigation of C-peptide interference with Zn<sup>2+</sup>-HSA binding. Results of equilibrium-dialysis study to measure the impact of C-peptide on Zn<sup>2+</sup> binding to HSA. n= 3, Error = std. dev. compartment was quantified and reported in Figure 2.12. This figure shows that the presence of C-peptide makes no impact on the binding of Zn<sup>2+</sup> to HSA, as the free concentration of Zn<sup>2+</sup> is statistically the same whether C-peptide is present in solution or not.

## 2.5.8 C-peptide Diffusion Time Studies

The performance of the equilibrium-dialysis device and technique to study the binding of C-peptide to proteins was assessed by measuring the time required for a fluorescent analogue of C-peptide to diffuse from the sample compartment, through the membrane, and reach a steady concentration in the buffer compartment. The resulting data are shown in Figure 2.13 and show an incubation time of approximately over 48 hours needed to reach equilibrium.

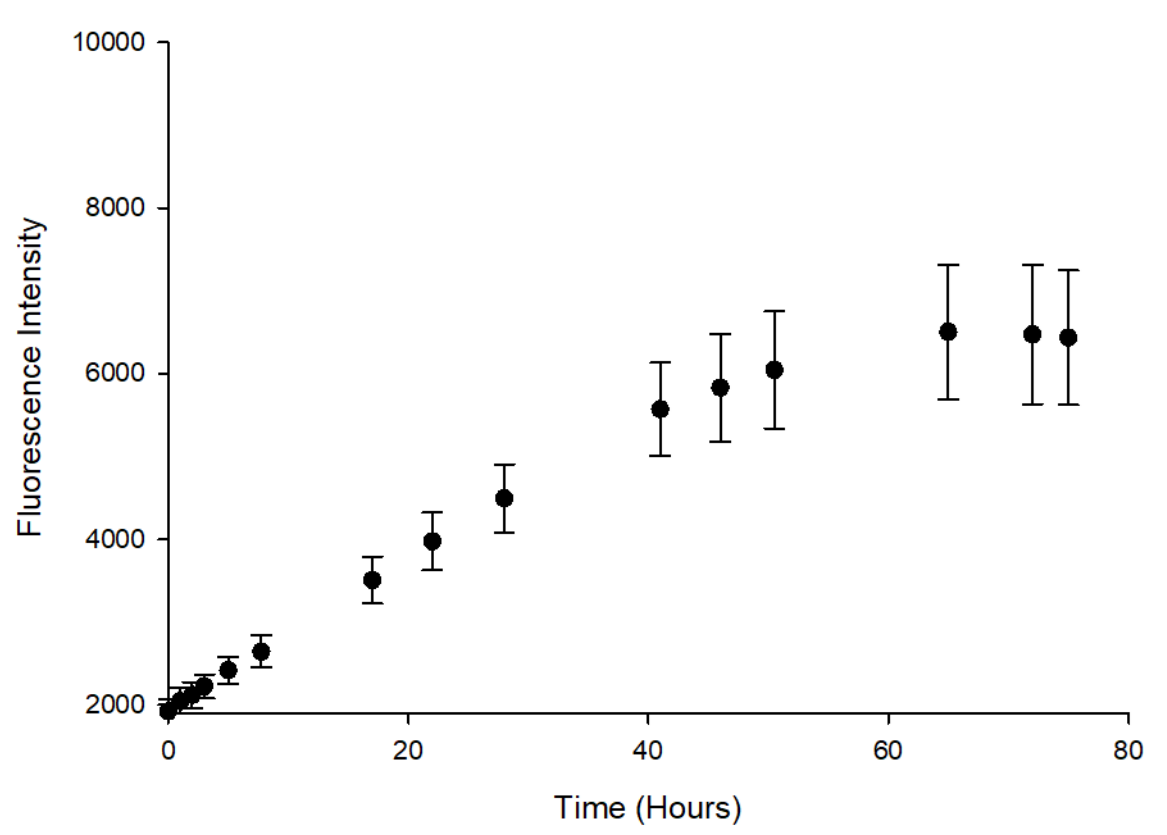


Figure 2.13 **FITC-C-peptide Equilibration Time**. A plot of FITC-C-peptide diffusion from the sample compartment into the buffer compartment over the course of several days by measuring the fluorescence intensity of the buffer compartment periodically. n=3 Error = std. dev.

#### 2.6 Discussion

Here, a device was fabricated using novel 3D-printing technologies to measure the binding constants between small ligands to large proteins. A new technique was developed, called Print-Pause-Print, for integrating membranes directly into Polyjet printed devices. Print-Pause-Print allows researchers to use any commercially purchased membrane to perform membrane-based separations on a device. The device fits into a plate reader for direct measurements of analyte ligands. The device was successfully used to measure the binding of fluorescein to BSA, as well as Zn<sup>2+</sup> to HSA. The device is a platform technology that allows the user to make real-time measurements of analytes diffusing through any commercially available membrane. The information gained from using the device could be used to investigate diffusion rates of molecules through membranes under a variety of conditions or membrane characterization studies. A novel feature of this technology is that it allows real-time detection of when the analyte-ligand has reached equilibrium in the device. This new feature saves time and resources, as a single sample can be monitored for equilibration time, then quantified to calculate a binding constant, without removing the sample from the device, therefore the sample is neither disturbed nor destroyed. Further applications of the device will be discussed in Chapter 5, including using the device to measure the diffusion of a drug through a confluent layer of cells to study cell/tissue permeability. The Print-Pause-Print approach has now been used on a variety of different membrane types, including polycarbonate, polyether-sulfone, and regenerated cellulose.

This device was used to investigate the hypothesis that C-peptide facilitates Zn<sup>2+</sup> uptake to RBCs by altering its ability to bind HSA, which was measured by a competitive binding

experiment. No difference was seen in binding between  $Zn^{2+}$  and HSA in the presence of C-peptide. This leads the authors to believe that  $Zn^{2+}$  and C-peptide bind independently of one another to HSA; however, C-peptide to HSA binding measurements need to be performed in order to be conclusive. Once these measurements are completed, then they should be carried out using human plasma, allowing more information to be discerned about the mechanism of how C-peptide,  $Zn^{2+}$ , and HSA interact with RBCs to increase ATP release from the cells.

The device was also used to investigate the feasibility of measuring C-peptide binding to HSA via equilibrium dialysis; however, the incubation time needed to make the measurement was very long (48+ hours). Incubation times this long are undesirable, as they may lead to unwanted error from a variety of variables, including: inadequate incubation time, bacterial contamination, slow evaporation, protein denaturation, etc. Therefore, Chapter 3 describes the development of ultrafiltration techniques for rapid measurements of C-peptide binding to HSA under a variety of conditions, such as those seen in diabetes.

**REFERENCES** 

#### REFERENCES

- 1. Meyer, J. A.; Froelich, J. M.; Reid, G. E.; Karunarathne, W. K.; Spence, D. M., Metal-activated C-peptide facilitates glucose clearance and the release of a nitric oxide stimulus via the GLUT1 transporter. *Diabetologia* **2008**, *51* (1), 175-182.
- 2. Medawala, W., *Mechanistic and Functional Studies of Zinc (II) Activation of C-peptide and Its Effect on Red Blood Cell Metabolism.* Michigan State University, Department of Chemistry: 2011.
- 3. Liu, Y.; Chen, C.; Summers, S.; Medawala, W.; Spence, D. M., C-peptide and zinc delivery to erythrocytes requires the presence of albumin: implications in diabetes explored with a 3D-printed fluidic device. *Integr. Biol.* **2015**, *7* (5), 534-543.
- 4. Peters Jr, T., *All about albumin: biochemistry, genetics, and medical applications*. Academic press: 1995.
- 5. Koch-Weser , J.; Sellers , E. M., Binding of Drugs to Serum Albumin. *New England Journal of Medicine* **1976**, *294* (6), 311-316.
- 6. Oshannessy, D. J.; Brighamburke, M.; Soneson, K.; Hensley, P.; Brooks, I., Determination of rate and equilibrium binding constants for macromolecular interactions using surface plasmon resonance: use of nonlinear least squares analysis methods. *Anal. Biochem.* **1993**, *212*, 457-468.
- 7. Vuignier, K.; Schappler, J.; Veuthey, J.-L.; Carrupt, P.-A.; Martel, S., Drug–protein binding: a critical review of analytical tools. *Anal. Bioanal. Chem.* **2010**, *398*, 53-66.
- 8. Loo, J. A., Studying noncovalent protein complexes by electrospray ionization mass spectrometry. *Mass Spectrom. Rev.* **1997**, *16* (1), 1-23.
- 9. Melten, J. W.; Wittebrood, A. J.; Willems, H. J.; Faber, G. H.; Wemer, J.; Faber, D. B., Comparison of equilibrium dialysis, ultrafiltration, and gel permeation chromatography for the determination of free fractions of phenobarbital and phenytoin. *J. Pharm. Sci.* **1985**, *74*, 692-694.
- 10. Lebowitz, J.; Lewis, M. S.; Schuck, P., Modern analytical ultracentrifugation in protein science: a tutorial review. *Protein Sci.* **2002**, *11* (9), 2067-2079.
- 11. Hage, D. S., Analysis of Biological Interactions by Affinity Chromatography: Clinical and Pharmaceutical Applications. *Clin. Chem.* **2017**.
- 12. Mallik, R.; Yoo, M. J.; Briscoe, C. J.; Hage, D. S., Analysis of drug–protein binding by ultrafast affinity chromatography using immobilized human serum albumin. *J. Chromatogr. A* **2010**, *1217*, 2796-2803.
- 13. Katz, S. A.; Paritt, C.; Purdy, R., Equilibrium dialysis: A laboratory experiment. *J. Chem. Educ.* **1970,** *47* (10), 721.

- 14. Reinard, T.; Jacobsen, H.-J., An inexpensive small volume equilibrium dialysis system for protein-ligand binding assays. *Anal. Biochem.* **1989,** *176* (1), 157-160.
- 15. Zamek-Gliszczynski, M. J.; Ruterbories, K. J.; Ajamie, R. T.; Wickremsinhe, E. R.; Pothuri, L.; Rao, M. V. S.; Basavanakatti, V. N.; Pinjari, J.; Ramanathan, V. K.; Chaudhary, A. K., Validation of 96-well Equilibrium Dialysis with Non-radiolabeled Drug for Definitive Measurement of Protein Binding and Application to Clinical Development of Highly-Bound Drugs. *J. Pharm. Sci.* **2011**, *100* (6), 2498-2507.
- 16. Rowe, D. J.; Bobilya, D. J., Albumin facilitates zinc acquisition by endothelial cells. *Proceedings of the Society for Experimental Biology and Medicine* **2000**, *224* (3), 178-186.
- 17. Ockner, R. K.; Weisiger, R. A.; Gollan, J. L., Hepatic uptake of albumin-bound substances: albumin receptor concept. *American Journal of Physiology-Gastrointestinal and Liver Physiology* **1983**, *245* (1), G13-G18.
- 18. Waters, N. J.; Jones, R.; Williams, G.; Sohal, B., Validation of a rapid equilibrium dialysis approach for the measurement of plasma protein binding. *J. Pharm. Sci.* **2008**, *97*, 4586-4595.
- 19. Pinger, C. W.; Heller, A. A.; Spence, D. M., A Printed Equilibrium Dialysis Device with Integrated Membranes for Improved Binding Affinity Measurements. *Anal. Chem.* **2017**, *89* (14), 7302-7306.
- 20. Cannon, D. M.; Kuo, T.-C.; Bohn, P. W.; Sweedler, J. V., Nanocapillary array interconnects for gated analyte injections and electrophoretic separations in multilayer microfluidic architectures. *Anal. Chem.* **2003**, *75*, 2224-2230.
- 21. Genes, L. I.; Tolan, N. V.; Hulvey, M. K.; Martin, R. S.; Spence, D. M., Addressing a vascular endothelium array with blood components using underlying microfluidic channels. *Lab Chip* **2007**, *7*, 1256-1259.
- 22. Li, F.; Smejkal, P.; Macdonald, N. P.; Guijt, R. M.; Breadmore, M. C., One step fabrication of a microfluidic device with an integrated membrane and embedded reagents by multimaterial 3D printing. *Anal. Chem.* **2017**, *89*, 4701–4707.
- 23. Hawkins, B. T.; Egleton, R. D., Fluorescence imaging of blood–brain barrier disruption. *Journal of Neuroscience Methods* **2006**, *151* (2), 262-267.
- 24. Spencer, T.; Phillips, R. P.; Sharp, P. F.; Forrester, J. V., Automated detection and quantification of microaneurysms in fluorescein angiograms. *Graefe's archive for clinical and experimental ophthalmology* **1992**, *230* (1), 36-41.
- 25. Nagataki, S.; Matsunaga, I., Binding of fluorescein monoglucuronide to human serum albumin. *Investigative ophthalmology & visual science* **1985**, *26* (8), 1175-1178.
- 26. Li, W.; Rockey, J. H., Fluorescein binding to normal human serum proteins demonstrated by equilibrium dialysis. *Archives of Ophthalmology* **1982**, *100* (3), 484-487.
- 27. Goumakos, W.; Laussac, J.-P.; Sarkar, B., Binding of cadmium (II) and zinc (II) to human and dog serum albumins. An equilibrium dialysis and 113Cd-NMR study. *Biochem. Cell Biol.* **1991**, *69*, 809-820.

# <u>Chapter 3: Measuring C-peptide and Zinc Binding to Glycated Human Serum Albumin via 3D-Printed Ultrafiltration Devices</u>

#### 3.1 Introduction

In 2016, the Spence group reported that the delivery of C-peptide and Zn<sup>2+</sup> to red blood cells (RBCs) requires the carrier protein albumin.<sup>1</sup> It was reported that RBCs under flow-conditions release significantly more ATP when exposed to a combination of C-peptide and Zn<sup>2+</sup>, but only in the presence of albumin, as seen in Figure 3.1. The discovery of the importance of albumin to the efficacy of C-peptide creates questions regarding albumin as a variable in C-peptide's mechanism of action.

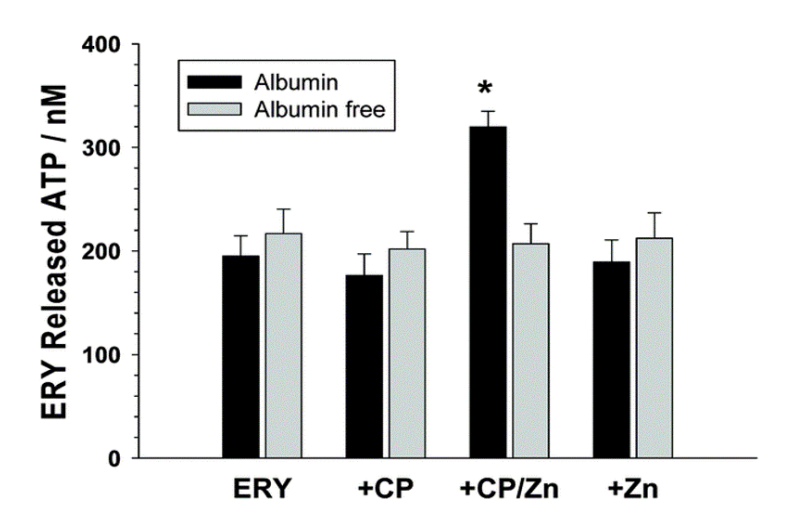


Figure 3.1 ATP release from flowing RBCs treated with C-peptide, Zn<sup>2+</sup>, and albumin. Liu et al: Healthy RBCs were treated with different combinations C-peptide (CP), Zn<sup>2+</sup>, and albumin. The cells were then flowed through a 3D-printed device and the subsequent ATP release from the cells was quantified.

There is literature dating over 30 years regarding diabetic human serum albumin (HSA) and its differences from albumin in non-diabetic subjects.<sup>2-6</sup> Under the high-glucose conditions found in the diabetic bloodstream, glucose reaction with plasma proteins (such as HSA) are enhanced.<sup>7-9</sup> The covalent addition of glucose to HSA results in major structural and functional changes to the protein, creating what is called glycated human serum albumin (gHSA).<sup>7, 10-13</sup> Some of these

changes include altering the secondary and tertiary structure of HSA and changing the binding affinity of specific ligands such as drugs, hormones, and fatty acids to HSA.<sup>5, 7, 12, 14-20</sup> These changes in binding affinity can alter how the ligands are transported throughout the body and alter their bioavailability.

The mechanism of HSA glycation, known as the Maillard reaction, is featured in Figure 3.2. $^{7/2}$  The extent of HSA glycation in a person's bloodstream directly correlates with the average glucose concentration in the bloodstream, with healthy subjects having approximately  $4.7 \pm 0.8\%$  of their HSA in the glycated form, compared to  $23.3 \pm 4.5\%$  in T1D patients. $^{17/22}$  Therefore, the individual interactions between C-peptide,  $Zn^{2+}$ , RBCs, and gHSA are of significant interest and measuring these interactions are important because HSA glycation may alter the bioavailability of C-peptide to RBCs in people with diabetes. If this is the case, gHSA may interfere with the bioactivity of C-peptide in the T1D bloodstream, and administering non-glycated HSA to T1D patients as part of a C-peptide replacement therapy may be required.

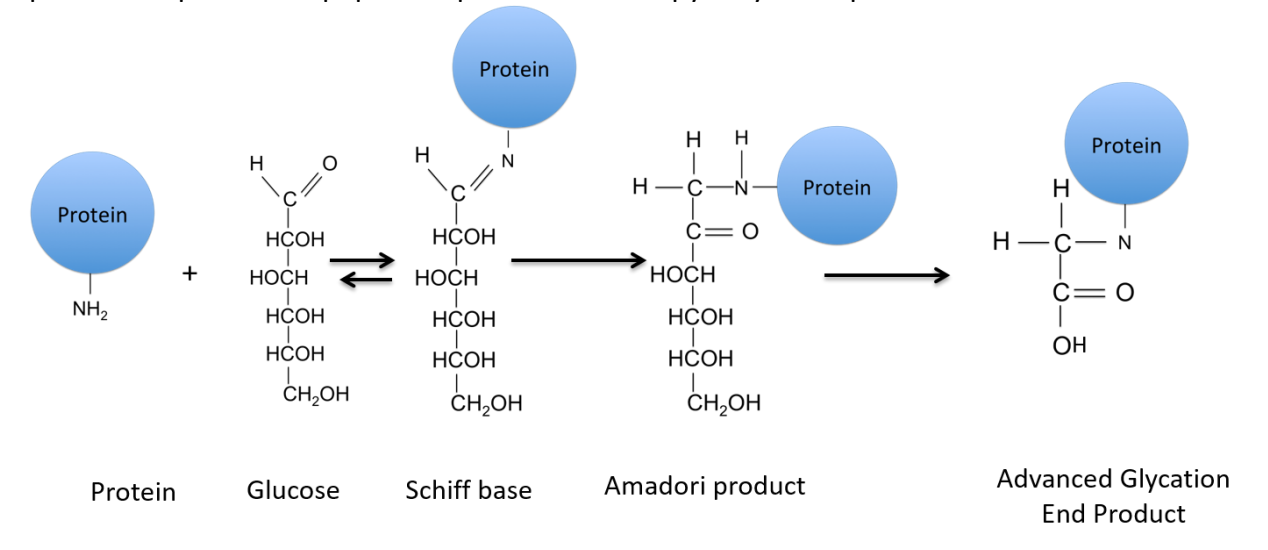


Figure 3.2 The Maillard Reaction of Protein Glycation. An open-chain molecule of glucose interacts with a terminal amine group on a protein to form a labile Schiff base. Over time, the Schiff base reconfigures into a more stable Amadori product. These glycation reactions can be followed by additional events to form irreversible advanced glycation end products (AGEs) such as carboxymethyl-lysine.

Two new 3D-printed ultrafiltration devices were created and used for performing binding measurements to better understand the interactions between HSA, C-peptide, and Zn<sup>2+</sup> under diabetic conditions (i.e. glycation/high glucose). Ultrafiltration uses pressure to drive solution and low molecular weight compounds through a size-exclusion membrane while retaining high molecular weight compounds.<sup>23-25</sup> This technique requires a small volume of sample to be separated from the bulk solution for analysis. In ultrafiltration, the equilibrium of the binding system is not affected when the separated portion (the ultrafiltrate) is low in volume (<10% of the total volume), as there is only a minimal change to the protein concentration. Therefore, the concentration of ligand in the ultrafiltrate equals the concentration of free-ligand in the bulk sample. Commercial devices exist for performing protein binding experiments by ultrafiltration; however, we propose that custom-made filtration devices provide a cost effective, adaptable, and contaminate-free membrane system. Here, a 3D-printed syringe-compatible device and a centrifuge-compatible device were developed for the determination of binding constants between proteins and ligands. The syringe-based system was used to investigate the binding of Zn<sup>2+</sup> and C-peptide to normal HSA (nHSA) and a commercially purchased gHSA that closely mimics the HSA found in people with T1D, to determine if glycation of HSA affects the ligand-protein interactions. The centrifuge-compatible device was characterized by measuring Zn<sup>2+</sup> binding to nHSA, and then used for competitive binding assays to investigate whether Zn<sup>2+</sup> or glucose impacts the binding of C-peptide to HSA.

#### 3.2 Methods

## 3.2.1 Membrane Preparation

Spectra/Por® flat sheet dialysis membranes (12-14 kilodalton MW cut off, regenerated cellulose, Spectrum Laboratories, Inc. Rancho Dominguez, CA) were used as received, and Slide-a-Lyzer™ dialysis cassettes (20 kilodalton MW cut off, ThermoFisher Scientific, Waltham, MA) were used after the membrane portion was removed with a razor blade. The membrane sheets were placed between two sheets of wax paper and cut with an H-Series 5th Generation CO₂ Desktop Laser cutter (Full Spectrum Laser, Las Vegas NV) to make circles with a dimeter of 15mm. The laser cutter is housed at the Main Library at Michigan State University. The power of the laser cutter was set to 22% and a speed of 100%. Alternatively, the membranes could be punched out using a steel hole-punch.

### 3.2.2 Support-Free Printing for Direct Membrane Integration

A membrane-holding O-ring was designed using CAD software (Autodesk Inventor Professional, San Rafael, CA) and submitted to a J750 Multi-Material Polyjet 3D-printer (Stratasys, Eden Prairie, MN) as a .STL file. The exact dimensions of this O-ring are shown in Figure 3.3. An important feature of this O-ring was that it was printed without the use of support material, a waxy substrate the printer uses to maintain certain structures. The printer was set to print without the use of support material by accessing the Stratasys Parameters Manager page on the computer embedded within the printer. Here, the following parameters were changed from their previous values to zero millimeters: Carpet\_height, Carpet\_protectorZ, and ImproveSupport thickOfPedestal. Changing these values instructs the printer to not add any

support-material to the bottom of the final device, in this case, the O-ring. The need for this strategy is shown in Figure 3.3, where support material is covering the membrane. In order to seamlessly seal the membrane into the device without the use of glue or adhesives, the membranes were integrated into the device by a *Print-Pause-Print* technique previously described. The printer is started and allowed to print half of the device before the printer was paused and the freshly cut membranes were laid on the center of the O-rings. Then, the printing process was resumed, layering material over the edges of the membrane, and curing the material with UV-light thereby sealing the membrane into the device. The final product without any post-processing is shown in Figure 3.3.

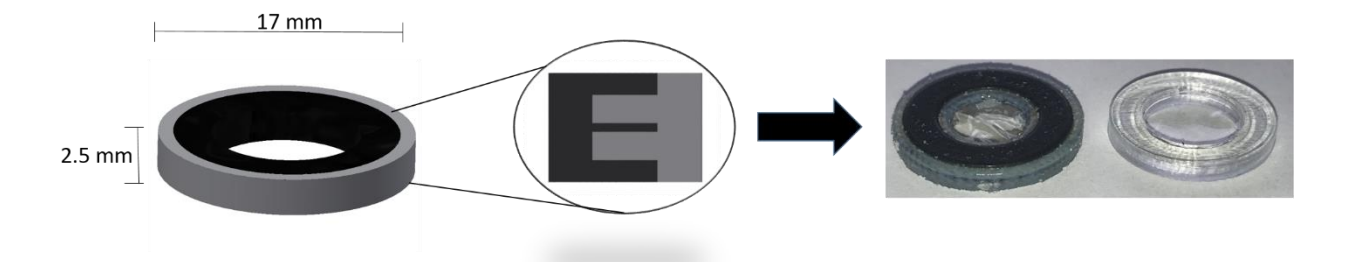


Figure 3.3 **Membrane-Holding O-ring.** Left: Diagram showing dimensions of the O-ring drawn in CAD software. Right: Membrane containing O-ring printed with and without support material. Note: The O-ring printed with support material is printed in TangoBlack and VeroClear, where the O-ring without support is in clear Tango+ and VeroClear.

## 3.2.3 Design and Fabrication of the 3D-Printed Syringe Device for Ultrafiltration

A device was fabricated to house the membrane-holding O-ring and to fit on the end of a 1 mL plastic syringe. The device has four major components: the top, the bottom, the membrane support, and the membrane-holding O-ring. The four parts, shown in Figure 3.4A, are assembled by threading the top into the bottom, thereby holding the O-ring and support in between.

The device utilizes the ability of the Polyjet 3D printer to print multiple materials that have rubber-like properties (Tango+) or hard plastic properties (VeroClear). The top has a Tango+

gasket in which the syringe is inserted, resulting in a sealed connection. The device has 3D printed threads with a standard metric thread size/pattern of M20x1 RH. The device features a layer of Tango+ on both the top and bottom pieces to provide a gasket to give a water-tight seal around the membrane O-ring. The membrane support is printed out of VeroClear and features a 1 mm x 1 mm grid to prevent the membrane from stretching or deforming during the separation. The assembled device is shown in Figure 3.4.

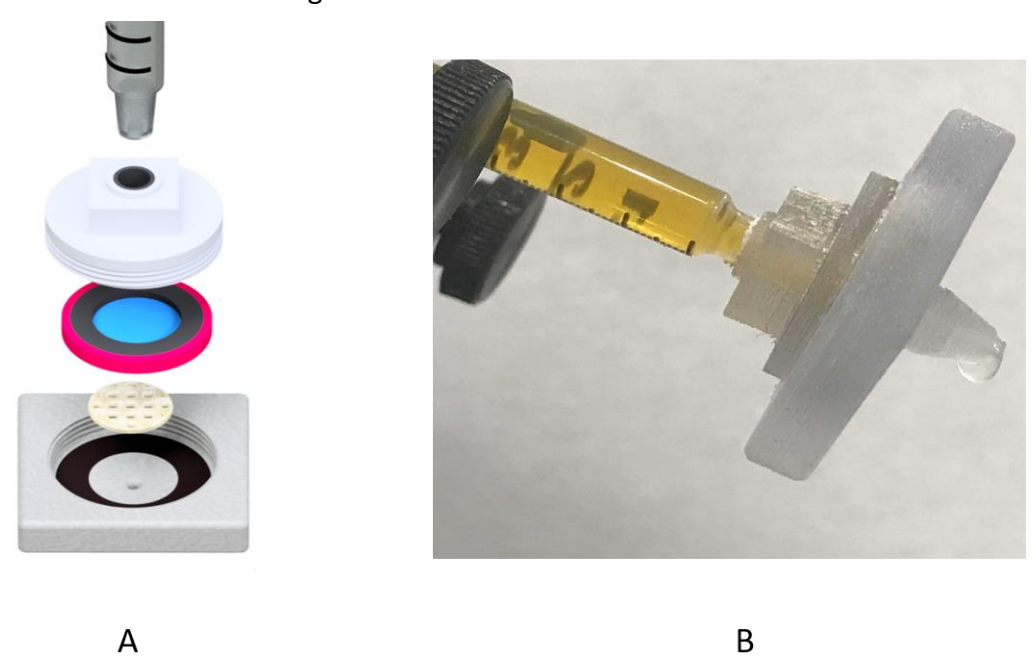


Figure 3.4 **3D-Printed Syringe-Enabled Ultrafiltration Device. A.** A schematic diagram showing how all of the parts of the syringe-based device fit together. **B.** A photograph shows an orange-colored protein solution in the syringe which cannot pass through the membrane, and therefore a clear drop of buffer is eluted from the device

#### 3.2.4 3D-printed Centrifuge-Enabled Ultrafiltration Device

First, three different .stl files were created, as seen in Figure 3.5. The bottom layer is a hard plastic support, the next two layers are a tacky Tango+ material that is designed to hold a polycarbonate membrane, the third and fourth layers were also designed to hold another membrane, and the fifth layer was designed to hold the liquid sample. The device was designed

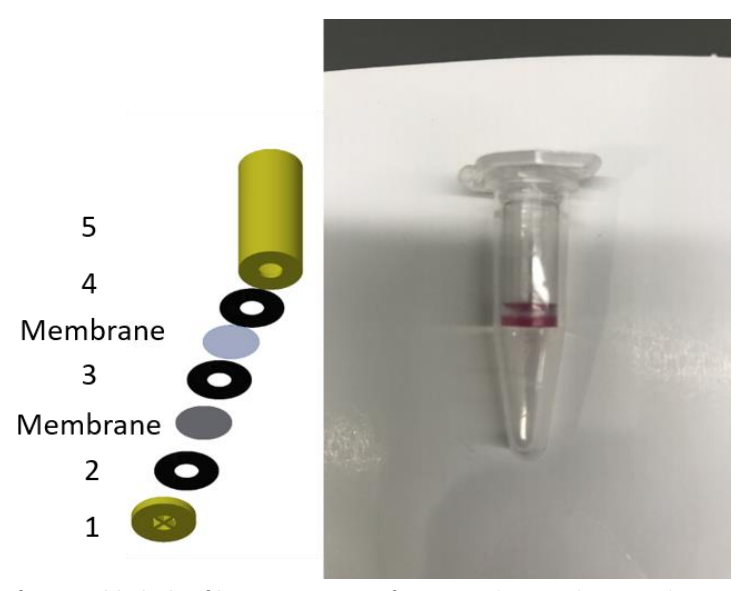


Figure 3.5 **3D-printed Centrifuge-Enabled Ultrafiltration** Device Left:. A CAD drawn schematic diagram showing the individual parts of the 3D-printed device, including both membranes. The numbers refer to the order in which each part was printed. Right: A photograph of the device ready to be used by being placed into a centrifuge tube.

as a small cup with holes in the bottom that fits into a 1.7 mL centrifuge tube, seen in Figure 3.5.

The printer was set to "support free" mode, as previously described and the first layer was printed to completion. Then, the printer settings were accessed to instruct the printer to lower the build tray a distance equal to the height of the object previously printed. The next model (layer 2) was submitted to the printer as a new device, instructing the printer to lay material (a 0.1 millimeter layer of Tango+) on top of the previous object. Once this model was completed, a polycarbonate membrane (0.4 micrometer pores) was set on top of the new layer, and once again the build tray was lowered and the next layer was printed (0.1 millimeter layer of Tango+). A dialysis membrane was then inserted, and the process of lowering the print tray and printing a layer of Tango+ was repeated. The final part of the device, which holds the liquid sample, was then printed to create the final model shown in Figure 3.5, a 3D-printed ultrafiltration device. This novel printing process allows for complex geometries to be 3D-printed without the use of support-material. Desirable centrifuge-times and speeds were characterized by loading the

device (containing a 20kDa MWCO membrane) with 200  $\mu$ L of H<sub>2</sub>O, centrifuging at different rates and times, and massing the ultrafiltrate to produce the graph seen in Figure 3.6.

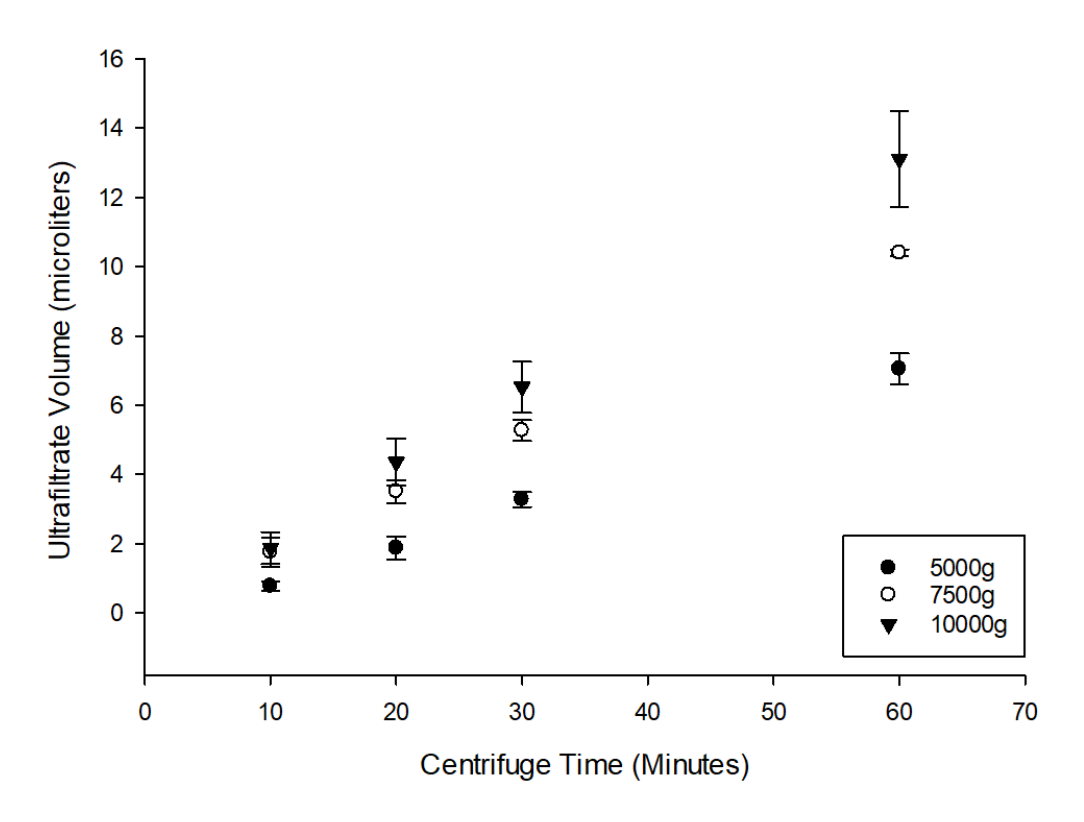


Figure 3.6 **Centrifuge-Device Speed and Time characterization.** A graph showing the effect of different centrifuge speeds and times required to produce an ultrafiltrate sample. From this data, an optimal centrifuge setting of 10,000g and 60 minutes was used for future studies. n=3, error = s.d.

#### 3.2.5 Sample Preparation

Human serum albumin (nHSA, product number: A3782) and glycated human serum albumin (gHSA, product: A8301, lot: SLBT1722) were purchased from Sigma (Sigma Aldrich, St. Louis MO). The gHSA was reported by the manufacturer to have a degree of modification of approximately 3 moles of hexose per mole of albumin. A buffer containing 10.5 mM Tris (pH 7.4) and 150 mM NaCl was prepared. Approximately 10 mg of either nHSA or gHSA were diluted to 1 mL with the Tris-NaCl buffer, and sterile filtered through Millex-GV 0.22 micron filter units from Merck

Millipore (Burlington, MA). The protein concentration was then quantitatively determined using the Pierce bicinchoninic acid (BCA) assay (ThermoFisher Scientific) prior to experiments.

For Zn<sup>2+</sup>-protein binding experiments, a 1 mL solution containing 10  $\mu$ M nHSA or gHSA and radioactive <sup>65</sup>ZnCl<sub>2</sub> stock (PerkinElmer) was prepared in the Tris-NaCl buffer, such that the final Zn<sup>2+</sup> concentrations ranged from 1.5  $\mu$ M to 32.5  $\mu$ M. The influence of glucose on Zn<sup>2+</sup> binding to nHSA was assessed by creating a separate buffer solution containing 20 mM glucose that was used to make a final sample containing 182  $\mu$ M glucose, 10  $\mu$ M nHSA, and 5  $\mu$ M Zn<sup>2</sup>.

Crude C-peptide was purchased from Peptide 2.0 (Chantilly, VA) and purified to > 99% by HPLC. To measure the binding of C-peptide to nHSA, a C-peptide stock of approximately ~100  $\mu$ M was prepared in distilled and deionized water (DDW). An aliquot of the peptide solution was then mixed with either nHSA or gHSA in buffer to make 0.7 mL samples containing a final albumin concentration of 10  $\mu$ M and varying C-peptide concentrations from 1-30  $\mu$ M.

Samples for use in the centrifugation device were prepared in 1.7 mL tubes as follows. For comparing the centrifuge device to the syringe device, a 1 mL sample of 10 μM HSA and 5.0 μM radioactive Zn<sup>2+</sup> was prepared in the Tris/NaCl buffer. To measure the effect of glucose on the affinity of C-peptide binding to HSA, a 13 mM glucose solution was prepared by weighing out an appropriate amount of dextrose (Sigma Aldrich, St. Louis, MO) and diluting to 50 mL with Tris/NaCl buffer. Also, to measure the effect of Zn<sup>2+</sup> on the affinity of C-peptide to HSA, ZnCl<sub>2</sub> was dried and weighed out to create a 50 mL solution of 2.0 mM Zn<sup>2+</sup>. Samples were then prepared up to 1 mL and prepared to contain 5 mg/mL HSA and 20 nM C-peptide with either 1.1 mM or 0.0 mM dextrose. Samples were also prepared with 5 mg/mL HSA and 20 nM C-peptide with

either 200 or 0  $\mu$ M Zn<sup>2+</sup>. Lastly, a sample was prepared to contain 5 mg/mL gHSA and 20 nM C-peptide to confirm the measurement made by the syringe-device, and also to study whether glycation changed the affinity of C-peptide to HSA when determined at more relevant concentration ratios of HSA to C-peptide.

#### 3.2.6 Syringe-Device Setup

Some parts of the syringe device, particularly the threaded top and bottom parts, contained support material requiring removal by hand. These parts were soaked overnight in a 500-mL solution that was over-saturated with sodium bicarbonate. The sodium bicarbonate increases the pH of the solution that helps to solubilize the remaining support-material for easy removal. The parts were then thoroughly rinsed in DDW to remove the remaining support-material and dried with compressed air. A 1-mL syringe was then inserted firmly into the top component, and subsequently filled with a 1-mL aliquot of sample. The membrane O-ring was then placed into the top portion followed by the membrane support (which was shown assembled in Figure 3.4A) and the device was thread together. The entire device was vortexed for approximately one second, which helps to move any trapped air-bubbles above the membrane to the top of the syringe. Finally, the entire device was connected to a syringe pump set to a flow rate of  $500 \, \mu L/m$  min to push a 12-15  $\mu L$  aliquot of sample through the membrane. All experiments were performed at room temperature.

## 3.2.7 Centrifuge Device Set Up

Once printed, the device required zero post processing before use due to the novel printing techniques described above. The device was loaded with 200  $\mu$ L of sample and centrifuged at 10,000g for 60 minutes, pushing approximately 13  $\mu$ L of ultrafiltrate through to the bottom of the centrifuge tube. Then 10  $\mu$ L of the sample were removed for analysis.

## 3.2.8 Sample Analysis of Zn<sup>2+</sup>

The syringe device was placed over a 1.7 mL centrifuge tube, allowing the 12-15  $\mu$ L drop to be collected in the tube. Next, 10  $\mu$ L of sample were pipetted into a 96-well scintillation plate and mixed with 100  $\mu$ L of scintillation cocktail. A calibration curve was prepared with external standards to quantitatively determine signals obtained from samples. Each standard was determined by adding a 10  $\mu$ L aliquot of each standard into the plate wells and mixed with the scintillation cocktail. The plate was inserted into a scintillation counter (PerkinElmer MicroBeta TriLux 1450) set with a delay of 30 minutes prior to measurement.

## 3.2.9 Sample Analysis for C-peptide

A 12-15  $\mu$ L drop was collected as described above; however, the C-peptide was quantitatively determined using an ELISA kit for Human C-peptide from ALPCO (Salem, NH) by comparing the sample to standards provided with the ELISA kit.

#### 3.2.10 Calculations and Data Analysis

The concentration of free ligand (either Zn<sup>2+</sup> or C-peptide) in the sample was determined by quantifying the amount of ligand eluted through the membrane. After quantifying the amount

of free-ligand in the sample, the amount of ligand bound to protein was calculated using Equation 3.1, and the percentage bound to protein was calculated using Equation 3.2.

$$(3.1)$$
:  $[Bound\ Ligand] = [Total\ ligand] - [Free\ ligand]$ 

(3.2): 
$$Percent \ Protein \ Bound = \frac{[Bound \ ligand]}{[Total \ ligand]}$$

The concentration of bound ligand was determined by subtracting the concentration of free ligand from that of the total ligand in the sample. A plot of the free vs. bound ligand was created to examine the saturation binding-curve, which was then analyzed by non-linear regression software (SigmaPlot 13.0) for the calculation of a binding ( $K_d$ ) and stoichiometry (n) constant.

#### 3.3 Results

## 3.3.1 Zn<sup>2+</sup> to HSA – Syringe Device

The ability of the device to effectively determine ligand-protein binding affinity was characterized by measuring the binding affinity of Zn<sup>2+</sup> to nHSA (Figure 3.7), followed by comparison with

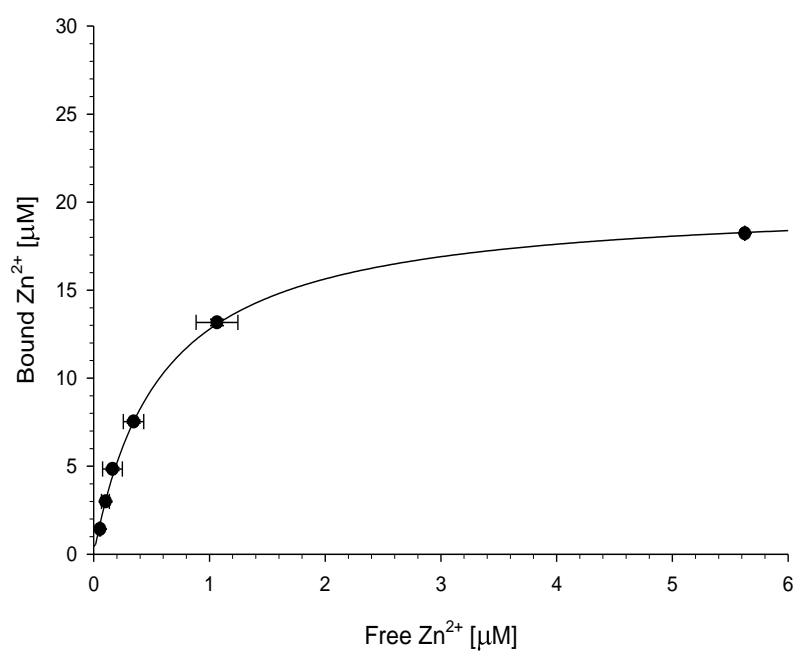


Figure 3.7 **Saturation Binding Curve between Zn^{2+} and HSA.** A saturation binding curve was plotted from ultrafiltration data measured using  $Zn^{2+}$  and HSA. The data was analyzed using non-linear regression software (SigmaPlot 13.0) and the  $K_d$  and binding stoichiometry was calculated. The goodness of fit was calculated as  $R^2 = 0.9989$ . n = 3-4. error = s.d.

literature values. The experimentally determined binding constant ( $K_d = 5.77 \pm 0.19 \times 10^{-7} \, M$ ) and stoichiometry ( $n=2.0 \pm 0.2$ ) are statistically equal to values measured by equilibrium dialysis ( $K_d = 5.62 \pm 0.93 \times 10^{-7} \, M$ ,  $n=1.6 \pm 0.2$ ) in Chapter 2, as well as literature values. <sup>26-27</sup> Collection of a 12-15  $\mu$ L drop of sample through a 12-14 kDa MWCO membrane required an average of 36.0  $\pm$  5.1 minutes (n=4) using the syringe-pump settings described above. To determine the effect of glucose on  $Zn^{2+}$  binding to HSA, a study was performed where glucose was added directly to the protein sample, followed by addition of  $Zn^{2+}$  and subsequent ultrafiltration. Additionally, a

commercially purchased glycated form of HSA was used, as it contains molecules of glucose covalently attached to the protein as a result of a long-term glucose incubation. Both of these

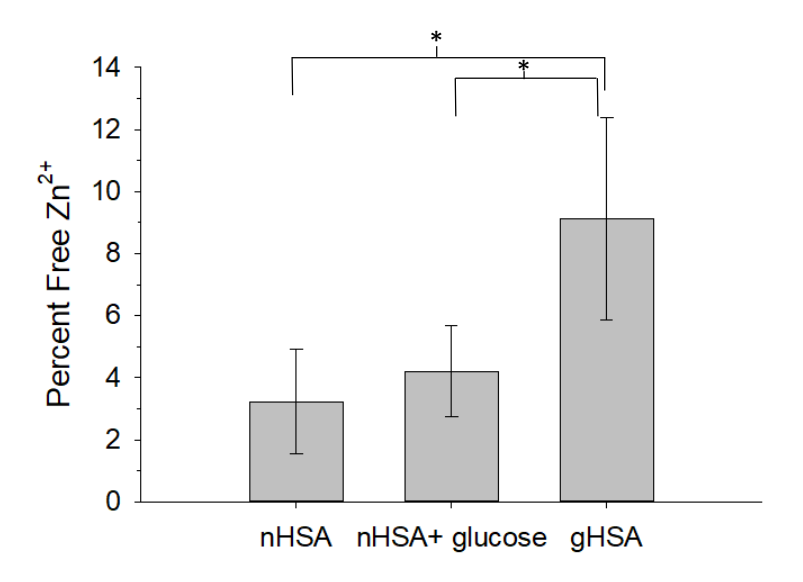


Figure 3. 8 Ultrafiltration data for  $Zn^{2+}$  binding to HSA with and without glucose or glycated HSA. The percentage of free  $Zn^{2+}$  in the sample containing glucose (n=5) was not statistically different than the control that contained no glucose (n=3). The glycated HSA sample (n=5) contained statistically more free- $Zn^{2+}$ \*(p<0.05) than both the control sample and the sample containing glucose., error = s.d.

samples were compared to a control sample, which contained no glucose and nHSA. Each sample contained 10.0  $\mu$ M nHSA or gHSA and 5.0  $\mu$ M Zn<sup>2+</sup>, while one of the nHSA samples contained a glucose concentration of 182  $\mu$ M, which is approximately equal to the concentration ratio of glucose-to-HSA in the bloodstream of people with diabetes (7-11 mM glucose: 0.63 mM HSA). The unbound, or free-Zn<sup>2+</sup> was determined and the percentage of free and bound Zn<sup>2+</sup> was calculated according to Equation 3.2 and shown in Figure 3.8. The percentage of free Zn<sup>2+</sup> in the nHSA sample and glucose-containing nHSA sample were not statistically different (3.2  $\pm$  1.7% (n=3) and 4.2  $\pm$  1.4% (n=5), respectively). However, the percentage of free Zn<sup>2+</sup> in the gHSA sample was approximately 2-3 fold higher than the nHSA sample (9.1  $\pm$  3.2 %, n=5). Therefore, the percentage of protein-bound Zn<sup>2+</sup> in the final samples were as follows: nHSA (96.7  $\pm$  1.7%), nHSA with added glucose (95.8  $\pm$  1.4%), and gHSA without added glucose (90.9  $\pm$  3.2%).

## 3.3.2 C-peptide to HSA - syringe device

The syringe device was then used to measure the binding affinity between C-peptide and nHSA. The syringe was loaded with 0.7 mL of sample and a 20 kDa MW cut off membrane was placed into the device. When the device was connected to the syringe pump with the same settings as mentioned above, it took 25.0  $\pm$  0.9 minutes to collect a 12-15  $\mu$ L sample, which was then analyzed by ELISA. A saturation binding curve of nHSA to C-peptide, shown in Figure 3.9, was analyzed and found to have an equilibrium binding constant of  $K_d$ = 2.4  $\pm$  0.3  $\times$  10<sup>-6</sup> M. The equilibrium binding constant measured is similar to results obtained using isothermal titration calorimetry (ITC) ( $K_d$  = 5.7  $\pm$  2.1  $\times$  10<sup>-6</sup> M at 25°C). Next, a single-point comparison experiment was performed to study the effect of glycation of HSA on binding to C-peptide (Figure 3.9), by making samples containing 10  $\mu$ M HSA and 5.0  $\mu$ M C-peptide. No significant difference in binding was observed between nHSA and gHSA binding to C-peptide (22.3  $\pm$  6.2% free and 21.2  $\pm$  7.4 %, free, respectively). This equates to a percent protein bound C-peptide in the sample to be 77.7  $\pm$  6.2% and 78.8  $\pm$  7.4 %, for the normal and glycated forms of HSA, respectively. These data suggest that HSA, glycated or normal, binds C-peptide with equal affinity.

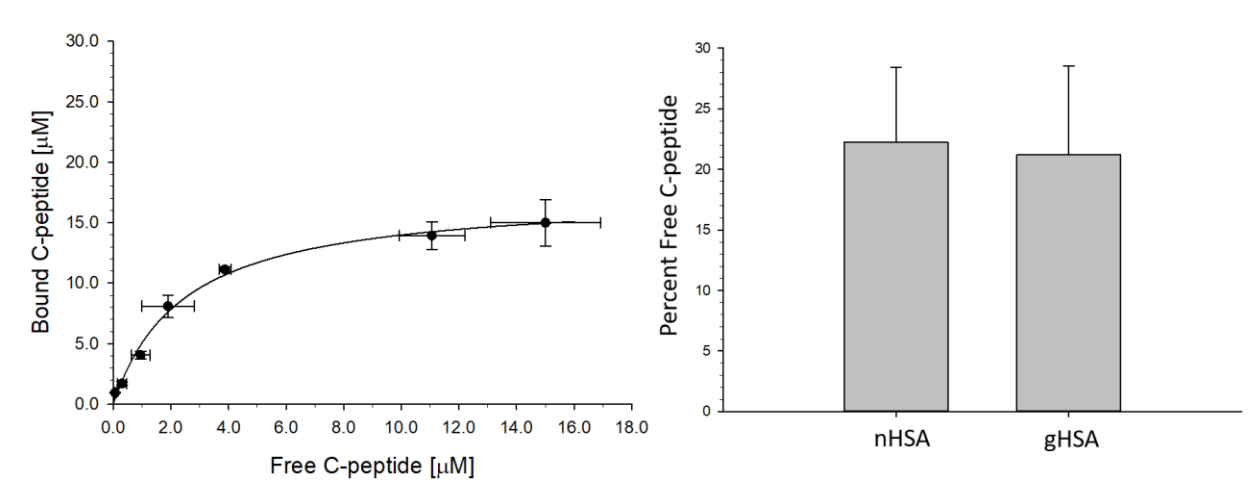


Figure 3.9 Saturation binding Curve Between C-peptide and HSA and Comparison to Glycated HSA. A saturation binding curve was plotted from ultrafiltration data measured using C-peptide and nHSA. The data was analyzed using non-linear regression software (SigmaPlot 13.0) and the  $K_d$  and binding stoichiometry was calculated. The goodness of fit was calculated as  $R^2$ = 0.992. n=3. error = s.d. The percentage of free C-peptide in the glycated HSA sample was not statistically different than the control.

#### 3.3.3 C-peptide binding to HSA, with Zinc or Glucose – centrifuge device

First, the performance of the centrifuge-enabled ultrafiltration device to be used for determining ligand-protein binding affinities was characterized by analyzing the free  $Zn^{2+}$  in a  $Zn^{2+}$ /HSA sample and comparing the result to that obtained by the syringe-device. The result, shown in Figure 3.10 shows no significant difference between the two devices. Then, the device was used to measure the effect of  $Zn^{2+}$  on C-peptide binding to HSA. The concentrations of HSA

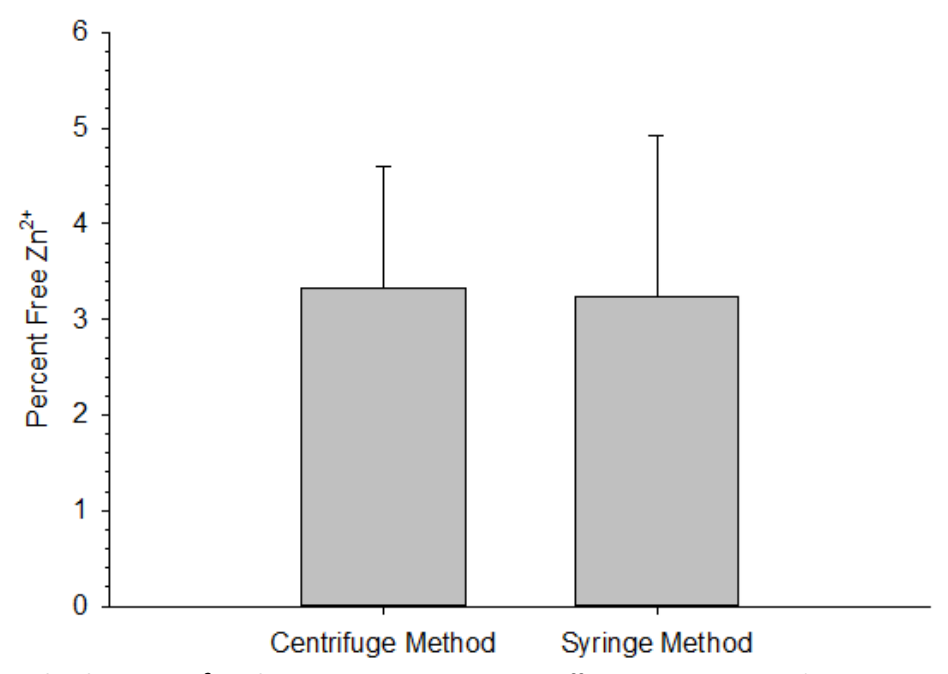


Figure 3.10 **Binding between Zn^{2+} and HSA - Comparison Between Different Devices.** A sample containing 10  $\mu$ M HSA and 5  $\mu$ M  $Zn^{2+}$  was made and the free  $Zn^{2+}$  in the sample was analyzed by measuring the  $Zn^{2+}$  in the ultrafiltrate using both the centrifuge-enabled device as well as the syringe-enabled device. There is no statistical difference in the results obtained from using either device.

and C-peptide in the sample were prepared to be 75  $\mu$ M and 20 nM, respectively, as these concentrations are more relevant and used regularly in experiments in the literature for biological assays of C-peptide. The chosen concentration of Zn<sup>2+</sup> was made to be in 2-3x excess of HSA, in order to confidently saturate the HSA to study its effect on C-peptide binding. Figure 3.11 shows the percentage of C-peptide bound to HSA in the sample (92.7  $\pm$  0.7%), which is not statistically different than that of the control sample containing no Zn<sup>2+</sup> (89.5  $\pm$  4.4%). The effect of immediate glucose addition on C-peptide binding to HSA was also analyzed by spiking a sample with a saturating concentration of glucose, 1.2 mM. The concentration of glucose was chosen as

it is mimics a ratio of glucose to HSA found in the bloodstream of diabetics (10 mM glucose/0.63 mM HSA). As shown in Figure 3.11, the percentage of C-peptide bound to HSA in the sample (93.3  $\pm$  1.1) is not statistically different from the control (89.5  $\pm$  4.4%), which contained no glucose. Lastly, the device was used to re-measure the binding of C-peptide to gHSA. There was no difference in binding affinity between C-peptide and nHSA or gHSA under these conditions (89.5  $\pm$  4.4% and 93.0  $\pm$  0.7% bound, respectively).

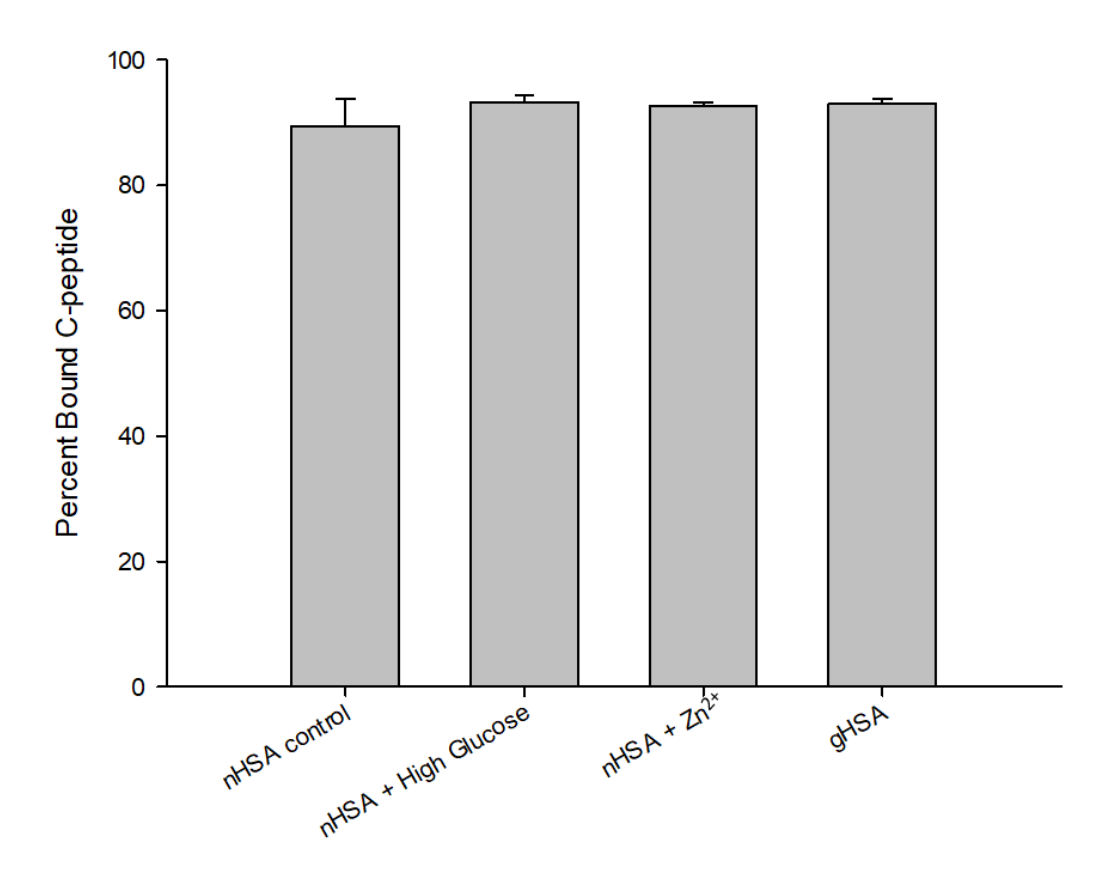


Figure 3.11 Ultrafiltration Data Analyzing the Impact of Glucose,  $Zn^{2+}$ , and HSA-Glycation on the binding of C-peptide to HSA. Ultrafiltration was performed on samples containing C-peptide and HSA and the concentration of C-peptide in the ultrafiltrate was analyzed by ELISA. Neither the addition of glucose (p=0.14) or  $Zn^{2+}$  (p=0.21) affected the amount of C-peptide bound to HSA. The substitution of glycated human serum albumin for normal human serum albumin did not affect the binding of C-peptide (p=0.2). n=4 error = s.d.

#### 3.4 Discussion

Ultrafiltration was successfully used to measure binding constants between proteins and ligands. The techniques shown here enable users to rapidly create their own ultrafiltration devices using any membrane, and use their choice of either a syringe pump or a centrifuge to drive the ultrafiltrate-solution through the membrane. The devices were used to determine binding constants between proteins and ligands comparable to those reported in the literature, therefore it is appropriate to use these devices for other protein-ligand binding experiments.

Using the custom ultrafiltration device, it was discovered that gHSA has an impaired binding affinity for Zn<sup>2+</sup> compared to nHSA. In pharmacokinetics, it is reported that unbound ligands in the bloodstream are more rapidly filtered out and excreted in the urine. Interestingly, diabetics are known to have impaired zinc homeostasis and hyperzincuria, or excess zinc in the urine. <sup>28-29</sup> The cause of hyperzincuria is reportedly unknown. The discovery that Zn<sup>2+</sup> binds to gHSA with weaker affinity may provide an etiology for this condition and should be studied further. An important follow-up study should be to use HSA obtained directly from diabetic patients and measure its affinity for Zn<sup>2+</sup>, as compared to HSA obtained from non-diabetic controls.

The high-affinity binding site of Zn<sup>2+</sup> on HSA has been characterized by X-ray crystallography, as seen in Figure 3.12. HSA consists of three homologous domains, and the primary Zn<sup>2+</sup> binding site is measured to lie at the interface of domain I and II.<sup>30</sup> The binding site consists of four different amino acids, two from domain I (histidine-67 and asparagine-99) and two from domain II (histidine-247 and aspartic acid-249) which coordinate together to bind Zn<sup>2+</sup> with a high affinity. It is reported that glycation of HSA causes changes in the proteins conformation by altering its

secondary and tertiary structure.<sup>7, 10, 31-32</sup> Here, I hypothesize that the covalent addition of a glucose molecule to HSA modifies the structure of the protein, therefore disrupting the primary Zn<sup>2+</sup> binding site by moving domains I and II, and thus the four aforementioned amino acids, out of optimal proximity to each other, consequently decreasing the affinity between HSA and Zn<sup>2+</sup>. The devices were used to study the binding of C-peptide to HSA under normal and diabetic conditions, and also to see if Zn<sup>2+</sup> impacts this binding. Interestingly, the binding of C-peptide to

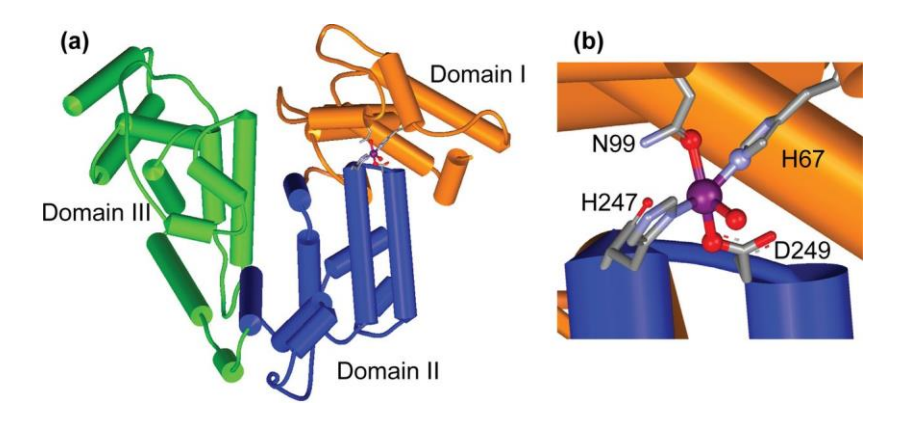


Figure 3.12 Model of the high-affinity Zn²+binding site on HSA based on X-ray crystal structure. HSA is composed of three homologous domains. The primary Zn²+binding site is at the interface of domains I (orange) and II (blue) and is composed of two amino acids from domain I (His67 and Asn99), two amino acids from domain II (His247 and Asp249). This figure is borrowed from Lu et al.

HSA was unaffected by both immediate addition of glucose as well as covalent glycation of HSA. Also, the binding of C-peptide to HSA was unaffected by saturating levels of Zn<sup>2+</sup>, further proving that the two species bind independently of one another. The following chapter will aim to use mass spectrometry to characterize the differences between gHSA and nHSA, both commercially purchased samples as well as samples from healthy and diabetic subjects. Then, their impact on the interaction of C-peptide and Zn<sup>2+</sup> with red blood cells will be evaluated using ELISA techniques and ATP-release measurements.

**REFERENCES** 

#### **REFERENCES**

- 1. Liu, Y.; Chen, C.; Summers, S.; Medawala, W.; Spence, D. M., C-peptide and zinc delivery to erythrocytes requires the presence of albumin: implications in diabetes explored with a 3D-printed fluidic device. *Integr. Biol.* **2015**, *7* (5), 534-543.
- 2. Kemp, S. F.; Kearns, G. L.; Turley, C. P., Alteration of phenytoin binding by glycosylation of albumin in IDDM. *Diabetes* **1987**, *36* (4), 505-509.
- 3. Cohen, M. P.; Sharma, K.; Jin, Y.; Hud, E.; Wu, V.-y.; Tomaszewski, J.; Ziyadeh, F. N., Prevention of diabetic nephropathy in db/db mice with glycated albumin antagonists. A novel treatment strategy. *The Journal of clinical investigation* **1995**, *95* (5), 2338-2345.
- 4. Ruiz-Cabello, F.; Erill, S., Abnormal serum protein binding of acidic drugs in diabetes mellitus. *Clinical Pharmacology & Therapeutics* **1984**, *36* (5), 691-695.
- 5. Vorum, H.; Fisker, K.; Otagiri, M.; Pedersen, A. O.; Kragh-Hansen, U., Calcium ion binding to clinically relevant chemical modifications of human serum albumin. *Clin. Chem.* **1995**, *41* (11), 1654-1661.
- 6. Peters Jr, T., *All about albumin: biochemistry, genetics, and medical applications*. Academic press: 1995.
- 7. Anguizola, J.; Matsuda, R.; Barnaby, O. S.; Hoy, K. S.; Wa, C.; DeBolt, E.; Koke, M.; Hage, D. S., Review: Glycation of human serum albumin. *Clin. Chim. Acta* **2013**, *425*, 64-76.
- 8. Dolhofer, R.; Wieland, H., Glycosylation of serum albumin: Elevated glycosyl-albumin in diabetic patients. *FEBS Lett.* **1979**, *103* (2), 282-286.
- 9. John, W.; Jones, A., Affinity chromatography: a precise method for glycosylated albumin estimation. *Ann. Clin. Biochem.* **1985**, *22* (1), 79-83.
- 10. Kisugi, R.; Kouzuma, T.; Yamamoto, T.; Akizuki, S.; Miyamoto, H.; Someya, Y.; Yokoyama, J.; Abe, I.; Hirai, N.; Ohnishi, A., Structural and glycation site changes of albumin in diabetic patient with very high glycated albumin. *Clin. Chim. Acta* **2007**, *382* (1), 59-64.
- 11. Kohzuma, T.; Koga, M., Lucica® GA-L Glycated Albumin Assay Kit. *Molecular diagnosis & therapy* **2010**, *14* (1), 49-51.
- 12. Furusyo, N.; Hayashi, J., Glycated albumin and diabetes mellitus. *Biochimica et Biophysica Acta (BBA)-General Subjects* **2013**, *1830* (12), 5509-5514.
- 13. Abidin, D.; Liu, L.; Dou, C.; Datta, A.; Yuan, C., An improved enzymatic assay for glycated serum protein. *Analytical Methods* **2013**, *5* (10), 2461-2469.
- 14. Barnaby, O. S.; Cerny, R. L.; Clarke, W.; Hage, D. S., Comparison of modification sites formed on human serum albumin at various stages of glycation. *Clin. Chim. Acta* **2011**, *412* (3–4), 277-285.

- 15. Matsuda, R.; Anguizola, J.; Joseph, K.; Hage, D. S., High-performance affinity chromatography and the analysis of drug interactions with modified proteins: binding of gliclazide with glycated human serum albumin. *Anal. Bioanal. Chem.* **2011**, *401* (9), 2811.
- 16. Barnaby, O. S.; Cerny, R. L.; Clarke, W.; Hage, D. S., Quantitative analysis of glycation patterns in human serum albumin using 16O/18O-labeling and MALDI–TOF MS. *Clin. Chim. Acta* **2011**, *412* (17–18), 1606-1615.
- 17. Blache, D.; Bourdon, E.; Salloignon, P.; Lucchi, G.; Ducoroy, P.; Petit, J.-M.; Verges, B.; Lagrost, L., Glycated albumin with loss of fatty acid binding capacity contributes to enhanced arachidonate oxygenation and platelet hyperactivity: relevance in patients with type 2 diabetes. *Diabetes* **2014**, DB 140879.
- 18. Rahnama, E.; Mahmoodian-Moghaddam, M.; Khorsand-Ahmadi, S.; Saberi, M. R.; Chamani, J., Binding site identification of metformin to human serum albumin and glycated human serum albumin by spectroscopic and molecular modeling techniques: a comparison study. *J. Biomol. Struct. Dyn.* **2015**, *33* (3), 513-533.
- 19. Shaklai, N.; Garlick, R. L.; Bunn, H. F., Nonenzymatic glycosylation of human serum albumin alters its conformation and function. *J. Biol. Chem.* **1984**, *259* (6), 3812-3817.
- 20. Qian, M.; Liu, M.; Eaton, J. W., Transition metals bind to glycated proteins forming redox active "glycochelates": implications for the pathogenesis of certain diabetic complications. *Biochem. Biophys. Res. Commun.* **1998**, *250* (2), 385-389.
- 21. Nursten, H. E., *The Maillard reaction: chemistry, biochemistry, and implications*. Royal Society of Chemistry: 2005.
- 22. Hirata, T.; Saisho, Y.; Morimoto, J.; Kasayama, S.; Koga, M.; Maruyama, T., The ratio of glycated albumin to HbA1c is correlated with diabetes duration according to decreases in insulin secretion in patients with autoimmune type 1 diabetes and type 2 diabetes. *J Genet Syndr Gene Ther* **2013**, *4* (168), 2.
- 23. Melten, J. W.; Wittebrood, A. J.; Willems, H. J.; Faber, G. H.; Wemer, J.; Faber, D. B., Comparison of equilibrium dialysis, ultrafiltration, and gel permeation chromatography for the determination of free fractions of phenobarbital and phenytoin. *J. Pharm. Sci.* **1985**, *74*, 692-694.
- 24. Li, C. M.; Lu, Y.; Ahn, S.; Narayanan, R.; Miller, D. D.; Dalton, J. T., Competitive mass spectrometry binding assay for characterization of three binding sites of tubulin. *J. Mass Spectrom.* **2010**, *45* (10), 1160-1166.
- 25. Liu, D.; Guo, J.; Luo, Y.; Broderick, D. J.; Schimerlik, M. I.; Pezzuto, J. M.; Van Breemen, R. B., Screening for ligands of human retinoid X receptor-α using ultrafiltration mass spectrometry. *Anal. Chem.* **2007,** *79* (24), 9398-9402.
- 26. Pinger, C. W.; Heller, A. A.; Spence, D. M., A Printed Equilibrium Dialysis Device with Integrated Membranes for Improved Binding Affinity Measurements. *Anal. Chem.* **2017**, *89* (14), 7302-7306.
- 27. Goumakos, W.; Laussac, J.-P.; Sarkar, B., Binding of cadmium (II) and zinc (II) to human and dog serum albumins. An equilibrium dialysis and 113Cd-NMR study. *Biochem. Cell Biol.* **1991**, *69*, 809-820.

- 28. Salgueiro, M. J.; Krebs, N.; Zubillaga, M. B.; Weill, R.; Postaire, E.; Lysionek, A. E.; Caro, R. A.; De Paoli, T.; Hager, A.; Boccio, J., Zinc and diabetes mellitus. *Biol. Trace Elem. Res.* **2001**, *81* (3), 215-228.
- 29. Cunningham, J. J.; Fu, A.; Mearkle, P. L.; Brown, R. G., Hyperzincuria in individuals with insulindependent diabetes mellitus: concurrent zinc status and the effect of high-dose zinc supplementation. *Metabolism* **1994**, *43* (12), 1558-1562.
- 30. Lu, J.; Stewart, A. J.; Sadler, P. J.; Pinheiro, T. J.; Blindauer, C. A., Albumin as a zinc carrier: properties of its high-affinity zinc-binding site. Portland Press Limited: 2008.
- 31. Coussons, P. J.; Jacoby, J.; McKay, A.; Kelly, S. M.; Price, N. C.; Hunt, J. V., Glucose Modification of Human Serum Albumin: A Structural Study. *Free Radical Biol. Med.* **1997**, *22* (7), 1217-1227.
- 32. Rondeau, P.; Bourdon, E., The glycation of albumin: structural and functional impacts. *Biochimie* **2011,** *93* (4), 645-658.

# <u>Chapter 4: Analysis of Glycated Albumin and its Effect on the Interaction Between C-peptide,</u> Zn<sup>2+</sup>, and Red Blood Cells

#### 4.1 Introduction

The previous chapter showed that the affinity of Zn<sup>2+</sup> to the glycated human serum albumin (gHSA) sample was significantly weaker than its affinity to normal human serum albumin (nHSA), however the affinity of C-peptide to gHSA was not changed (in comparison to nHSA). A higher concentration of glucose is found in the diabetic bloodstream (7-11 mM) as compared to non-diabetics (4-7 mM), which causes an increase in the non-enzymatic glycation of proteins in the bloodstream by the Maillard reaction (Figure 3.2). Human serum albumin (HSA), the most prevalent protein in the blood-plasma, is reported to become glycated by this reaction. Glycated HSA has been reported throughout the literature to have properties different from those of non-glycated HSA, as the modification results in changes in the structure of the protein. In the bloodstream, HSA functions as a carrier protein by binding ligands, such as drugs and hormones, and transporting them throughout the body. Glycation of HSA has been reported to alter the proteins ability to bind certain ligands, sometimes causing them to bind stronger, or weaker, depending on the ligand. An analysis of the HSA samples used in Chapter 3 is needed in order to interpret the relevance of the results.

The extent of glycation of HSA in the bloodstream is reported to be directly correlated to the average concentration of glucose in the bloodstream, therefore, some researchers advocate that its analysis and quantitation could provide a valuable biomarker of glycemic control. There are several techniques reported throughout the literature for studying the extent of glycation of HSA. Each technique has advantages and disadvantages. The earliest reported and most widely

used technique is by boronate-affinity chromatography. 13-14 This technique involves flowing the HSA sample through a column with a boronate stationary phase. The boronate groups bind to the cis-diol groups on the glucose attached to the HSA and retain it on the column, allowing the non-glycated HSA to be eluted and quantified by absorbance spectroscopy. The retained HSA can then be eluted using a buffer with high pH and the chromatographic peak can be measured using absorbance spectrophotometry and compared to the unretained species, enabling the user to calculate the percentage of glycated HSA. Another common technique for analyzing the extent of HSA glycation is by a commercially available enzymatic assay, Diazyme GlycoGap<sup>®</sup>. <sup>15</sup> This technique reports the average number of molecules of glucose bound per molecule of protein (x mol hexose/protein). A disadvantage of the chromatographic technique is that it only reports the percentage of total protein that is glycated, and not the amount of molecules of glucose that are attached to each protein molecule. Conversely, a disadvantage of this enzymatic technique is that it does not report the relative amounts of glycated and non-glycated protein in the sample. There are several other techniques less widely used for analyzing HSA glycation, such as the Lucica® Glycated Albumin kit and matrix-assisted laser desorption ionization (MALDI) time of flight mass spectrometry. 16-17

Here, we use time of flight mass spectrometry coupled with electrospray ionization to analyze intact samples of commercially purchased normal and glycated HSA as well as HSA isolated from plasma of type-1 diabetic and non-diabetic individuals. This technique allows the determination of the relative amount of glycated and non-glycated molecules in the sample. The resulting spectra also reveal the heterogeneity of the samples, a feature that is not offered by the other

mentioned techniques. The analysis performed here is similar to that described by Naldi *et al* and Bar-Or *et al* for studying modifications of HSA in disease states. <sup>18-19</sup>

Discussions of HSA molecular state become important when considering its role when treating red blood cells (RBCs) with a combination of C-peptide and Zn<sup>2+</sup> in an HSA-containing buffer. This formulation results in the cells releasing significantly more adenosine triphosphate (ATP) when pumped through a fluidic device, but only when HSA is present in the buffer.<sup>20</sup> However, it is reported throughout the literature that HSA found in the bloodstreams of people with diabetes has different properties than that found in non-diabetics, including both structural and functional changes. 1, 3 Therefore, we hypothesize that glycated HSA interferes with the interaction between C-peptide/Zn<sup>2+</sup> and RBCs. To test this hypothesis, we measured the binding between C-peptide and RBCs in the presence of glycated HSA and normal HSA. Also, we measured the resultant ATP release from RBCs treated with a combination of C-peptide and Zn<sup>2+</sup> in the presence of glycated and normal HSA. As described in Chapter 1, ATP is known to regulate microvascular blood flow by signaling nitric oxide production in the endothelium.<sup>21-23</sup> Therefore, decreases in ATP released by RBCs may cause impaired microvascular blood flow and downstream microvascular complications. The results of these studies may help to explain the failures and inconsistencies of C-peptide replacement trials in diabetic humans. These experiments were performed in collaboration with Monica Jacobs and Suzanne Summers.

### 4.2 Methods

#### 4.2.1 Isolation of RBCs from Whole Blood

Approximately 10-20 mL of whole blood was obtained from consenting donors via venipuncture and collected into heparinized tubes. The tubes were then centrifuged at 500*g* for 10 minutes and the plasma was removed and stored in a 15 mL polypropylene tube. The buffy coat was removed and discarded, and the cells were washed 3 times in a physiological salt solution buffer (PSS). PSS was prepared to contain 4.7 mM KCl, 2.0 mM CaCl<sub>2</sub>, 140.5 mM NaCl, 12.0 mM MgSO<sub>4</sub>, 21 mM tris (hydroxymethyl) amino methane, 5.5 mM glucose, and 5 g/L bovine serum albumin at pH 7.40. After the final wash the supernatant was removed leaving a solution of packed RBCs. The hematocrit of this solution was measured using a CritSpin microcentrifuge system, and the resulting hematocrit was approximately 65-80%.

## 4.2.2 Isolation of HSA from Human Plasma

Plasma was obtained from whole blood of consenting donors and stored in a 15 mL polypropylene tube at -20°C. until thawing at room temperature on the day of use. The HSA was isolated from the plasma using an immunoprecipitation method described in the literature.<sup>9</sup> Briefly, approximately 550 μL of the plasma sample was diluted to 1100 μL with phosphate buffered saline (PBS) (pH 7.40, 1.44 g Na<sub>2</sub>HPO<sub>4</sub>, 0.2 g KCl, 8 g NaCl, 0.24 g KH<sub>2</sub>PO<sub>4</sub> diluted in 1 liter of DDW). PureProteome<sup>TM</sup> Albumin Magnetic Beads from Millipore (Burlington, MA) were used, the beads are coated with antibodies for HSA. A 4 mL aliquot of the bead solution was removed from the original vial and pipetted into a 15 mL polypropylene tube. The beads were washed three times with 10 mL of PBS by placing the tube into a magnetic holder and decanting the

solution. Then, 540 μL of the diluted plasma were added directly to the beads in the tube, and then incubated for one hour on a small orbital shaker (260 rpm) at room temperature. The tube was placed back into the magnetic holder and the solution was decanted off. The bead-samples were then washed three times with PBS. Then, 3 mL of glycine buffer (pH 3.0, 0.1 M glycine, pH adjusted with HCl) was added to the beads to elute the HSA from the antibodies, and the tube was incubated for 1 minute at room temperature. The tube was placed into the magnetic holder again and approximately 2.5 mL of the solution were then removed and added to a separate tube containing 50 µL of 420 mM Tris buffer pH 8.0 in order to adjust the pH of the samples to be approximately 7-8. The process of adding glycine buffer to the beads, incubating, and removing it, was repeated four times. Then, all of the fractions were combined (approx. 4 mL) and added to an Amicon Ultra-15 ultrafiltration centrifugal filter unit (10 kDa MWCO) from Millipore (Burlington, MA) followed by addition of 10 mL of DDW. The device was centrifuged at 3260g for 12 minutes so that only 0.4-1mL of the protein sample remained above the membrane, then DDW was added to reconstitute the protein in 15 mL of solution, and the centrifugation step was repeated. This was repeated for a total of 7 filtration cycles to remove buffer salts from the protein sample. The remaining protein solution was lyophilized and stored at -20°C.

#### 4.2.3 Electrospray Ionization-Time of Flight Mass Spectrometry

A Waters (Milford, MA) Xevo G2-XS® time of flight mass spectrometer was used at the Michigan State University Mass Spectrometry and Metabolomics Core Facility for analysis of HSA samples. The mass spectrometer is paired with electrospray ionization and an ultra-high pressure liquid chromatography (UPLC) system for sample introduction into the instrument, which was operated in positive-ion mode. An aliquot of the sample was injected via an autosampler onto

the UPLC desalting column (cyanopropyl guard column) coupled to the mass spectrometer, with a gradient mobile phase consisting of 0.1% formic acid in water (solvent A) and acetonitrile (solvent B). The LC gradient gradually increased the amount of solvent B in the mobile phase over the course of 15 minutes. Spectra were obtained in the m/z range of 200 to 2000 daltons. The MassLynx software provided a chromatogram showing the time range which the protein sample eluted from the guard column, resulting in a peak. The spectra collected from the chromatographic peak were summed for each sample and then baseline subtracted. The spectrum deconvolution and data analysis were carried out with the MaxEnt tool in the MassLynx software before being exported into spreadsheet software for analysis. Using MaxEnt, the spectra were processed in the range of 66,200 to 67,200 daltons. The extent of glycation was assessed by centroiding the peaks on the spectrum and summing the ion counts of the peaks shifted +162 Da and multiples of +162 Da from the lowest-mass main peak (66,425 ± 13 Da) and then dividing those counts by the total ion count of the spectrum. Also included were peaks shifted +162 Daltons from different HSA isoforms, such as cysteinylated-HSA (+119 Da), HSA+SO<sub>2</sub>H (+31 Da), and potassium-HSA (+39.1 Da). The sulfinic acid isoform (HSA+SO<sub>2</sub>H) occurs when Cys-34 on HSA becomes oxidized. A spectrum library of known HSA isoforms was used for peak identification.<sup>19</sup>

#### 4.2.4 Preparation of C-peptide

Crude C-peptide was purchased from Peptide 2.0 and purified by HPLC as reported previously in the literature to remove any transition metals and obtain a peptide purity of approximately 99%, as confirmed by mass spectrometry. <sup>24-26</sup> The peptide was then lyophilized and stored at - 20°C. Approximately 0.3 mg of the peptide was weighed out into a 1 mL tube. The solution was

inverted several times and incubated at room temperature for approximately 20 minutes to let the peptide dissolve. The solution was centrifuged (1500g for 3 minutes) and the supernatant was transferred to another tube in order to remove any undissolved peptide or particulates. Then, the concentration of the sample was confirmed by ELISA (Eagle Biosciences, Nashua, NH) and the solution was diluted appropriately to make several one-mL solutions containing 8.0 micromolar C-peptide in distilled and deionized water (DDW,  $18M\Omega$ ). The aliquots were stored at 5°C for up to three weeks until use.

## 4.2.5 Buffer Preparation

An albumin-free PSS buffer was prepared to contain 4.7 mM KCl, 2.0 mM CaCl<sub>2</sub>, 140.5 mM NaCl, 12.0 mM MgSO<sub>4</sub>, 21 mM tris (hydroxymethyl) amino methane, and 5.5 mM glucose at pH 7.40. The buffer was diluted to 500 mL using volumetric glassware and then sterile filtered and used on athe day of preparation. Then approximately 5.0 ± 0.3 mg of either glycated human serum albumin (gHSA, Sigma) or normal human serum albumin (nHSA, Sigma) were placed into 1.7 mL centrifuge tubes, followed by the addition of 1.0 mL of albumin-free PSS to create gHSA-PSS and nHSA-PSS.

#### 4.2.6 C-peptide Binding to RBCs

For the binding experiments, 25  $\mu$ L of the 800 nM C-peptide was pipetted into a centrifuge tube followed by an appropriate amount (approximately 875  $\mu$ L) of the freshly prepared gHSA-PSS or nHSA-PSS solution and then RBCs to create a 1 mL sample containing 7% RBCs and 20 nM C-peptide. This was repeated using buffer without RBCs to make a control sample. The samples were incubated for 2 hours at 37°C. Meanwhile, standards were prepared ranging in

concentration from 0-25 nM C-peptide in PSS. After the incubation, samples were centrifuged at 500g for 5 minutes and the supernatant of the samples was removed and placed in separate tubes and stored at -20°C for future analysis. On the day of analysis, the samples and standards were thawed and diluted 1:20 in DDW (50  $\mu$ L of sample with 950  $\mu$ L of DDW). Then, the diluted samples and standards were analyzed by C-peptide ELISA (Eagle Biosciences, Nashua, NH) to quantify the amount of C-peptide remaining in the supernatant. The blood used in these experiments was drawn from three different blood draws from consenting non-diabetic donors.

#### 4.2.7 ATP Release

ATP was measured using the luciferin/luciferase chemiluminescence assay. To quantitatively determine the amount of ATP released from RBCs treated under different conditions, samples were prepared by adding 25 μL of 800 nM C-peptide and 25 μL of 800 nM ZnCl<sub>2</sub>, or 50 μL of DDW, were first added to 1.7 mL tubes, followed by addition of gHSA-PSS or nHSA-PSS (approximately 850 μL), followed by immediate addition of packed RBCs (approximately 100 μL) to create a 1 mL sample containing 7% RBCs, 20 nM C-peptide, and 20 nM Zn<sup>2+</sup>. These samples were incubated for 3 hours at 37°C. Then, the samples were transferred into a 1 mL syringe, placed onto a syringe pump set (flow rate: 5mL/hour), and pushed through a silica capillary (27 cm length) with an inside diameter of 250 micrometers to simulate flow conditions. The samples were collected in tubes at the other end of the capillary and then centrifuged at 750g for 3 minutes. The supernatant was removed from the sample and 100 μL of each supernatant was placed into a 96-well plate. A luciferin/luciferase stock solution was prepared by dissolving 5 mg of potassium luciferin and 100 mg firefly lantern extract into 5 mL of DDW. Then, 200 μL of the luciferin-luciferase solution were placed into a row of a different 96-well plate. This plate was loaded into

the middle-tray of the plate-reader as a reagent-plate followed by the sample-plate in the bottom tray. The plate reader was programmed to simultaneously inject 50  $\mu$ L of the luciferin/luciferase reagent into each well containing sample and subsequently measure the resulting chemiluminescence from the well. Afterwards, another 100  $\mu$ L of each sample was loaded into the plate in a different order and the measurement process was repeated so that an average of 3 different chemiluminescence signals could be calculated. The RBCs used in these experiments were obtained from four different blood draws from consenting non-diabetic donors.

A control experiment was performed to confirm that the difference in chemiluminescence intensity between nHSA and gHSA samples is not simply due to quenching of the chemiluminescence signal by gHSA. In this experiment, nHSA-PSS and gHSA-PSS were spiked with an ATP standard to each contain 128 nM ATP. Then, the samples were treated with luciferin/luciferase exactly as described above and the resulting chemiluminescence of the samples was measured.

#### 4.3 Results

## 4.3.1 Mass Spectrometry Analysis of Albumin Samples

The extent of glycation of HSA samples, both commercially purchased and isolated from human donors, was assessed by time-of-flight mass spectrometry and the resulting spectra are presented in Figure 4.1. The purchased nHSA and gHSA samples used for binding experiments in chapter 3, as well as cell studies in this chapter, were measured to contain approximately 23% and 67% glycated HSA, respectively. HSA was isolated from both a non-diabetic human donor and a Type-1 diabetic human donor using a magnetic-bead immunoprecipitation method. The

non-diabetic HSA sample contained approximately 15% glycated HSA, while the Type-1 diabetic sample contained approximately 41% glycated HSA.

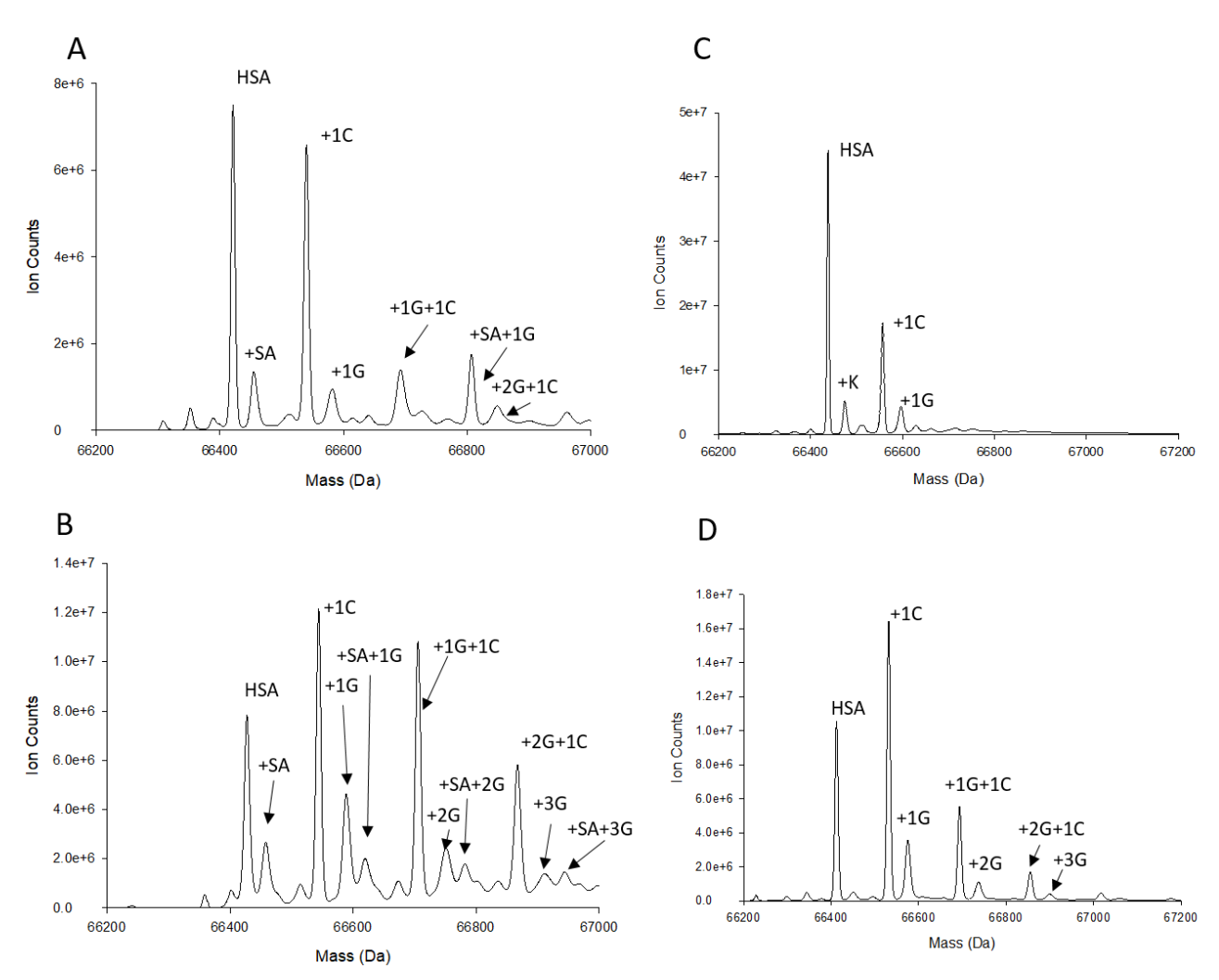


Figure 4.1 Mass Spectra of Human Serum Albumin Samples. Time-of-flight mass spectra used to analyze the relative extent of glycation of four different human serum albumin samples. G=glycation (+162). C=cysteinylation (+119). SA = sulfinic acid (SO<sub>2</sub>H) (+31), K=potassium. A: Purchased human serum albumin from Sigma, approximately 23% glycated. B: Purchased glycated human serum albumin from Sigma, approximately 67% glycated. C: Albumin isolated from plasma from a non-diabetic donor, approximately 15% glycated. D: Albumin isolated from plasma from a subject with Type-1 diabetes, approximately 41% glycated.

# 4.3.2 C-peptide Uptake by RBCs

The binding of C-peptide to healthy RBCs in the presence of normal and glycated HSA was assessed by incubating a 7% solution of RBCs with 20 picomoles of C-peptide in a buffer solution

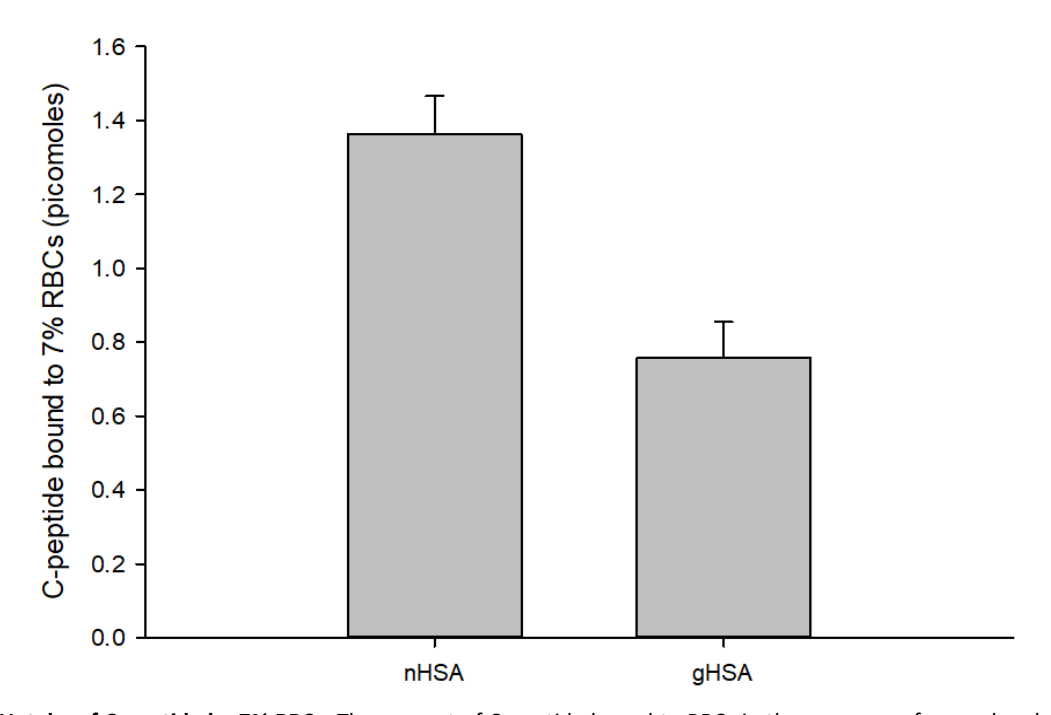


Figure 4.2 **Uptake of C-peptide by 7% RBCs**. The amount of C-peptide bound to RBCs in the presence of normal and glycated HSA. The RBCs in the sample containing nHSA bound  $1.4 \pm 0.1$  picomoles of C-peptide, while the samples containing gHSA bound  $0.8 \pm 0.1$  picomoles. p<0.05. n=3 blood draws, error = std error of the mean.

that contained either type of HSA. The samples were incubated for 2 hours and then centrifuged. The supernatant was removed and analyzed by ELISA and compared to a set of external standards. The amount of C-peptide bound to the cells (Figure 4.2) was calculated by measuring the amount of C-peptide in the supernatant and subtracting that from the amount originally added to the sample (20.0 picomoles). RBCs in the presence of glycated HSA bound significantly less C-peptide (0.8  $\pm$  0.1 picomoles) than RBCs in the presence of the normal HSA (1.4  $\pm$  0.1 picomoles) (p<0.05).

#### 4.3.3 ATP Release from RBCs

The amount of ATP released from RBCs subjected to flow conditions when treated with C-peptide and  $Zn^{2+}$  and either normal or glycated HSA was measured. Figure 4.3 shows a significant increase (2.1  $\pm$  0.2 fold) in the chemiluminescence intensity due to ATP released from RBCs treated with C-peptide and  $Zn^{2+}$  in the presence of purchased nHSA as compared to the control sample, which contained 7% RBCs and neither C-peptide nor  $Zn^{2+}$ . The chemiluminescence from ATP released from RBCs treated with C-peptide and  $Zn^{2+}$  in the presence of purchased gHSA was

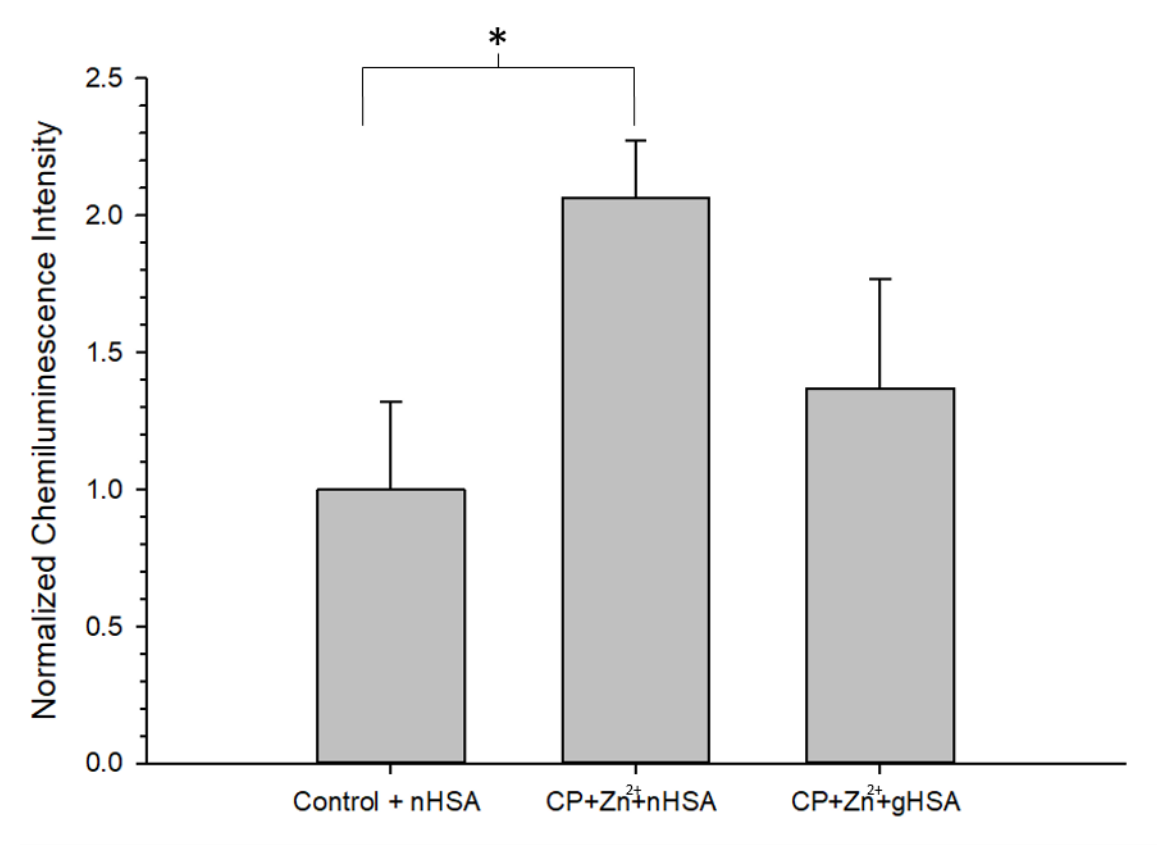


Figure 4.3 ATP release from RBCs treated with C-peptide,  $Zn^{2+}$ , and different forms of HSA. The ATP released from RBCs treated with C-peptide/ $Zn^{2+}$  and nHSA was higher than in the control sample which contained 7% RBCs and no C-peptide/ $Zn^{2+}$ . The ATP in the sample containing C-peptide/ $Zn^{2+}$ /gHSA was not statistically different than the control sample (p=0.48). n=4 blood draws. \*asterisks denote p<0.05. error = std. error of the mean.

increased 1.4  $\pm$  0.4 fold higher than the control, but the difference was not statistically significant.

In a separate control experiment, the resulting chemiluminescence signal (relative luminescence units) from samples containing equal concentrations of ATP and either nHSA-PSS ( $8.7 \pm 0.7 \times 10^4$  RLU) or gHSA-PSS ( $8.9 \pm 1.3 \times 10^4$  RLU) was determined to be statistically equal when subjected to the luciferin/luciferase assay. This experiment confirms that the difference in chemiluminescence signals between the gHSA and nHSA samples in Figure 4.3 is due to different amounts of ATP released from the RBCs in the samples, and not a spectral interference caused by the difference in proteins.

### 4.4 Discussion

Mass spectrometry was used to analyze the glycation of purchased-HSA compared to HSA isolated from human plasma. The purchased nHSA sample contained similar amounts of glycated HSA (approx. 23%) as the sample isolated from the non-diabetic subject (approx. 15%). The purchased gHSA sample contained more glycated HSA (approx. 67%) than the sample isolated from the T1D subject (approx. 41%). Though the average non-diabetic is reported to have  $4.7 \pm 0.8\%$  of their HSA in the glycated form compared to  $23.3 \pm 4.5\%$  for T1D patients, these numbers vary widely throughout the literature and subjects with diabetes have been reported to have as high as 94% glycated HSA.  $^{10, 27-28}$  Therefore, due to ease of preparation, the purchased nHSA and gHSA samples were used to mimic non-diabetic HSA and T1D-HSA, respectively, for the experiments involving RBCs.

Previous literature reports that C-peptide binding to RBCs is dependent upon albumin. It is hypothesized that the C-peptide receptor on RBCs is actually a receptor for albumin, which carries and delivers C-peptide and  $Zn^{2+}$  to the cell. Using an ELISA technique, it was found that

C-peptide binding to RBCs is diminished in the presence of the gHSA sample compared to the nHSA sample. Further, the ability of C-peptide and Zn<sup>2+</sup> to stimulate ATP release from RBCs was also diminished in the presence of gHSA. The etiology of this occurrence is unknown, but I hypothesize that the gHSA competes with nHSA to bind the C-peptide in the sample (as measured in Chapter 3), but only the nHSA can then interact with the RBC to deliver C-peptide to the proper receptor. Further experiments that could be performed to prove or disprove this hypothesis will be discussed in Chapter 5.

The discovery that gHSA interferes with the interaction between C-peptide and RBCs may have practical clinical importance. As mentioned in Chapter 1, administering C-peptide to T1D human patients has failed to produce improvements in microvascular complications in several small clinical trials and one large clinical trial.<sup>29-30</sup> The results of the studies in this chapter suggest that in order for C-peptide and Zn<sup>2+</sup> to provide therapeutic effects, non-glycated HSA may also need to be administered to T1D patients. The experiments in this chapter should be repeated using RBCs from T1D patients. The ability of C-peptide and Zn<sup>2+</sup> to cause RBCs to release more ATP is a phenomenon that is hypothesized to regulate microvascular blood flow. The increased ATP can signal increased nitric oxide production in the endothelium, and downstream vasodilation. The deficiency of C-peptide in T1D may be a cause of poor microvascular blood flow by blocking this pathway, leading to downstream microvascular complications. C-peptide replacement therapy has been hypothesized by many researchers to alleviate microvascular complications in T1D; however, the research in this chapter suggests that further *in vitro* experiments should be performed to determine an optimal preparation and administration

strategy for this therapeutic.<sup>31-32</sup> Future studies that need to be performed to better understand this pathway will be addressed in Chapter 5.

It should be noted that in all of the RBC samples used in this study, the RBCs were washed in a PSS buffer containing bovine serum albumin (BSA). The packed RBC solution, which had a hematocrit of approximately 70%, contained roughly 22  $\mu$ M BSA. Therefore, when 100  $\mu$ L of RBCs was added to each RBC sample, approximately 2.2 nanomoles of BSA was also added. The amount of nHSA and gHSA in each final RBC sample was approximately 64 nanomoles. In future experiments, the RBCs should be washed and prepared in buffer that contains the appropriate HSA (either nHSA or gHSA) that the samples will be made in.

- 1. Furusyo, N.; Hayashi, J., Glycated albumin and diabetes mellitus. *Biochimica et Biophysica Acta (BBA)-General Subjects* **2013**, *1830* (12), 5509-5514.
- 2. Baraka-Vidot, J.; Guerin-Dubourg, A.; Bourdon, E.; Rondeau, P., Impaired drug-binding capacities of in vitro and in vivo glycated albumin. *Biochimie* **2012**, *94* (9), 1960-1967.
- 3. Anguizola, J.; Matsuda, R.; Barnaby, O. S.; Hoy, K. S.; Wa, C.; DeBolt, E.; Koke, M.; Hage, D. S., Review: Glycation of human serum albumin. *Clin. Chim. Acta* **2013**, *425*, 64-76.
- 4. Peters Jr, T., *All about albumin: biochemistry, genetics, and medical applications*. Academic press: 1995.
- 5. Koch-Weser, J.; Sellers, E. M., Binding of Drugs to Serum Albumin. *New England Journal of Medicine* **1976**, *294* (6), 311-316.
- 6. Rahnama, E.; Mahmoodian-Moghaddam, M.; Khorsand-Ahmadi, S.; Saberi, M. R.; Chamani, J., Binding site identification of metformin to human serum albumin and glycated human serum albumin by spectroscopic and molecular modeling techniques: a comparison study. *J. Biomol. Struct. Dyn.* **2015**, *33* (3), 513-533.
- 7. Barnaby, O. S.; Cerny, R. L.; Clarke, W.; Hage, D. S., Comparison of modification sites formed on human serum albumin at various stages of glycation. *Clin. Chim. Acta* **2011**, *412* (3–4), 277-285.
- 8. Matsuda, R.; Anguizola, J.; Joseph, K.; Hage, D. S., High-performance affinity chromatography and the analysis of drug interactions with modified proteins: binding of gliclazide with glycated human serum albumin. *Anal. Bioanal. Chem.* **2011**, *401* (9), 2811.
- 9. Anguizola, J.; Joseph, K.; Barnaby, O. S.; Matsuda, R.; Alvarado, G.; Clarke, W.; Cerny, R. L.; Hage, D. S., Development of affinity microcolumns for drug–protein binding studies in personalized medicine: interactions of sulfonylurea drugs with in vivo glycated human serum albumin. *Anal. Chem.* **2013**, *85* (9), 4453-4460.
- 10. Hirata, T.; Saisho, Y.; Morimoto, J.; Kasayama, S.; Koga, M.; Maruyama, T., The ratio of glycated albumin to HbA1c is correlated with diabetes duration according to decreases in insulin secretion in patients with autoimmune type 1 diabetes and type 2 diabetes. *J Genet Syndr Gene Ther* **2013**, *4* (168), 2.
- 11. Koga, M.; Hashimoto, K.; Murai, J.; Saito, H.; Mukai, M.; Ikegame, K.; Ogawa, H.; Kasayama, S., Usefulness of glycated albumin as an indicator of glycemic control status in patients with hemolytic anemia. *Clin. Chim. Acta* **2011**, *412* (3-4), 253-257.
- 12. Raghav, A.; Ahmad, J., Glycated serum albumin: a potential disease marker and an intermediate index of diabetes control. *Diabetes & Metabolic Syndrome: Clinical Research & Reviews* **2014**, *8* (4), 245-251.

- 13. Shima, K.; Ito, N.; Abe, F.; Hirota, M.; Yano, M.; Yamamoto, Y.; Uchida, T.; Noguchi, K., High-performance liquid chromatographic assay of serum glycated albumin. *Diabetologia* **1988**, *31* (8), 627-631.
- 14. Hage, D. S., Affinity chromatography: a review of clinical applications. *Clin. Chem.* **1999**, *45* (5), 593-615.
- 15. Abidin, D.; Liu, L.; Dou, C.; Datta, A.; Yuan, C., An improved enzymatic assay for glycated serum protein. *Analytical Methods* **2013**, *5* (10), 2461-2469.
- 16. Kohzuma, T.; Koga, M., Lucica® GA-L Glycated Albumin Assay Kit. *Molecular diagnosis & therapy* **2010**, *14* (1), 49-51.
- 17. Bai, X.; Wang, Z.; Huang, C.; Wang, Z.; Chi, L., Investigation of non-enzymatic glycosylation of human serum albumin using ion trap-time of flight mass spectrometry. *Molecules* **2012**, *17* (8), 8782-8794.
- 18. Bar-Or, D.; Bar-Or, R.; Rael, L. T.; Gardner, D. K.; Slone, D. S.; Craun, M. L., Heterogeneity and oxidation status of commercial human albumin preparations in clinical use. *Critical care medicine* **2005**, *33* (7), 1638-1641.
- 19. Naldi, M.; Giannone, F.; Baldassarre, M.; Domenicali, M.; Caraceni, P.; Bernardi, M.; Bertucci, C., A fast and validated mass spectrometry method for the evaluation of human serum albumin structural modifications in the clinical field. *Eur. J. Mass Spectrom.* **2013**, *19* (6), 491-496.
- 20. Liu, Y.; Chen, C.; Summers, S.; Medawala, W.; Spence, D. M., C-peptide and zinc delivery to erythrocytes requires the presence of albumin: implications in diabetes explored with a 3D-printed fluidic device. *Integr. Biol.* **2015**, *7* (5), 534-543.
- 21. Ellsworth, M. L.; Ellis, C. G.; Goldman, D.; Stephenson, A. H.; Dietrich, H. H.; Sprague, R. S., Erythrocytes: oxygen sensors and modulators of vascular tone. *Physiology* **2009**, *24* (2), 107-116.
- 22. Sprague, R. S.; Olearczyk, J. J.; Spence, D. M.; Stephenson, A. H.; Sprung, R. W.; Lonigro, A. J., Extracellular ATP signaling in the rabbit lung: erythrocytes as determinants of vascular resistance. *American Journal of Physiology-Heart and Circulatory Physiology* **2003**, *285* (2), H693-H700.
- 23. Sprague, R. S.; Stephenson, A. H.; Ellsworth, M. L., Red not dead: signaling in and from erythrocytes. *Trends in Endocrinology & Metabolism* **2007**, *18* (9), 350-355.
- 24. Medawala, W., Mechanistic and Functional Studies of Zinc (II) Activation of C-peptide and Its Effect on Red Blood Cell Metabolism. Michigan State University, Department of Chemistry: 2011.
- 25. Meyer, J. A.; Froelich, J. M.; Reid, G. E.; Karunarathne, W. K.; Spence, D. M., Metal-activated C-peptide facilitates glucose clearance and the release of a nitric oxide stimulus via the GLUT1 transporter. *Diabetologia* **2008**, *51* (1), 175-182.
- 26. Meyer, J., *Successful and reproducible bioactivity with C-peptide via activation with zinc.* MICHIGAN STATE UNIVERSITY: 2009.

- 27. Kisugi, R.; Kouzuma, T.; Yamamoto, T.; Akizuki, S.; Miyamoto, H.; Someya, Y.; Yokoyama, J.; Abe, I.; Hirai, N.; Ohnishi, A., Structural and glycation site changes of albumin in diabetic patient with very high glycated albumin. *Clin. Chim. Acta* **2007**, *382* (1), 59-64.
- 28. Blache, D.; Bourdon, E.; Salloignon, P.; Lucchi, G.; Ducoroy, P.; Petit, J.-M.; Verges, B.; Lagrost, L., Glycated albumin with loss of fatty acid binding capacity contributes to enhanced arachidonate oxygenation and platelet hyperactivity: relevance in patients with type 2 diabetes. *Diabetes* **2014**, DB\_140879.
- 29. Wahren, J.; Foyt, H.; Daniels, M.; Arezzo, J. C., Long-acting C-peptide and neuropathy in type 1 diabetes: a 12-month clinical trial. *Diabetes care* **2016**, *39* (4), 596-602.
- 30. Ekberg, K.; Brismar, T.; Johansson, B.-L.; Jonsson, B.; Lindström, P.; Wahren, J., Amelioration of Sensory Nerve Dysfunction by C-Peptide in Patients With Type 1 Diabetes. *Diabetes* **2003**, *52* (2), 536-541.
- 31. Pinger, C-Peptide replacement therapy in type 1 diabetes: are we in the trough of disillusionment? *Molecular bioSystems* **2017**, *13* (8), 1432.
- 32. Sima, A. A., *Diabetes & C-peptide: Scientific and Clinical Aspects*. Springer Science & Business Media: 2011.

### **Chapter 5: Conclusions and Future Directions**

### **5.1 Conclusions**

The  $\beta$ -cells of the pancreas normally secrete insulin, along with C-peptide and Zn<sup>2+</sup>, in response to increased levels of blood glucose. In T1D, the  $\beta$ -cells are destroyed by an autoimmune response, therefore T1D patients must administer exogenous insulin in order to survive; however, they do not receive exogenous C-peptide or Zn<sup>2+</sup>. Unfortunately, even with paired with proper diet, exercise, and close glucose control, insulin therapy alone does not preclude T1D patients from developing secondary complications with high prevalence, such as blindness (retinopathy), kidney failure (nephropathy), and nerve damage (neuropathy). <sup>1-3</sup>

Previously, it was believed that C-peptide was not biologically active after secretion from the pancreatic β-cells.<sup>4-5</sup> However, over the past two decades, researchers have reported numerous functions of C-peptide, many of which are hypothesized to protect against diabetic complications.<sup>6-8</sup> In contrast to successful *in vitro* studies, recent human clinical trials of C-peptide have found limited success, typically obtaining results that are not statistically different from placebo.<sup>9-10</sup> These results have lead researchers to question whether or not C-peptide is truly biologically active.

The Spence group reported that C-peptide alone is not biologically active when it is purified by HPLC.<sup>11-12</sup> Specifically, we reported that when combined with a transition metal (such as Zn<sup>2+</sup>), C-peptide interacts with red blood cells (RBCs) and results in the release of increased concentrations of ATP. RBCs regulate blood flow by releasing ATP when subjected to deformation or hypoxia.<sup>13-16</sup> The ATP released from RBCs can stimulate endothelial nitric oxide synthase

(eNOS) in endothelial cells, causing them to release the vasodilator nitric oxide, which is an important signaling molecule in the relaxation of smooth muscle cells surrounding blood vessels, thus enabling the dilation of the vessel lumen. <sup>13-16</sup> Interestingly, RBCs from diabetic patients are less deformable and release less ATP than those from non-diabetic patients, which is believed to be a determinant in the problematic microvascular blood flow associated with diabetic complications. <sup>17-18</sup> Therefore, it is hypothesized that treating T1D patients with C-peptide and Zn<sup>2+</sup> may alleviate secondary complications associated with T1D, such as retinopathy, nephropathy, and neuropathy, by interacting with RBCs and improving their ability to regulate blood flow. <sup>11, 19-20</sup>

In 2015, the Spence group reported that C-peptide and Zn<sup>2+</sup> delivery to RBCs requires albumin.<sup>19</sup> Albumin is the most prevalent protein in the blood plasma (35-50 g/L, or approximately 0.6 mM) and is reported to act as a carrier protein for many different ligands, hormones, metals, and drugs.<sup>21</sup> Albumin is modified by high concentrations of glucose in the bloodstream, such as that found in the bloodstream of a person with T1D, forming glycated albumin.<sup>22-23</sup> Glycated albumin is reported to have many different properties than non-glycated albumin, such as an altered secondary and tertiary structure, and altered ligand-binding properties.<sup>23-30</sup> The work in Chapters 3 and 4 of this dissertation show that when albumin becomes increasingly glycated its ability to bind Zn<sup>2+</sup> and deliver C-peptide to RBCs are both decreased. The resulting consequence of these binding and delivery deficiencies of glycated albumin is reduced stimulation of RBC-derived ATP release by C-peptide and Zn<sup>2+</sup>. Therefore, we hypothesize that treating T1D patients with C-peptide and Zn<sup>2+</sup> alone may not improve secondary complications.

In the clinic, bolus injections of albumin are already given to patients with hypoalbuminemia, hypovolemia, and burn victims. <sup>31-32</sup> Albumex is an FDA approved 20% albumin solution that is used by physicians. <sup>33</sup> Future studies should include supplementing glycated albumin samples with Albumex and repeating the RBC experiments performed in Chapter 4. <sup>33</sup> The results of these *in vitro* studies could help inform researchers planning *in vivo* clinical trials for C-peptide replacement therapy.

## **5.2 Receptor Studies**

The results of the ultrafiltration experiments in Chapter 3 show no difference in the binding affinity between C-peptide and glycated or normal albumin. However, the results of experiments in Chapter 4 show that glycated albumin interferes with the ability of C-peptide to bind to RBCs. It should be noted that the receptor mechanism for C-peptide to RBCs is unknown.<sup>34</sup> The results of the studies reported by Liu *et al* suggest that the C-peptide receptor is actually a receptor for albumin, or a C-peptide/albumin complex, which delivers C-peptide to the cells.<sup>19, 35</sup> The results of the studies in this dissertation suggest that both non-glycated and glycated albumin bind C-peptide in solution, however, only the non-glycated albumin can interact with RBCs and deliver C-peptide. An important follow up study should focus on directly measuring the binding interaction between RBCs and albumin in its glycated and non-glycated form. Unpublished data mentioned in a paper from 1983 reports that RBCs bind albumin in a saturable manner (10<sup>4</sup> receptors/cell) with moderately high affinity.<sup>36</sup> The prospect of an albumin-ligand complex receptor on cells has been previously proposed by Ockner et al (see Figure 5.1).<sup>36-37</sup> The

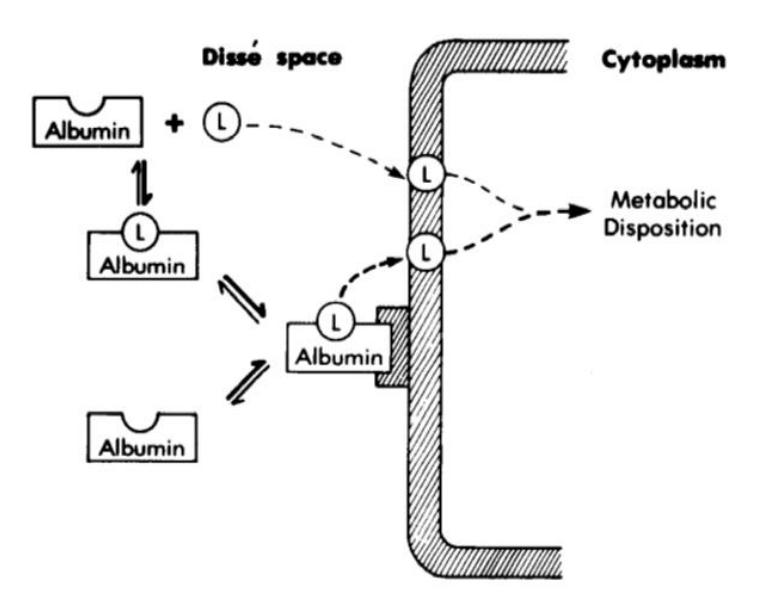


Figure 5.1 A schematic representation of the albumin-ligand complex receptor model proposed by Ockner.<sup>23</sup> The diagram indicates that uptake of ligand (L) can happen by the specific interaction of the albumin-ligand complex with its putative receptor (predominant pathway), or result from direct uptake of unbound (free) ligand (conventional model, minor pathway).

mechanism for this receptor model proposes that albumin, with a bound ligand, binds to the receptor on the cell and results in the ligand being taken up by the cell, and that this is the predominant pathway for the ligand to enter the cell. This same mechanism may be true for C-peptide uptake by RBCs, however, the glycated albumin may not be able to interact with the cell-receptor. To verify this proposed mechanism, albumin binding to RBCs must be quantitatively measured simultaneously with C-peptide uptake to the cells.

The presence of an albumin-receptor on RBCs needs to be confidently measured in order to confirm the hypothesis that C-peptide binds to RBCs via the mechanism described above. Numerous publications report measuring the presence of an albumin receptor on other cell types, but the data for an albumin receptor on RBCs is unpublished. 38-40 Currently, our group is working on measuring this receptor by treating RBCs with technetium-99m (99mTc) labelled albumin. 99mTc is a radioactive isotope (140 keV) commonly used in the field of nuclear medicine. To perform these experiments, RBCs are treated with the radiolabeled-albumin, washed

thoroughly, and the radiation remaining on the RBCs can be measured and correlated to the amount of albumin bound to the cells. Using this technique and Scatchard analysis, the amount of albumin bound to cells can be quantified, and the binding-affinity and number of receptors on each cell can be calculated. Different forms of albumin, such as glycated-albumin isolated from T1D patients, can then be used to understand whether glycation interferes with the interaction of albumin and RBCs. Once this measurement is established, samples should be spiked with varying levels of C-peptide and Zn<sup>2+</sup> and the interaction between <sup>99m</sup>Tc-albumin and RBCs should be repeated, which may or may not reveal a separate receptor for C-peptide/Zn<sup>2+</sup>/albumin. This would be evident if the data fits to a two-site binding model using non-linear regression software (GraphPad Prism or SigmaPlot). Future studies should also focus on the interaction of albumin with RBCs from patients with different diseases, such as type-1 and type-2 diabetes, as well as multiple sclerosis. Our group has measured a difference in the binding of C-peptide to RBCs isolated from subjects with these different diseases, compared to healthy non-disease subjects. If a difference in albumin-receptors also exists, this may support the hypothesis that C-peptide binds via an albumin receptor.

A major criticism of C-peptide research is the lack of an identified receptor. Attempts at identifying the receptor by: screening cDNA expression libraries and also by co-immunoprecipitation assays have failed.<sup>4</sup> It should be noted that, according to the methods section of the publication, no albumin was used in the co-immunoprecipitation procedure.<sup>4</sup> Therefore, a future study should be performed to identify the C-peptide/albumin receptor on RBCs. Here, I propose performing a *crosslinking protein-interaction analysis*, a well-defined technique for isolating and characterizing proteins involved in protein-protein interactions

involving cells. 41-43 In this experiment, C-peptide and albumin would be added to RBCs, exactly as in section 4.2.6, to allow C-peptide to bind to the cells. Then, a chemical crosslinker would be added to the sample to covalently bind the C-peptide/albumin/receptor together in a stable complex. Once the complex is stable, the cells can be lysed, and the lysate can be subjected to gel electrophoresis (SDS-PAGE) and western blot analysis. When two proteins are covalently crosslinked, the migration patterns of both proteins in the gel shift in relation to the uncrosslinked proteins. Then, the user may attempt to use an anti-C-peptide antibody and western blot analysis to detect the interacting proteins. Then, the samples from the gel can be excised, digested, and subjected to a mass spectrometry procedure that can be used to identify the linked proteins, therefore, hopefully revealing the receptor.

### 5.3 Future studies on in vivo glycated HSA

The glycated human serum albumin sample used in experiments in Chapters 3 and 4 was purchased from Sigma, where it was prepared by exposing normal human serum albumin to high concentrations of glucose *in vitro* for long periods of time. In Chapter 4, albumin was isolated from the blood of a person with T1D as well as a healthy control subject. The albumin was analyzed via mass spectrometry and compared to purchased normal and glycated albumin samples. In Chapter 3, the purchased albumin samples were subjected to binding experiments where it was found that *in vitro* glycated albumin has a weaker affinity for Zn<sup>2+</sup> than normal albumin. Then, it was found that the *in vitro* glycated albumin interfered with the binding of C-peptide to RBCs. Future experiments should include obtaining blood plasma from at least ten T1D patients and ten non-diabetic subjects and isolating their albumin by the method described in section 4.3. Then, the extent of *in vivo* glycation of each albumin sample should be measured

via mass spectrometry, as described in section 4.4. Once characterized, the different albumin samples should be used in Zn<sup>2+</sup> binding experiments. If glycation directly affects the ability of albumin to bind Zn<sup>2+</sup>, then an analysis could be performed to correlate the extent of glycation of the albumin samples to their affinity for Zn<sup>2+</sup>. Similarly, experiments should be performed to measure the binding of C-peptide to T1D RBCs in the presence of the T1D albumin. This information is crucial to understanding the effect of administering C-peptide to T1D patients. Finally, the ATP release studies in Chapter 4 should also be revisited with the T1D albumin/ T1D RBC samples. These studies could provide comprehensive evidence of the damage of *in vivo* glycation to albumin.

# 5.4 3D-printing Techniques and a Cell-Culture Permeability Device

3D-printing technology has accelerated scientific research by allowing scientists to rapidly design and create tools to fit their individual research needs. Further, the implementation of non-printed items into 3D-printed devices by techniques such as *Print-Pause-Print* (seen in Chapter 2) is expanding the capabilities of the tools that can be created. In Chapter 2, an equilibrium-dialysis device was created that enabled direct real-time measurement of diffusion of the free analyte-ligand. This technology was used to optimize equilibrium-dialysis binding measurements, however, this technology may have broader utility. To simplify, the device allowed automated real-time monitoring of analyte migration across a barrier into a secondary compartment with automated calibration. Currently, we are developing the device to be a cell/tissue permeability measurement platform (Figure 5.1). In this application, Whatman 105 paper is integrated into

inserts via the *Print-Pause-Print* technique, and placed into the device. Researchers have shown that this paper is a suitable scaffold for cell culture. In this model, multiple pieces of paper with

Confluent Cell Layer Monolayer

on Porous Membrane

After Time

Figure 5.2 **An illustration of the principle of cell permeability assays.** The blue triangles represent a drug or small molecule of interest different cells cultured on each piece can be incorporated into the device in order to mimic complex tissues and organs. The paper-substrate could be integrated into the device and subsequent spectroscopic measurements of analyte migration across the cell layers could be

assessed in an automated manner, by placing the device directly into a plate reader.

- 1. Fowler, M. J., Microvascular and macrovascular complications of diabetes. *Clinical diabetes* **2008**, *26* (2), 77-82.
- 2. Wahren, J., C-peptide and the pathophysiology of microvascular complications of diabetes. *Journal of Internal Medicine* **2017**, *281* (1), 3-6.
- 3. Dugan, J.; Pfotenhauer, K.; Young, C.; Shubrook, J. H., Diabetes Microvascular Complications. *Primary Care Reports* **2017**, *23* (5).
- 4. Luzi, L.; Zerbini, G.; Caumo, A., C-peptide: a redundant relative of insulin? *Diabetologia* **2007**, *50* (3), 500-502.
- 5. Hoogwerf, B. J.; Bantle, J. P.; Gaenslen, H. E.; Greenberg, B. Z.; Senske, B. J.; Francis, R.; Goetz, F. C., Infusion of synthetic human C-peptide does not affect plasma glucose, serum insulin, or plasma glucagon in healthy subjects. *Metabolism* **1986**, *35* (2), 122-125.
- 6. Henriksson, M.; Nordling, E.; Melles, E.; Shafqat, J.; Ståhlberg, M.; Ekberg, K.; Persson, B.; Bergman, T.; Wahren, J.; Johansson, J., Separate functional features of proinsulin C-peptide. *Cellular and Molecular Life Sciences* **2005**, *62* (15), 1772-1778.
- 7. Sima, A. A., *Diabetes & C-peptide: Scientific and Clinical Aspects*. Springer Science & Business Media: 2011.
- 8. Pujia, A.; Gazzaruso, C.; Montalcini, T., An update on the potential role of C-peptide in diabetes and osteoporosis. *Endocrine* **2017**, 1-5.
- 9. Ekberg, K.; Brismar, T.; Johansson, B.-L.; Jonsson, B.; Lindström, P.; Wahren, J., Amelioration of Sensory Nerve Dysfunction by C-Peptide in Patients With Type 1 Diabetes. *Diabetes* **2003**, *52* (2), 536-541.
- 10. Wahren, J.; Foyt, H.; Daniels, M.; Arezzo, J. C., Long-acting C-peptide and neuropathy in type 1 diabetes: a 12-month clinical trial. *Diabetes care* **2016**, *39* (4), 596-602.
- 11. Meyer, J. A.; Froelich, J. M.; Reid, G. E.; Karunarathne, W. K.; Spence, D. M., Metal-activated C-peptide facilitates glucose clearance and the release of a nitric oxide stimulus via the GLUT1 transporter. *Diabetologia* **2008**, *51* (1), 175-182.
- 12. Keltner, Z.; Meyer, J. A.; Johnson, E. M.; Palumbo, A. M.; Spence, D. M.; Reid, G. E., Mass spectrometric characterization and activity of zinc-activated proinsulin C-peptide and C-peptide mutants. *Analyst* **2010**, *135* (2), 278-288.
- 13. Sprague, R. S.; Olearczyk, J. J.; Spence, D. M.; Stephenson, A. H.; Sprung, R. W.; Lonigro, A. J., Extracellular ATP signaling in the rabbit lung: erythrocytes as determinants of vascular resistance. *American Journal of Physiology-Heart and Circulatory Physiology* **2003**, *285* (2), H693-H700.

- 14. Sprague, R. S.; Stephenson, A. H.; Ellsworth, M. L., Red not dead: signaling in and from erythrocytes. *Trends in Endocrinology & Metabolism* **2007**, *18* (9), 350-355.
- 15. Ellsworth, M. L.; Ellis, C. G.; Goldman, D.; Stephenson, A. H.; Dietrich, H. H.; Sprague, R. S., Erythrocytes: oxygen sensors and modulators of vascular tone. *Physiology* **2009**, *24* (2), 107-116.
- 16. Richards, J. P.; Yosten, G. L.; Kolar, G. R.; Jones, C. W.; Stephenson, A. H.; Ellsworth, M. L.; Sprague, R. S., Low O2-induced ATP release from erythrocytes of humans with type 2 diabetes is restored by physiological ratios of C-peptide and insulin. *American Journal of Physiology-Regulatory, Integrative and Comparative Physiology* **2014**, *307* (7), R862-R868.
- 17. Carroll, J.; Raththagala, M.; Subasinghe, W.; Baguzis, S.; Oblak, T. D.; Root, P.; Spence, D., An altered oxidant defense system in red blood cells affects their ability to release nitric oxide-stimulating ATP. *Molecular BioSystems* **2006**, *2* (6-7), 305-311.
- 18. McMillan, D. E.; Utterback, N. G.; La Puma, J., Reduced erythrocyte deformability in diabetes. *Diabetes* **1978**, *27* (9), 895-901.
- 19. Liu, Y.; Chen, C.; Summers, S.; Medawala, W.; Spence, D. M., C-peptide and zinc delivery to erythrocytes requires the presence of albumin: implications in diabetes explored with a 3D-printed fluidic device. *Integr. Biol.* **2015**, *7* (5), 534-543.
- 20. Medawala, W.; McCahill, P.; Giebink, A.; Meyer, J.; Ku, C.-J.; Spence, D. M., A molecular level understanding of zinc activation of C-peptide and its effects on cellular communication in the bloodstream. *Rev Diabet Stud* **2009**, *6* (3), 148.
- 21. Peters Jr, T., *All about albumin: biochemistry, genetics, and medical applications*. Academic press: 1995.
- 22. Shima, K.; Ito, N.; Abe, F.; Hirota, M.; Yano, M.; Yamamoto, Y.; Uchida, T.; Noguchi, K., High-performance liquid chromatographic assay of serum glycated albumin. *Diabetologia* **1988**, *31* (8), 627-631.
- 23. Furusyo, N.; Hayashi, J., Glycated albumin and diabetes mellitus. *Biochimica et Biophysica Acta (BBA)-General Subjects* **2013**, *1830* (12), 5509-5514.
- 24. Kisugi, R.; Kouzuma, T.; Yamamoto, T.; Akizuki, S.; Miyamoto, H.; Someya, Y.; Yokoyama, J.; Abe, I.; Hirai, N.; Ohnishi, A., Structural and glycation site changes of albumin in diabetic patient with very high glycated albumin. *Clin. Chim. Acta* **2007**, *382* (1), 59-64.
- 25. Baraka-Vidot, J.; Guerin-Dubourg, A.; Bourdon, E.; Rondeau, P., Impaired drug-binding capacities of in vitro and in vivo glycated albumin. *Biochimie* **2012**, *94* (9), 1960-1967.
- 26. Anguizola, J.; Matsuda, R.; Barnaby, O. S.; Hoy, K. S.; Wa, C.; DeBolt, E.; Koke, M.; Hage, D. S., Review: Glycation of human serum albumin. *Clin. Chim. Acta* **2013**, *425*, 64-76.
- 27. Anguizola, J.; Joseph, K.; Barnaby, O. S.; Matsuda, R.; Alvarado, G.; Clarke, W.; Cerny, R. L.; Hage, D. S., Development of affinity microcolumns for drug—protein binding studies in personalized medicine:

interactions of sulfonylurea drugs with in vivo glycated human serum albumin. *Anal. Chem.* **2013**, *85* (9), 4453-4460.

- 28. Blache, D.; Bourdon, E.; Salloignon, P.; Lucchi, G.; Ducoroy, P.; Petit, J.-M.; Verges, B.; Lagrost, L., Glycated albumin with loss of fatty acid binding capacity contributes to enhanced arachidonate oxygenation and platelet hyperactivity: relevance in patients with type 2 diabetes. *Diabetes* **2014**, DB\_140879.
- 29. Raghav, A.; Ahmad, J., Glycated serum albumin: a potential disease marker and an intermediate index of diabetes control. *Diabetes & Metabolic Syndrome: Clinical Research & Reviews* **2014**, *8* (4), 245-251.
- 30. Rahnama, E.; Mahmoodian-Moghaddam, M.; Khorsand-Ahmadi, S.; Saberi, M. R.; Chamani, J., Binding site identification of metformin to human serum albumin and glycated human serum albumin by spectroscopic and molecular modeling techniques: a comparison study. *J. Biomol. Struct. Dyn.* **2015**, *33* (3), 513-533.
- 31. McCann, K. B.; Vucica, Y.; Famulari, S.; Bertolini, J., Effect of processing methods on colouration of human serum albumin preparations. *Biologicals* **2009**, *37* (1), 32-36.
- 32. Farrugia, A., Albumin usage in clinical medicine: tradition or therapeutic? *Transfusion medicine reviews* **2010**, *24* (1), 53-63.
- 33. Wolf, M.; Kronenberg, H.; Dodds, A.; Miach, P.; Isbister, J.; Levidiotis, M.; Dear, K., A safety study of Albumex<sup>®</sup> 5, a human albumin solution produced by ion exchange chromatography. *Vox sanguinis* **1996**, *70* (4), 198-202.
- 34. Janabi, A. M. H. Proinsulin C-peptide-mediated signalling and the search for its receptor. Department of Molecular and Cell Biology, 2017.
- 35. Liu, Y., Delivery of a pancreatic beta cell-derived hormone to erythrocytes by albumin and downstream cellular effects. Michigan State University: 2015.
- 36. Ockner, R. K.; Weisiger, R. A.; Gollan, J. L., Hepatic uptake of albumin-bound substances: albumin receptor concept. *American Journal of Physiology-Gastrointestinal and Liver Physiology* **1983**, *245* (1), G13-G18.
- Weisiger, R.; Gollan, J.; Ockner, R., Receptor for albumin on the liver cell surface may mediate uptake of fatty acids and other albumin-bound substances. *Science* **1981**, *211* (4486), 1048-1051.
- 38. Schnitzer, J. E.; Carley, W. W.; Palade, G. E., Albumin interacts specifically with a 60-kDa microvascular endothelial glycoprotein. *Proceedings of the National Academy of Sciences* **1988**, *85* (18), 6773-6777.
- 39. Antohe, F.; Dobrila, L.; Heltianu, C.; Simionescu, N.; Simionescu, M., Albumin-binding proteins function in the receptor-mediated binding and transcytosis of albumin across cultured endothelial cells. *European journal of cell biology* **1993**, *60* (2), 268-275.

- 40. Birn, H.; Fyfe, J. C.; Jacobsen, C.; Mounier, F.; Verroust, P. J.; Ørskov, H.; Willnow, T. E.; Moestrup, S. K.; Christensen, E. I., Cubilin is an albumin binding protein important for renal tubular albumin reabsorption. *The Journal of clinical investigation* **2000**, *105* (10), 1353-1361.
- 41. ThermoFisher Crosslinking Protein Interaction Analysis. <a href="https://www.thermofisher.com/us/en/home/life-science/protein-biology/protein-biology-learning-center/protein-biology-resource-library/pierce-protein-methods/sample-preparation-mass-spectrometry.html">https://www.thermofisher.com/us/en/home/life-science/protein-biology/protein-biology-learning-center/protein-biology-resource-library/pierce-protein-methods/sample-preparation-mass-spectrometry.html</a>.
- 42. Simpson, R. J.; Adams, P. D.; Golemis, E., *Basic methods in protein purification and analysis*. Cold Spring Harbor Laboratory Press: 2009.
- 43. Yang, L.; Tang, X.; Weisbrod, C. R.; Munske, G. R.; Eng, J. K.; Von Haller, P. D.; Kaiser, N. K.; Bruce, J. E., A photocleavable and mass spectrometry identifiable cross-linker for protein interaction studies. *Anal. Chem.* **2010**, *82* (9), 3556-3566.